Fermi National Accelerator Laboratory

FERMILAB-Pub-95/264-E

CDF

Properties of the W Boson from the Fermilab Tevatron

S.E. Kopp

Fermi National Accelerator Laboratory
P.O. Box 500, Batavia, Illinois 60510

Enrico Fermi Research Institutes
University of Chicago
5640 South Ellis Avenue
Chicago, Illinois 60637

August 1995

Invited review paper for the *International Journal of Modern Physics A*

Operated by Universities Research Association Inc. under Contract No. DE-AC02-76CHO3000 with the United States Department of Energy

Disclaimer

FERMILAB-PUB-95/264-E
CDF/PUB/ELECTROWEAK/PUBLIC/3293

Properties of the W Boson from the Fermilab Tevatron

Sacha E. Kopp

Enrico Fermi Research Institutes, University of Chicago,
5640 South Ellis Avenue, Chicago, Illinois 60637§

1 May 1995

Abstract

The experimental knowledge of the charged intermediate vector boson, the W, is reviewed. Measurements of the electroweak properties of the W boson, such as its mass, decay width, couplings to fermions, and leptonic branching ratios are summarized. As well, I review production properties of the W as measured in $p\bar{p}$ collisions and how they can be used as tests of perturbative QCD. I also discuss searches that make use of the W signature, such as new charged electroweak bosons and the now-confirmed discovery of the top quark.

CONTENTS:

Invited review paper for the International Journal of Modern Physics A

1. Introduction

Within the unified electroweak theory of Weinberg,[1] Salam,[2] and Glashow,[3] the massive $W^{\pm}$ and Z^0 particles are the intermediate vector bosons which carry the weak force. The theory allows us to predict many of their properties given atomic and lepton-hadron scattering data at low Q^2. Their discovery in 1983 by the UA1[4] and UA2[5] experiments at the CERN $p\bar{p}$ collider has provided an outstanding confirmation of the electroweak theory. The precision studies of the Z^0 resonance at the LEP and SLD experiments[6], furthermore, have tested the electroweak theory to higher orders in perturbation theory. The importance of precise direct measurements of the W and Z^0 is that they may reveal discrepencies with the low-Q^2 extrapolations due to new physics at higher mass scales, as shown schematically in Figure 1. These data also allow us to make precise extrapolations of the charged current interation to the Q^2 scale of the W. The purpose of this article is to review direct measurements made of the W boson. A number of new results are available from data collected in 1992-1993 by the CDF and DØ experiments at the Fermilab Tevatron collider. I attempt here to summarize the status of our experimental knowledge as we head into the next phase of study of the W with future runs of LEP-200 and of the Fermilab Main Injector.

In the Standard Model of the electroweak force[7], the intermediate vector bosons arise from the hidden gauge group $SU(2) \times U(1)$, where the gauge-covariant derivative introduces three $SU(2)$ gauge bosons, W^i_μ and one boson, B_μ, associated with the $U(1)$ group:

$$D_\mu = \delta_\mu - i\,(gW^i_\mu \tau^i + g'B_\mu Y)$$

The parameters g, g' are the coupling constants of the two groups, $\tau^i = \sigma^i / 2$, and Y denotes the weak hypercharge. Through the introduction of a complex scalar doublet, the Higgs field, with a vacuum expectation value $\langle\phi(x)\rangle = \frac{1}{\sqrt{2}}\binom{0}{v}$, the gauge fields arrange into the mass eigenstates:

$$\begin{aligned} W^{\pm} &= \tfrac{1}{\sqrt{2}}\left(W^1_\mu \mp W^2_\mu\right) & M_W &= \tfrac{g}{2}v \\ Z^0 &= \left(\cos\theta_W W^3_\mu - \sin\theta_W B_\mu\right) & M_Z &= \tfrac{\sqrt{g^2+g'^2}}{2}v \\ A &= \left(\sin\theta_W W^3_\mu + \cos\theta_W B_\mu\right) & m_\gamma &= 0 \end{aligned} \qquad [1]$$

where $\tan\theta_W \equiv g'/g$. The charged current carrier, the $W^{\pm}$, is responsible for the familiar low-energy atomic β decay. A remarkable aspect of the theory, as far as the charged-current carrier, the $W^{\pm}$, is concerned, is that it is predicted to have one single, universal coupling g to all fermions. The same feature was actually postulated in the Fermi four-point theory of the weak

interaction. Unlike the Fermi theory, however, the Standard Model weak interaction is predicted to be diminished in strength at low-Q^2 because of the large boson masses[8], even though the couplings are similar to the electromagnetic coupling: $g = e / \sin\theta_W$, $g' = e / \cos\theta_W$.

At lowest order the parameters of the Standard Model are interrelated, and, given other measurements, the theory may predict the parameters of the W. An important relation holds at lowest order between the boson masses and the weak mixing angle: $\rho \equiv M_W/M_Z\cos\theta_W = 1$. Thus, given a measurement[6] of the weak mixing angle, $\sin^2\theta_W = 0.2322 \pm 0.0003$ from deep inelastic scattering data, forward-backward and left-right asymmetries at the Z^0 pole, and the mass, $M_Z = 91188 \pm 4\ MeV/c^2$, of the Z^0 boson, the theory predicts a lowest-order value for the W mass. Furthermore, because low-Q^2 weak processes like μ decay described by a universal coupling $G_F = 1.16632 \times 10^{-5}\ GeV^{-2}$ in the Fermi effective theory are just the $Q^2 \to 0$ limit of the weak coupling times the W propagator, $-ig^2 / (Q^2 - M_W^2 - i\varepsilon)$ in the Standard Model, the universal coupling g in the Standard Model may be predicted as $g^2 = \frac{8}{\sqrt{2}} G_F M_W^2$.

At higher order in the Standard Model, the electroweak observables of both the W and the Z^0 receive corrections due to Feynman graphs such as those in Figure 2. Since next-to-leading order corrections may be roughly estimated as $\frac{\alpha}{4\pi} M_W \sim 100\ MeV$, we see that present experimental measurements begin to probe the next-to-leading order in the Standard Model. At next-to-leading order, the W propagator changes to:[9]

$$\frac{-i}{Q^2 - M_W^2 - i\varepsilon} \rightarrow \frac{-i}{Q^2 - M_W^2 - \Pi_{WW}(Q^2)}$$

where $\Pi_{WW}(Q^2)$ is the vacuum polarization of the W. The vacuum polarization has ramifications for both the mass and the width of the W. Because the graphs of Figure 2 give $\mathrm{Re}\,\Pi_{WW}(M_W^2) \neq 0$, the mass of the pole changes from its lowest-order value, and $\mathrm{Im}\,\Pi_{WW}(Q^2)$ is interpreted as the W decay width. The corrections to observables of the W and Z^0 that enter through vacuum polarization corrections and that retain the intrinsic Lorentz and gauge symmetry properties as the tree-level calculations are sometimes called "oblique corrections."[10] The importance of these corrections is that the theoretical predictions for the W depend upon the masses of new particles that enter through the oblique corrections (see Figure 2). Hence, the direct measurements of the W performed at $p\bar{p}$ colliders check the theory and constrain the masses of new particles through constraints on the sizes of the radiative corrections.

One major question that has lingered over the last decade is why the top quark is so heavy. In the Standard Model, the W and Z^0 couple to the left-handed components of three families of weak isodoublets, divided into the leptons and the quarks:

Leptons: $\begin{pmatrix} e \\ \upsilon_e \end{pmatrix}$ $\begin{pmatrix} \mu \\ \upsilon_\mu \end{pmatrix}$ $\begin{pmatrix} \tau \\ \upsilon_\tau \end{pmatrix}$

Quarks: $\begin{pmatrix} u \\ d \end{pmatrix}$ $\begin{pmatrix} c \\ s \end{pmatrix}$ $\begin{pmatrix} t \\ b \end{pmatrix}$

The existence of three isodoublet families of each type is required in the Standard Model in order for the theory to be renormalizable. The families each exhibit a remarkable mass heirarchy which has no explanation in the Standard Model. For example, $m_e = 0.511\ keV/c^2$, while $m_\tau = 1.778\ GeV/c^2$. Similarly, the masses of the lightest quarks are a few tens of MeV/c^2, but the now-confirmed top quark has a mass of 176 GeV/c^2, making this fundamental fermion nearly as heavy as a Tungsten nucleus.

In the presence of this large top mass, W and Z^0 self-mass effects[11] alter the so-called ρ parameter, $\rho \equiv M_W/M_Z\cos\theta_W$, where M_W and M_Z are the measured boson masses and $\sin^2\theta_W$ is the weak coupling measured at the Z^0. At $O(m_t^2)$ we have:

$$\rho \cong 1 + \frac{3\alpha}{16\pi \sin^2\theta_W}\left(\frac{m_t}{M_W}\right)^2$$

A direct measurement of m_{top} is of paramount importance as a test against the value for m_{top} extracted from the radiative corrections of the measured W and Z^0 parameters. The top mass also has implications for many other sectors of the Standard Model, such as the ratio of CP-violating parameters ε'/ε measured in kaon decays[12], but these will not be discussed here.

This article will proceed as follows: Section 2 will describe the collection of W's at $p\bar{p}$ colliders. In Section 3, I attempt to stress the interplay between Standard Model predictions and the direct measurements of the W, including the W mass, leptonic branching ratio, total decay width, universality of the coupling g, and tests of V-A in the weak interaction. Section 4 describes properties of W production in $p\bar{p}$ collisions and tests of perturbative QCD that are possible. Section 5 describes new particle searches that can be performed using W decays, such as new (possibly right-handed) W' bosons, W + jet(s) resonances, and the now-confirmed observation of top quark. Finally, Section 6 concludes and ponders where we go from here.

2. Experimental Considerations of Observing W Bosons

In this section I review the experiments which currently observe W bosons. Because of the limited energies available at e^+e^- colliders, measurements pertaining to the W have been to date the purview of $p\bar{p}$ colliders. The Fermilab Tevatron, with center-of-mass energy $\sqrt{s} = 1800\ GeV$, is the only such accelerator facility currently running. The Sp$\bar{p}$S collider at CERN also collided protons on antiprotons at $\sqrt{s} = 546$ and $630\ GeV$, featuring the UA1[4,13] and UA2[5] detectors, but was shut down in 1989. Two detectors are now recording data at the Fermilab collider, the Collider Detector at Fermilab (CDF) and the DØ collider experiment.

2.1 The Fermilab Tevatron

A schematic view of the Fermilab Tevatron[14] is shown in Figure 3. At Fermilab, protons are accelerated to $200\ MeV$ in the Linac and then to $8\ GeV$ in the Booster accelerator. The protons are then transferred to the Main Ring, an accelerator in the main tunnel, and accelerated to $150\ GeV$. The protons are then either transferred to the superconducting Tevatron accelerator or are extracted to strike a Tungsten target, where $\bar{p}$'s are produced and momentum-selected into the Accumulator ring. When a large number of $\bar{p}$'s is collected in the Accumulator, they are also inserted into the Tevatron, rotating in the opposite direction, and raised to $900\ GeV$.

The luminosity is given by $\mathcal{L} = \frac{N_p N_{\bar{p}} B f}{A}$, where N_p ($N_{\bar{p}}$) is the number of p's ($\bar{p}$'s) in each bunch, $B = 6$ is the number of bunches in the Tevatron, $f = 50\ kHz$ is the accelerator revolution frequency, and A is the cross-sectional area of the $p\bar{p}$ bunches at the collision point, measured to be $A \sim 1.4 \times 10^{-4}\ cm^2$ (see Figure 4). During the collider run from August, 1992 to June, 1993, the Tevatron delivered an integrated luminosity $\int \mathcal{L} dt = 27.3\ pb^{-1}$, with typical instantaneous luminosities of $4.0 \times 10^{30}\ cm^{-2}sec^{-1}$ and a peak instantaneous luminosity of $9.7 \times 10^{30}\ cm^{-2}sec^{-1}$. CDF wrote $19.7\ pb^{-1}$ of data to tape and DØ recorded $12.4\ pb^{-1}$. Approximately 20,000 and 13,000 leptonic decays of W bosons, respectively, were recorded by each experiment.

2.2 The CDF and DØ Detectors

CDF[15] is a cylindrical detector surrounding the $p\bar{p}$ ring with a central barrel region $|\eta| < 1.1$,[16] end-cap regions ($1.1 < |\eta| < 2.4$) closing the barrel, and far-forward detector regions ($2.2 < |\eta| < 4.2$) (see Figure 5). It has electromagnetic (EM) and hadronic (Had) calorimeters arranged in projective tower geometry and charged particle tracking chambers. The

EM calorimeter measures electron energies with resolution $(\sigma_E/E)^2 = (13.5\%)^2/E + (1\%)^2$. The Central Tracking Chamber measures the curvature of charged particles with $|\eta| < 1.5$ in a 1.4 T magnetic field provided by a superconducting solenoidal magnet coil. The CTC momentum resolution is $\delta p_T/p_T^2 = 0.001$. Drift chambers outside the calorimeters for muon detection cover the region $|\eta| < 1.0$. Scintillator planes, called Beam-Beam Counters (BBC's), are mounted at $3.2 < |\eta| < 5.9$ in order to signal inelastic collisions and act as luminosity monitors.

CDF has installed a Silicon Vertex Detector (SVX)[17], a four-layer silicon microvertex detector, to provide precise r-ϕ information for charged particle tracks. This device truly revolutionized the analysis of $p\bar{p}$ collisions. The SVX provides 13 μm hit resolution and an impact parameter resolution of $\sigma_d \sim 30$ μm (see Figure 4), which, for tracks with $p_T > 1$ GeV/c, is dominated by the uncertainty in the primary interaction position (see Figure 4). The impact parameter discriminates daughters of long-lived heavy quarks (for b quarks $<\gamma\beta c\tau_b> \sim 2000$ μm) from those originating from the primary vertex of the $p\,\bar{p}$ collision, as shown in Figure 6. Two or more tracks with large impact parameters may be fit to the hypothesis of originating from a common secondary vertex (such as the decay point of a b) separated from the primary. This process is referred to as 'b tagging,' and is revisited in later sections.

The DØ detector[18] (see Figure 7) consists of a Uranium-liquid Argon calorimeter covering the pseudorapidity range $|\eta| < 4.2$ and a charged particle tracking chamber which measures the trajectories and specific ionizations of charged particle tracks. The EM calorimeter resolution is $(\sigma_E/E)^2 = (15\%)^2/E + (2\%)^2$. A transition radiation detector aids in electron identification. The DØ calorimeter was designed to have better hermeticity than CDF and drift chambers outside the calorimeters to provide superior solid angle coverage for muon detection.[19] The DØ detector, however, has no solenoidal magnet, relying solely upon calorimetric information for electrons and jets. Having no magnetic field in the tracking volume, they have installed toroid magnets between the layers of the muon chambers in order to measure muon momenta, resulting in a muon momentum resolution $\delta p_T/p_T^2 \sim 20\%$.

2.3 High-P_T Lepton Identification

In practice, only leptonic decay modes of the W are used by experiments since they provide the unique signature of an energetic lepton. The decays such as $W \to q\bar{q}'$, in contrast, appear identical to the dijet topology in QCD $q\bar{q}$ or gg scattering, which occurs at a cross section 10^2 times bigger than the W cross section.[20] One remarkable exception is provided by the

UA2 experiment,[21] whose excellent mass resolution could resolve a dijet excess near the W mass (see Figure 8). Similarly, $W \rightarrow \tau\upsilon$ decays are frequently not used because the hadronic tau decays look like quark or gluon jets, and the leptons from $\tau \rightarrow \ell\upsilon_\tau\bar{\upsilon}_\ell$ are of lower transverse momentum.[22] The signature of high-p_T leptons, while having some backgrounds from $b \rightarrow c\ell\upsilon$, decay in flight, *etc.*, tends to be much more distinct. The transverse energy spectrum of electrons from the CDF experiment is shown in Figure 9. A shoulder from W and Z^0 decays is apparent.

Neutrinos from W decays are non-interacting, so may be identified by the presence of a large energy imbalance in the calorimeters. The $\not\!\!E_T$, or missing transverse energy, is defined as $\not\!\!E_T \equiv |\sum_i \vec{E}^{\,i}_T|$ where $\vec{E}^{\,i}_T$ is a vector whose magnitude is the transverse energy in a calorimeter cell which points from the event vertex to the center of the cell. For events with muons, the $\not\!\!E_T$ calculation includes $\vec{p}^{\,\mu}_T$, as measured with tracking, since the muon is mimimum-ionizing in the calorimeters. Only the transverse components of the neutrino can be reconstructed because many spectator particles from the $p\bar{p}$ collision escape undetected down the beam pipe.

2.4 Isolation of the *W* Signal

To suppress leptons from other sources, an 'isolation' variable is used. Leptons from QCD jet production, unlike leptons from W's, tend to be embedded in a jet of hadrons. The isolation variable suppresses events with significant energy flow near the lepton. Figure 10 shows the $\not\!\!E_T$ spectrum of CDF events with isolated and non-isolated electrons. The isolated electrons show a peak from the W at $\approx 40\ GeV$ in addition to the bump closer to zero from mismeasured jet events. The W's are selected by requiring an isolated lepton and $\not\!\!E_T > 20\ GeV$.

Because only the transverse components of the neutrino momentum can be inferred, the invariant mass of $W \rightarrow \ell\upsilon$ decays cannot be reconstructed. Instead, the "transverse mass," M_T, is used. It is defined as $M_T^2 \equiv (|\vec{p}^{\,\ell}_T| + |\vec{p}^{\,\upsilon}_T|)^2 - (\vec{p}^{\,\ell}_T + \vec{p}^{\,\upsilon}_T)^2$ where $\vec{p}^{\,\ell}_T$ and $\vec{p}^{\,\upsilon}_T$ are the lepton momenta in the transverse plane. The transverse mass of $W \rightarrow \ell\upsilon$ events from the UA1 experiment is shown in Figure 11. The transverse mass, in the limit of perfect detector resolutions and zero decay width, diverges at the W mass and shows no events with $M_T > M_W$. The resolutions and finite decay width of the W smear this divergence and cause some events to populate this region. A very useful property of the transverse mass is that it still peaks near M_W and is invariant to longitudinal boosts and, to first order, to boosts in the transverse plane.[23]

3. Electroweak Measurements of the W

3.1 The W Leptonic Branching Ratio

Two fundamental parameters that are calculable in the Standard Model are the W boson width, $\Gamma(W)$, and the W leptonic branching ratio, $\Gamma(W\to\ell\upsilon)/\Gamma(W)$. Because of its universal coupling, the W decays with approximately equal probability to each of three lepton families and to the two quark families kinematically available (with a color factor of three on the number of quark families). Hence, the branching ratio of the W into $(\ell,\bar{\upsilon}_\ell)$ is approximately $\frac{1}{9}$. The quark decays are enhanced by α_s/π to first order in QCD so that the leptonic branching ratio is:[24]

$$\Gamma(W\to\ell\upsilon)/\Gamma(W) = [3 + 6(1 + \alpha_s(M_W)/\pi)]^{-1} = 0.1084 \pm 0.0002,$$

where the 0.0002 uncertainty reflects the uncertainty in α_s at $Q^2 = M_W^2$. A precise measurement of the leptonic branching ratio is thus a sensitive search for new particles which couple to the W. A prediction may be made for the W total decay width by calculating the W leptonic partial width, $\Gamma(W\to\ell\upsilon) = g^2 M_W/48\pi$. Rosner *et al*,[24] find that the Standard Model expectation is:

$$\Gamma(W) = [3 + 6(1 + \alpha_s(M_W)/\pi)]\ \Gamma(W\to\ell\upsilon) = 2077 \pm 12\ MeV,$$

where the uncertainty in the prediction is dominated by the uncertainty in the measured W mass.

The W leptonic branching ratio may be extracted from a measurement of the ratio, R, of the cross sections times leptonic branching ratios of the W and Z^0 in $p\bar{p}$ collisions.[25] The ratio R may be expressed as:

$$R \equiv \frac{\sigma B(p\bar{p}\to W\to\ell\upsilon)}{\sigma B(p\bar{p}\to Z^0\to\ell\ell)} = \frac{\sigma(p\bar{p}\to W)}{\sigma(p\bar{p}\to Z^0)}\,\frac{\Gamma(W\to\ell\upsilon)}{\Gamma(Z^0\to\ell\ell)}\,\frac{\Gamma(Z^0)}{\Gamma(W)}$$

On the right hand side, the ratio $\sigma(p\bar{p}\to W)/\sigma(p\bar{p}\to Z^0)$ of the production cross sections may be calculated from the boson couplings and knowledge of the proton structure. The Z^0 total width, $\Gamma(Z^0)$, and the leptonic partial width, $\Gamma(Z^0\to\ell^+\ell^-)$, are well-measured by the LEP experiments.[6] Thus, a measurement of R yields a precise measurement of the W leptonic branching ratio $\Gamma(W\to\ell\upsilon)/\Gamma(W)$.

The measurement of R is the most precise way to measure $\Gamma(W\to\ell\upsilon)/\Gamma(W)$ because many experimental and theoretical uncertainties cancel in the ratio. Theoretically, the uncertainties in the calculations of the production cross sections nearly cancel in the ratio because W's and Z^0's have very similar production mechanisms[26]. Experimentally, the ratio of cross sections times branching ratios are found from:

$$R \equiv \frac{\sigma B(p\bar{p}\to W\to\ell\upsilon)}{\sigma B(p\bar{p}\to Z^0\to\ell\ell)} = \frac{N_W^{Candidates} - N_W^{Background}}{A_W\varepsilon_W\int\mathcal{L}dt} \quad \frac{A_Z\varepsilon_Z\int\mathcal{L}dt}{N_Z^{Candidates} - N_Z^{Background}}$$

where $N_W^{Candidates}$ and $N_Z^{Candidates}$ are the number of W and Z^0 candidates observed; A_W and A_Z are the "acceptances" for the W and Z^0 decays (the efficiency for the kinematic cuts on the leptons and the geometric acceptance of the detector) and are estimated with a Monte Carlo calculation; ε_W and ε_Z are the efficiencies for the W and Z^0 to pass the lepton identification criteria which can be measured with $Z^0\to\ell^+\ell^-$ and $J/\psi\to\mu^+\mu^-$ decays, and $\int\mathcal{L}dt$ is the integrated luminosity of the experiment. Quite importantly, the experimental determination of the luminosity (and its uncertainty) cancels completely.

The measurement of R has been performed with different techniques by the UA1,[27] UA2,[28] DØ,[29] and CDF[30,31] experiments. Since $R \sim 10$, the number of Z^0's limits the statistical uncertainty of this measurement. UA1, UA2, and DØ attempt to capture all Z^0's in their detectors in order to decrease the statistical uncertainty. CDF chose to require both W and Z^0 decays to be triggered by at least one charged lepton in the central, barrel region of their detector (approximately 80% efficient for Z^0's). In this way, the efficiencies of the lepton triggers, of the selection criteria for the central lepton, and the geometric efficiency of obtaining a central lepton (which appear in the factors $\varepsilon_W/\varepsilon_Z$ and A_W/A_Z) almost completely cancel out in R because they are common to both W's and Z^0's. The results are summarized in Tables 1, 2 and Figures 12, 13.

Table 1: Ratio R from the DØ Collaboration [29]

	$W\to e\upsilon$	$Z^0\to e^+e^-$	$W\to\mu\upsilon$	$Z^0\to\mu^+\mu^-$
Number of Candidates	10338	775	1665	77
Total Background	5.7 ± 0.4 %	4.0 ± 1.4 %	22.1 ± 1.9 %	10.1 ± 3.7 %
Acceptance: A_W or A_Z	46.1 ± 0.6 %	36.3 ± 0.4 %	24.8 ± 0.7 %	6.5 ± 0.4 %
Efficiency: ε_W or ε_Z	71.7 ± 1.5 %	75.0 ± 2.3 %	22.3 ± 2.6 %	53.8 ± 5.0 %
Luminosity	$12.4\pm1.5\ pb^{-1}$		$11.1\pm1.3\ pb^{-1}$	
$\sigma(W\to\ell\upsilon)/\sigma(Z^0\to\ell^+\ell^-)$	$10.82\ \pm0.41$ (*stat.*) ±0.24 (*sys.*)		$11.8\ ^{+1.8}_{-1.4}$ (*stat.*) ±1.1 (*sys.*)	

Table 2: Ratio R from the CDF Collaboration [30,31]

	$W\to e\nu$ a)	$Z^0\to e^+e^-$ a)	$W\to\mu\nu$ b)	$Z^0\to\mu^+\mu^-$ b)
Candidates:	13796	1312	1436	106
Signal (after bckgd subtraction)	$12096 \pm 117\,^{+163}_{-167}$	$1291 \pm 36 \pm 9$	$1216 \pm 38\,^{+27}_{-31}$	$106 \pm 10\,^{+0.2}_{-1.0}$
Acceptance: A_W or A_Z	0.342 ± 0.008	0.409 ± 0.005	0.190 ± 0.009	0.154 ± 0.009
A_W / A_Z	0.835 ± 0.013		1.234 ± 0.032	
Efficiencies: ε_W or ε_Z	0.720 ± 0.013	0.696 ± 0.017	0.821 ± 0.036	0.857 ± 0.041
$\varepsilon_W / \varepsilon_Z$	1.035 ± 0.016		0.958 ± 0.018	
Drell-Yan Correction	-	1.005 ± 0.002	-	1.01 ± 0.01
$\sigma(W\to\ell\nu)/\sigma(Z\to\ell\ell)$	10.90 ± 0.32 (*stat.*) ± 0.29 (*sys.*)		9.8 ± 1.1 (*stat.*) ± 0.4 (*sys.*)	

a) Collected in 19.6 pb^{-1} b) Collected in 3.54 pb^{-1}

In order to extract a value for the leptonic branching ratio of the W from the various measurements of R, we require the LEP[6] measurements of $\Gamma(Z^0) = 2497.4 \pm 3.8\ MeV$ and $\Gamma(Z^0\to\ell\ell) = 83.96 \pm 0.18\ MeV$, as well as a theoretical calculation of the ratio of production cross sections $\sigma(p\bar{p}\to W)/\sigma(p\bar{p}\to Z^0)$. Different collaborations have used different values for this cross section ratio, and I have left their cited values for σ_W/σ_Z, rather than use a common value.[32] The world average for the leptonic branching ratio (see Table 3) is:

$$\text{World Average: } \Gamma(W\to\ell\nu)/\Gamma(W) = 0.1078 \pm 0.0028.$$

The Standard Model prediction,[24] assuming $m_{top} > M_W - m_b$, is 0.1084 ± 0.0002. This measured branching ratio limits new decay modes X (such as $t\bar{b}$) of the W to have:

$$B.R.(W\to X) < 0.050 \qquad (95\%\ \text{C.L.})$$
$$\Gamma(W\to X) < 110\ MeV \qquad (95\%\ \text{C.L.}).$$

Some experiments have assumed the Standard Model value of $g^2 = \frac{8}{\sqrt{2}} G_F M_W^2$ in order to calculate the W leptonic partial width $\Gamma(W\to\ell\nu) = \frac{g^2 M_W}{48\pi}$ and obtain a value for $\Gamma(W)$ from the branching ratio measurement. It must be emphasized, however, that R, strictly speaking, measures only $\Gamma(W\to\ell\nu)/\Gamma(W)$. Multiplying the branching ratio measurement by this calculation gives only a figure of merit for the width within the Standard Model, since the prediction for g has been employed. An independent measurement must be made of the coupling g.

Table 3: World Average Results for $\Gamma(W\to\ell\nu)$ / $\Gamma(W)$

Collaboration		Decay Mode	Result for R	σ_W / σ_Z	$\Gamma(W\to\ell\nu)/\Gamma(W)$
UA1	[27]	$\mu\nu$, $\mu^+\mu^-$	9.5 ± 1.1	3.23 ± 0.05 [27]	0.099 ± 0.011
UA2	[28]	$e\nu$, e^+e^-	10.4 ± 0.8	3.26 ± 0.09 [33]	0.1072 ± 0.0089
CDF	[30]	$e\nu/ee + \mu\nu/\mu\mu$	10.0 ± 0.7	3.23 ± 0.03 [34]	0.1041 ± 0.0074
DØ	[29]	$e\nu/ee + \mu\nu/\mu\mu$	10.90 ± 0.49	3.34 ± 0.03 [35]	0.1097 ± 0.0051
CDF	[31]	$e\nu$, e^+e^-	10.90 ± 0.46	3.35 ± 0.03 [36]	0.1094 ± 0.0046
		World Average:			0.1078 ± 0.0028

3.2 Direct Measurement of $\Gamma(W)$

To test the Standard Model, it is also desirable to measure $\Gamma(W)$ as well as $\Gamma(W\to\ell\nu)/\Gamma(W)$. The W width receives electroweak corrections due to next-to-leading order graphs such as those in Figure 2 which alter the effective coupling g at the W-fermion vertex. The corrections to $\Gamma(W)$ depend upon the top and Higgs masses, since loops can exist at the W-fermion vertex involving the Z^0 boson, a scalar Higgs boson ϕ, and corrections to the W propagator from the top quark that are not absorbed into the W mass.[37] The vertex corrections from the Standard Model Higgs cause $\Gamma(W)$ to change by approximately 20 MeV as the Higgs mass varies from 50 GeV/c^2 to 1000 GeV/c^2, while the correction from $t\,\bar{b}$ loops changes $\Gamma(W)$ by approximately 80 MeV as the m_{top} varies from 80 GeV/c^2 to 200 GeV/c^2.[38] The vertex corrections to g are nearly identical for all fermions; hence, they cancel out of the leptonic branching ratio. Only a direct measurement of $\Gamma(W)$ is sensitive to these radiative corrections.

Direct measurements of $\Gamma(W)$ have been reported by the UA1[39] and UA2[40] Collaborations. Including systematic uncertainties, they obtained $\Gamma(W) = 2.8\ ^{+1.4}_{-1.5} \pm 1.3\ GeV$ and $\Gamma(W) < 7.0\ GeV$ (90% C.L.) respectively. These direct measurements result from fits of the W transverse mass distribution for the best values of M_W and $\Gamma(W)$. The fits were performed over a limited range in M_T near the M_W peak, and hence are sensitive to experimental resolutions.

A more powerful technique for measuring $\Gamma(W)$, as published recently by the CDF collaboration,[41] is to use the high-mass tail of the transverse mass distribution of $W\to\ell\nu$ decays. Events with $M_T > M_W$ can arise due to the calorimeter resolution or due to the non-zero W width. However, a precise measurement of $\Gamma(W)$ from the high-mass tail is possible as the transverse mass is invariant to boosts in the tranverse plane and because far above M_W the Breit-

Wigner tail of the W dominates over the gaussian resolution of the detector. In the CDF analysis $\Gamma(W)$ is determined from a log-likelihood fit of the transverse mass data in the region $M_T > 110\ GeV/c^2$. Events with central electrons with calorimeter transverse energy $E_T > 30\ GeV$ $\not\!\!E_T > 30\ GeV$ were selected, reducing backgrounds.

A cut of $P_T^W < 20\ GeV/c$ is imposed in order to further suppress many of the backgrounds in the fit region and to suppress the broader calorimeter resolution which arises at large P_T^W. This cut also suppresses $O(\alpha_s)$ diagrams of W production such as $qg \rightarrow Wq$ and $q\bar{q} \rightarrow Wg$, where the W is seen to recoil with large transverse momentum against a jet of hadrons. With this cut, the number of $W \rightarrow e\upsilon$ candidates is 9701 and the total background is 224 ± 44 events. The background in the fit region (dominated by hadron jets) is $\sim 10\%$ of the 58 events observed. Figure 14 shows the transverse mass distribution of the 9701 candidate events after the $P_T^W < 20\ GeV/c$ cut, along with the expected background.

The Monte Carlo program generates zeroth order diagrams of W production, $q\ \bar{q} \rightarrow W$, according to an energy-dependent Breit-Wigner distribution:[42]

$$\sigma(\hat{s}) \sim \frac{\hat{s}}{[(\hat{s} - M_W^2)^2 + \hat{s}^2\Gamma_W^2/M_W^2]}$$

where $\sqrt{\hat{s}}$ is the (possibly off-shell) $\ell\nu$ mass. This form of the cross section includes vacuum polarization contributions to the W propagator even far off the W pole. The real part of the vacuum polarization is shown to have negligible effect, even off the pole,[43] and in fact using only the lowest order approximation causes only a 6 MeV shift in the fitted width. The bosons are given P_T according to a previous measurement[44] of the P_T^W spectrum in order to mimic higher order diagrams for W production, but $q\ \bar{q}$ diagrams dominate because of the P_T^W cut.

The inset to Figure 14 shows the likelihood fit to the data to Monte Carlo templates of different widths. The most likely value is $\Gamma(W) = 2.04 \pm 0.28\ (stat.)\ GeV$. A small shift of $70 \pm 28\ MeV$, estimated with a different Monte Carlo program,[45] is applied to $\Gamma(W)$ due to the effect of radiative decays $W \rightarrow e\upsilon\gamma$, where the photon energy is not incorporated into the transverse mass. The most important systematic uncertainties pertain to the modeling of the resolution, which causes extra events to populate the fit region and can be controlled with larger control samples to model them. The final CDF result for the W width is:

$$\text{CDF:}\quad \Gamma(W) = 2.11 \pm 0.28(stat.) \pm 0.16(sys.)\ GeV.$$

This result yields a 15% measurement of the W width which is purely statistics limited. With the combined data set of 200 pb^{-1} from both the CDF and DØ detectors, a 100 MeV measurement is possible. This may be compared with the ultimate uncertainty[46] expected from the LEP-200 experiments of 200 MeV. With future runs of the Tevatron, a 30 MeV measurement is possible, which approaches the level of the radiative corrections to the width.[47]

With the present direct measurement of $\Gamma(W)$ by CDF, and the theoretical expectation[24] $\Gamma(W) = \frac{g^2 M_W}{48\pi} \frac{1}{0.1084 \pm 0.0002}$, we may extract a measurement of the W-fermion coupling, g, at $Q^2 = M_W^2$ (see Section 1). Using the world average $M_W = 80.27 \pm 0.15$ GeV/c^2, we find:

$$\text{CDF:} \quad g = 0.656 \pm 0.049.$$

Note that the Standard Model expectation is $g^2 = \frac{8}{\sqrt{2}} G_F M_W^2 = 0.425 \pm 0.002$, or $g = 0.652 \pm 0.001$. This measurement is unique as a measurement of g at $Q^2 = M_W^2$, and shows that the coupling constant does not run very much with Q^2 when G_F and M_W are used to parameterize g.

3.3 The *W* Boson Mass

Through the oblique corrections, the LEP and SLD Z^0 data, together with low energy deep-inelastic scattering data, may provide constraints upon the allowed W mass for different assumptions regarding m_{top} and m_{Higgs}, as shown in Figure 26.[48] With the measurement of the top mass (see Section 5.3) a measurement of the W mass sheds light on the Higgs. Note that the sensitivity of M_W to m_{top} is much greater than for m_{Higgs}, since the m_{top} dependence of the oblique correction is $(m_{top}/M_W)^2$, while the correction in m_{Higgs} is logarithmic in m_{Higgs}. As m_{top} varies from 80 GeV/c^2 to 200 GeV/c^2, M_W changes by 1 GeV/c^2, which is much larger than the anticipated experimental uncertainty. Furthermore, because of the remarkable radiative corrections to $\Gamma(Z^0 \rightarrow b\bar{b})$ (see Figure 2), where the top quark is uniquely involved because it is the weak isodoublet partner to the b (as opposed to entering through the oblique corrections, which are in some sense summations over all particles), there is independent sensitivity in the Z^0 data to m_{top}. Fitting simultaneously for m_{top} and M_W the LEP+SLD data predict $M_W = 80320 \pm 60$ MeV/c^2, while the LEP data alone predict $M_W = 80270 \pm 60$ MeV/c^2. The uncertainties in these fits are from the unknown top and Higgs masses. The direct measurement of the W and top masses, then, greatly help constrain the electroweak fits for the Higgs mass.

Table 4: Recent Experimental Values for the W Mass

Experiment	Mode	Mass (GeV/c^2)
UA1-86[49]	$e\upsilon$	83.5 ± 2.9
UA2-87[50]	$e\upsilon$	80.2 ± 1.5
UA1-89[51]	$\mu\upsilon$	81.8 ± 6.5
UA1-89[51]	$\tau\upsilon$	89 ± 7
CDF-90[52]	$e\upsilon,\mu\upsilon$	79.91 ± 0.39
UA2-92[53]	$e\upsilon$	80.36 ± 0.37
DØ-94[54]	$e\upsilon$	79.86 ± 0.40
CDF-95[55]	$e\upsilon,\mu\upsilon$	80.41 ± 0.18

The W boson mass is measured in $p\bar{p}$ collisions by fitting the transverse mass of leptonic decays of the the W. As mentioned in Section 1, the transverse mass is useful because it displays a prominent peak near M_W and is also relatively insensitive to boosts in the longitudinal and transverse directions. The measurement consists of two crucial components: modelling the transverse mass, which includes describing the detector resolutions, and establishing the experimental momentum scale. To suppress backgrounds, CDF and DØ require $p_T^\ell, \not\!\!E_T > 25\ GeV$, and no jets > 30 GeV. UA2 and DØ require $P_T^W < 20\ GeV/c$ because the $\not\!\!E_T$ resolution degrades at large P_T^W. CDF imposes a similar cut of $|\mathbf{u}| < 20\ GeV$, where the hadron recoil $\mathbf{u}$ is defined as $\mathbf{u} \equiv \sum_i \vec{E}_T^{\,i}$, and the sum is over all towers in the calorimeter except those near the lepton.

The techniques for measuring the mass fall along two lines: an absolute measurement in which the momentum scale of the experiment is known by independent means, and a relative measurement in which the calorimeter momentum scale is divided out by measuring M_W/M_Z. UA2 and DØ, which do not have magnetic fields, have performed the latter form of measurement using $W \to e\upsilon$ decays and multiplied their measurements by the LEP Z^0 mass. CDF, which has a magnetic field, measures M_W absolutely using $W \to e\upsilon$ and $W \to \mu\upsilon$ decays by calibrating their tracking chamber magnetic field, and then transfering this calibration to the calorimeters. The recent measurements of M_W are compiled in Table 4.

3.3.1 Tracking Scale Determination

At CDF, the momentum scale is determined by normalizing the observed invariant mass peak of $J/\psi \to \mu^+\mu^-$ decays to the world average[56] J/ψ mass. The J/ψ is produced copiously in $p\bar{p}$ collisions through both prompt production and through b quark production and decay (see Figure 6). The invariant mass of 60,000 $J/\psi \to \mu^+\mu^-$ candidates is shown in Figure 15. The raw

measured value is $M(\mu\mu) = 3097.3 \pm 0.1$ (*stat.*) $\pm$ 1.5 (*sys.*) MeV/c^2, to be compared with the world average $3096.93 \pm 0.09\ MeV/c^2$. This measurement indicates that the CDF momentum scale must be multiplied by 0.99986 ± 0.00048. The total correction and uncertainty on the W mass from the CTC momentum scale determination is $-11 \pm 40\ MeV/c^2$.

As a check of the momentum scale, CDF measures the invariant masses of several other dimuon mass resonances, as shown in Figure 16 and Table 5. The agreement is good for all the resonances, and the small disagreement with the Υ(3S) may result from the larger background fraction there. The measured Z^0 mass is in good agreement with the LEP value and provides a check in a p_T régime similar to that for W leptons. A simultaneous fit to the Z^0 width determines the tracking resolution: $\delta p_T/p_T^2 = 0.00081 \pm 0.00009\ (GeV/c)^{-1}$. Determining the scale absolutely thus has the advantage of leaving these resonances as checks of the method.

Table 5: CDF Cross Checks of Dimuon Resonances

Resonance	Corrected CDF Measured Mass (MeV/c^2)	World-Average Mass (MeV/c^2) [49]
$\Upsilon(1S) \rightarrow \mu^+\mu^-$	$9460 \pm 2 \pm 5$	9460.3 ± 0.2
$\Upsilon(2S) \rightarrow \mu^+\mu^-$	$10029 \pm 5 \pm 5$	10023.3 ± 0.3
$\Upsilon(3S) \rightarrow \mu^+\mu^-$	$10334 \pm 8 \pm 6$	10355.3 ± 0.5
$Z^0 \rightarrow \mu^+\mu^-$	$91020 \pm 210 \pm 50$	91188 ± 4

3.3.2 Calorimeter Scale Determination

The overall scale for electrons in UA2 and DØ is set using $Z^0 \rightarrow e^+e^-$ decays. They select a sample of di-electrons with $70 < M(ee) < 120\ GeV/c^2$. In this way, when W electrons are used to measure the W mass, systematic uncertainties due to the relative energy calibration will nearly cancel. The statistical uncertainties in their M_Z values, as well as uncertainties from calorimeter non-linearities in extrapolating the scale from M_Z to M_W feed into the their scale errors (see Table 6). The Z^0 mass peaks of DØ and UA2 are shown in Figure 17. DØ measures $M_Z = 87.11 \pm 0.18\ GeV/c^2$, where the uncertainty is statistical only and the overall scale is not yet fixed. UA2 measures $M_Z = 91.74 \pm 0.28\ GeV/c^2$. DØ hopes to decrease the statistical uncertainty on the scale by using the mass peaks of $J/\psi \rightarrow ee$ decays (see Figure 18) and $\pi^0 \rightarrow \gamma\gamma$ decays, along with the Z^0, to set the scale.[57]

The CDF calorimeter scale is set by fitting E/p to determine the scale, where E is the electron calorimeter energy and p is the momentum of its track measured in the magnetic field.

Figure 19 shows the E/p distribution of $W \rightarrow e\upsilon$ electrons from CDF. Since the momentum p is calibrated with J/ψ's, fitting E/p transfers the CTC scale to the calorimeter. In the fit, the E/p distribution must be modelled for the resolutions on E and p and the effect of Bremsstrahlung radiation by electrons in the tracking material which causes a high-side tail in E/p: the track momentum is that of the electron after it radiates, but the calorimeter energy is that of the electron plus the collinearly radiated γs. An important advantage of this calibration is that it is performed with electrons of the same $\langle E_T \rangle$ electrons as those used in the W mass determination.

Several checks are available in the CDF scale determination. The width of the E/p peak, given the electron resolution (measured from $Z^0 \rightarrow ee$ decays below), independently measures the tracking resolution, $\delta p_T/p_T^2 = 0.00081 \pm 0.00011$ $(GeV/c)^{-1}$, in good agreement with the value extracted from the width of the $Z^0 \rightarrow \mu\mu$ peak. The number of events in the far $1.8 < E/p < 2.0$ tail is used to measure the amount of material in the detector, which is found to be (8.9 ± 0.9) % X_0, in agreement with an independent study of photon conversions in the detector: (8.1 ± 0.4) % X_0. Another check is to use the scale determination to measure the Z^0 mass (see Figure 20). The calorimeter non-linearity, which is does not affect CDF's W mass measurement, must be estimated in order to measure M_Z since the W's were used to set the scale. CDF finds $M_Z = 90880 \pm 185$ $(stat.) \pm 200$ $(sys.)$ MeV/c^2. A simultaneous fit to the Z^0 width determines the electron resolution. The ability to use the Z^0 mass as a check and the large statistical and systematic uncertainties in M_Z underscore the advantage of calibrating the scale with W electrons.

3.3.3 Transverse Mass Modeling

All experiments compare the transverse mass distributions of their W candidates to Monte Carlo templates generated with different input values for the W mass. W's are generated according to a Breit-Wigner, convoluted with the parton distribution functions. Because the P_T^W and $\not{u}$ cuts suppress higher order diagrams, it is sufficient to use only $q\bar{q} \rightarrow W$ diagrams and boost the W either by a theoretical calculation of P_T^W (DØ) or the measured P_T^Z distribution (UA2 and CDF). UA2 and CDF assume that the P_T^Z and P_T^W distributions are similar (see Section 4.3).

The Monte Carlo models of the lepton resolutions vary slightly, but all in some way use $Z^0 \rightarrow \ell\ell$ data to characterize the neutrino resolution. The neutrino resolution depends upon the calorimeter response to the hadrons which recoil against the W. Z^0 events are similar to W events in that hadrons are seen to recoil against the Z^0, but differ in that P_T^Z is much better measured than the recoil and in that there are no neutrinos expected. The $Z^0 \rightarrow \ell\ell$ events are used to map

out **u** *vs.* P_T^Z, and this reponse function is then inserted into the W Monte Carlo. The performance of the DØ model, for example, in comparison to the data is shown in Figure 21.

3.3.4 Transverse Mass Fitting and Results

The experiments generate lineshapes at different values of the W mass and fit these to the data (see Figures 22-24). The transverse mass is used in the fits because it is most insensitive to P_T^W, although the lepton p_T distributions can also be fit for the W mass as checks. These and numerous other tests were performed, such as varying fitting windows, letting $\Gamma(W)$ also float in the fit, varying the **u** or P_T^W cuts, *etc.* The results are:

$$M_W^{CDF}(e) = 80490 \pm 145\ (stat.) \pm 130\ (sys.) \pm 120\ (scale)\ MeV/c^2$$
$$M_W^{CDF}(\mu) = 80310 \pm 205\ (stat.) \pm 120\ (sys.) \pm 45\ (scale)\ MeV/c^2$$
$$(M_W^{CDF}(e{+}\mu \text{ combined}) = 80410 \pm 180\ MeV/c^2\ )$$
$$M_W^{UA2}(e) = 80360 \pm 220(stat.) \pm 160\ (sys.) \pm 260\ (scale)\ MeV/c^2$$
$$M_W^{D\emptyset}(e) = 79860 \pm 160\ (stat.) \pm 200\ (sys.) \pm 310\ (scale)\ MeV/c^2$$

where the statistical uncertainties are those from the finite numbers of W candidates, and the systematic uncertainties are summarized in Tables 6 - 7. The UA2 uncertainties are arranged a little differently here than in their paper; I have put the uncertainty due to the finite number of Z^0's into the 'scale' error, rather than into the statistical uncertainty. Quoting it thusly allows for more ready comparison of the sources of error between the different experiments.

Combining these measurements with previous measurements of Table 4, we obtain:

$$M_W^{World} = 80270 \pm 150\ MeV/c^2,$$

where $\pm$ 85 MeV/c^2 from structure functions is treated as common to all experiments. We may place these measurements in an experimental and theoretical context by examining Figures 25 and 26. Figure 25 shows the W mass measurements and the world-average result against the SLD and LEP predictions based on electroweak measurements at the Z^0 pole. Figure 26 shows the world-average W mass with the CDF measurement of the top quark mass (see Section 5.3).

Table 6: Summary of UA2 and DØ uncertainties in the W mass measurement

Uncertainty	ΔM_W^{UA2} (MeV/c^2)	ΔM_W^{D0} (MeV/c^2)
I. Statistical	220	160
II. Energy Scale	260	310
1. Statistics of Z^0 sample	250	165
2. Extrapolating scale M_Z to M_W	80	260
III. Other Systematics	160	200
1. e or μ resolution	75	70
2. P_T^W modeling	60	50
3. Recoil modeling	80	155
4. e or μ ID and removal	30	50
5. Trigger	-	20
6. Backgrounds	-	30
7. Radiative Decays $W \rightarrow \ell\nu\gamma$	30	-
8. W width	-	20
9. Fitting Procedure	30	30
10. Proton Structure	85	70
Total Uncertainty	370	400

Table 7: Summary of CDF uncertainties in the W mass measurement

Uncertainty	ΔM_W^e (MeV/c^2)	ΔM_W^μ (MeV/c^2)	Common (MeV/c^2)
I. Statistical	145	205	
II. Energy Scale	120	45	45
1. Scale from J/ψ	40	40	40
2. False Curvatures	15	15	15
3. Calorimeter	110	-	-
a. Stat. uncert. on E/p	65		
b. Syst. uncert. on E/p	90		
III. Other Systematics	130	120	90
1. e or μ resolution	80	60	0
2. P_T^W modeling	45	45	25
3. Recoil modeling	60	60	60
4. e or μ ID and removal	25	25	5
5. Trigger	0	25	0
6. Backgrounds	10	25	0
7. Radiative Decays $W \rightarrow \ell\nu\gamma$	20	20	20
8. W width	20	20	20
9. Fitting Procedure	10	10	0
10. Proton Structure	50	50	50
11. W production corrections	18	18	18
Total Uncertainty	230	240	100

3.4 Tests of the Universality of the Coupling g

The universality of the coupling g has been tested using the leptonic decays of the W by the UA1[27], UA2[58], and CDF[30,59] collaborations. Through measuring the cross section of W production times branching ratios into $e\upsilon$, $\mu\upsilon$, and $\tau\upsilon$,

$$\frac{\sigma B(W\to\mu\upsilon)}{\sigma B(W\to e\upsilon)} = \left(\frac{g_\mu}{g_e}\right)^2 \quad \text{and} \quad \frac{\sigma B(W\to\tau\upsilon)}{\sigma B(W\to e\upsilon)} = \left(\frac{g_\tau}{g_e}\right)^2,$$

they obtain the ratios of the couplings squared to electrons, muons, and taus from direct W decays. The hadronic decays of the tau are identified by jets with the characteristic 1 and 3 charged track topologies. Again, because a ratio of cross sections is measured, many systematic uncertainties in the individual W cross section measurements cancel in the ratio. Similar studies of g_A and g_V have been performed in $Z^0\to\ell^+\ell^-$ decays at LEP.[6] The results obtained are:

$$\left(\frac{g_\tau}{g_e}\right) = 1.00 \pm 0.04 \qquad \left(\frac{g_\mu}{g_e}\right) = 0.990 \pm 0.030$$

Universality in charged current interactions has also been tested using leptonic decay of taus and muons. The ratio of the tau and muon couplings is extracted from the relation $\Gamma(\tau\to e\upsilon\upsilon)/\Gamma(\tau\to\mu\upsilon\upsilon) = \left(\frac{g_\tau}{g_\mu}\right)^2\left(\frac{m_\tau}{m_\mu}\right)^5 = \frac{\tau_\mu}{\tau_\tau}B_e$, where the the tau and muon lifetimes and masses, as well as the $\tau\to e\upsilon\upsilon$ branching ratio B_e, can be measured independently, yielding g_τ/g_μ. This technique has been revolutionized by the precise BES measurement of the tau mass, as well as the stabilization of the B_e measurement, giving[60] $g_\tau/g_\mu = 0.994 \pm 0.004$. A very precise value of $g_\mu/g_e = 1.0030 \pm 0.0023$ has also been extracted[61] from the ratio of $\pi\to e\upsilon/\pi\to\mu\upsilon$ decays.

3.5 Search for Rare Radiative Decay $W^\pm\to\pi^\pm\gamma$

With the copious numbers of leptonic decays of the W that have been collected, one can begin to look for rare decays of the W. The decay $W\to\pi^\pm\gamma$ is attractive because of its unambiguous final state of a single isolated, high-p_T photon and a single isolated, high-p_T charged pion. The decay is suppressed because of the behaviour of the meson form factor for $\sqrt{s} = M_W$, and in fact one expects $\Gamma(W\to\pi^\pm\gamma)/\Gamma(W) \sim 3\times10^{-9}$. However, new physics associated with strong interaction dynamics or the $W\gamma$ vertex (see Section 3.7) could enhance this rate.[62] A similar search for the decay $Z^0\to\pi^0\gamma$ by the DELPHI collaboration[63] establishes the limit $\Gamma(Z^0\to\pi^0\gamma)/\Gamma(Z^0) < 1.5\times10^{-4}$. A search by the CDF collaboration[64] in 17 pb^{-1} for $\pi^\pm\gamma$ events with $72.1 < M(\pi\gamma) < 88.3$ GeV/c^2 establishes the limit $\Gamma(W\to\pi^\pm\gamma)/\Gamma(W) < 2.1\times10^{-4}$ (95% C.L.).

3.6 Test of *V-A* in the Weak Interaction

As a consequence of the pure *V-A* coupling of the *W*, *W* bosons produced via Drell-Yan annihilation in $p\bar{p}$ collisions produce a large charge and angular asymmetry in the distribution of the daughter leptons. This can be seen schematically in Figure 27. A W^+ produced in $u\bar{d}$ annihilation, where the u comes from the proton, is longitudinally polarized along the antiproton direction, while a W^- is produced polarized along the proton direction. The positron, having a definite helicity, preferentially travels along the spin of the W^+ (antiproton direction), while an electron travels along the spin of the W^- (proton direction). The decay amplitude is[65] $\frac{d\Gamma}{d\Omega}(W\rightarrow\ell\upsilon) \propto (1+\cos\theta)^2$, where is the angle of the lepton with respect to the W spin direction.

A measurement of the charge asymmetry has been performed by UA1.[66] At the energy of the CERN $Sp\bar{p}S$ collider, valence-valence quark interactions dominate in *W* production, and sea-sea quark annihilations can be neglected.[67] Requiring $P_T^W < 15\ GeV/c$ suppresses processes such as $qg\rightarrow Wq$. The lepton direction in the *W* frame is deduced by constraining the $e\upsilon$ system to the *W* mass and calculating the longitudinal component of the υ momentum. This procedure gives two solutions for p_L^{υ}, and, at CERN energies, choosing the smaller solution usually yields the true one. Figure 28 shows the UA1 data, showing beautiful agreement with the *V-A* theory.

There has also been exhaustive study recently of decay asymmetries in $\mu\rightarrow\ell\upsilon\upsilon$[68] and $\tau\rightarrow\ell\upsilon\upsilon$[61] decays, which also arise as a result of the *V-A* coupling. The "Michel parameters" characterize the decay widths $\frac{d\Gamma}{d\Omega dx}$ (μ or $\tau\rightarrow\ell\upsilon\upsilon$) with respect to $x = p_{\ell}/E_{\mu}$ or p_{ℓ}/E_{τ}. I will not describe these parameters or their measurements in detail, but will only note the extreme precisions achieved. Data samples of several million tau's have been required in these indirect measurements, since some terms in the decay asymmetries are suppressed by $(m_{\ell}/m_{\mu})^2$ or $(m_{\ell}/m_{\tau})^2$ (this should be compared to the 75 events in the UA1 paper that demonstrated *V-A* !).

Table 8: Tests of *V-A* from Muon and Tau Decay Parameters.

Parameter	Muon Average[68]	Tau Average[61]	*V-A* Pred.
ρ	0.7518 ± 0.0026	0.757 ± 0.024	0.75
η	-0.007 ± 0.013	0.03 ± 0.022	0.00
ξ	1.003 ± 0.013	1.03 ± 0.12	1.00
δ	0.7486 ± 0.0038	0.75 ± 0.17	0.75

3.7 Measurement of the γW^+W^- Coupling

An important aspect of the Standard Model is the coupling of the W to the photon, for this is specified by the gauge invariance of the theory. The most general parameterization[69] of the W-γ couplings is characterized by two CP-conserving factors κ and λ which describe the magnetic dipole μ_W and electric quadrupole Q_W moments of the W and two CP-violating factors $\tilde{\kappa}$ and $\tilde{\lambda}$ which are related to the electric dipole d_W and magnetic quadrupole $\tilde{Q}_W$ moments:

$$\mu_W = \frac{e}{2M_W}(1+\kappa+\lambda) \qquad d_W = \frac{e}{2M_W}(\tilde{\kappa}+\tilde{\lambda})$$
$$Q_W = -\frac{e}{M_W^2}(\kappa-\lambda) \qquad \tilde{Q}_W = -\frac{e}{M_W^2}(\tilde{\kappa}-\tilde{\lambda})$$

It is well-known that tree-level unitarity, *e.g.* for the process $e^+e^- \rightarrow W^+W^-$, restricts the parameters to their Standard Model values $\kappa = 1$ and $\lambda = \tilde{\kappa} = \tilde{\lambda} = 0$ at asymptotically high energies.[70] Thus, any extensions of the Standard Model in which these parameters take on other values has to be described by form-factors with some implied symmetry-breaking scale $\Lambda_W >> M_W$. These form factors must reduce to the Standard Model values at high W-photon center of mass energies, or else the unitarity limit is exceeded.

In $p\bar{p}$ collisions, information about the strengths of these couplings can be extracted from events in which an energetic photon is produced in association with a W boson. The processes which give rise to such photons are radiation off of (a) an initial-state quark, (b) the W itself, and (c) the daughter lepton in the $W \rightarrow \ell\upsilon$ decay. Process (b) is of interest here, and (a) and (c) are backgrounds. At the Tevatron, W-γ masses of nearly 200 GeV/c^2 are probed. Both DØ[71] and CDF[72] have searched for $W\gamma$ production. The photon spectra are shown in Figure 29. Anomalous couplings are signified by photons of larger p_T^γ than expected by the Standard Model. CDF and DØ obtain similar limits on the couplings (Figure 30) by fitting the p_T^γ spectra.

A very interesting and complementary limit on the anomolous couplings is also obained by the $b \rightarrow s\gamma$ measurement of the CLEO collaboration.[73] In this radiative decay, the final-state photon is emitted either from a W boson or from the top quark appearing in the loop diagram, and anomalous couplings would alter the observed branching ratio.[74] Figure 30 shows the anomalous coupling limits derived from this measurement. The enhanced sensitivity of CLEO to κ relative to λ appears to be a feature of the coefficients of the various diagrams, which depend upon m_{top}. Because of the particularly large top mass, the sensitivity to κ is greatest.

4. Tests of QCD using W Bosons

4.1 W Production at $p\bar{p}$ Colliders

The W and Z^0 are predominantly produced in hadron-hadron collisions via the Drell-Yan[75] mechanism. The quark carries a momentum fraction x_1 of the proton momentum $p = \frac{1}{2}\sqrt{s}$, and the antiquark carries momentum fraction x_2, so the required center-of-mass energy squared of the parton-parton system is $\hat{s} = x_1 x_2 s \sim M_W^2$. W and Z^0 production is a convolution of Breit-Wigner resonances with the parton momentum distribution functions of the proton:[76]

$$\sigma(p\bar{p} \rightarrow W + X) = \sum_{ij} \int_0^1 dx_1 \int_0^1 dx_2 \, [q_i(x_1)\bar{q}_j(x_2) + q_j(x_1)\bar{q}_i(x_2)] \, \hat{\sigma}(x_1, x_2)$$

where $q_i(x)$ ($\bar{q}_i(x)$) is the fractional momentum distribution of the quark (antiquark) of type $i = u$, d, s, c in the proton and $\hat{\sigma}(x_1, x_2)$ is the parton-parton subprocess cross section to produce a W. Since the proton is predominantly made up of u and d quarks, W production is largely due to $u\bar{d}$ at $\sqrt{s} = 1800$ GeV.[77] W's and Z^0's are also produced at $O(\alpha_s)$ and above via processes such as $qg \rightarrow Wq$ or $q\bar{q} \rightarrow W + (n\,g)$, the diagrams for which have recently been calculated to $O(\alpha_s^3)$.[78]

The dominant uncertainty in the theoretical prediction for the W cross section is the parameterization of the parton momentum distributions. The current parameterizations from the CTEQ collaboration[79] and those of Martin-Roberts-Stirling[80] obtain quite different results for the sea quark and gluon distributions at small x ($O(0.01) < x < O(0.2)$), where DIS data are at present not available. Since W production at the Tevatron occurs at $x \sim M_W/\sqrt{s} \approx 0.04$, a precise measurement of the W production cross section could help to constrain the proton structure, particularly the gluons, in this region of x.

An experimentally challenging aspect of the W cross section measurement in $p\bar{p}$ collisions (see Section 3.1) is the determination of the integrated luminosity. The luminosity is monitored with scintillator planes in the far-forward direction ($3.2 < |\eta| < 5.9$) that detect the remnants that comprise the unstruck partons of proton-antiproton collisions. The observed monitor rate is converted to a luminosity by normalizing to the fraction of the proton-antiproton total cross section, $\sigma_{p\bar{p}}^{tot}$ accepted by the luminosity detector. Both the total cross section $\sigma_{p\bar{p}}^{tot}$ and the fraction seen by the luminosity monitors are difficult to calculate and must be measured.

Figure 31 shows the recent predictions for the W and Z^0 production cross sections as a function of $\sqrt{s}$. A recent improvement in the experimental luminosity determination has recently been accomplished by the CDF collaboration. They have measured[81] the elastic and total $p\bar{p}$ cross sections at $\sqrt{s} = 630$ and 1800 GeV, in which the CDF luminosity counters (BBC's) were used in the measurement, along with forward Silicon detectors installed around the beam pipe. The important aspect of their analysis is that the same detectors used in the $\sigma_{p\bar{p}}^{tot}$ measurement are used in monitoring the luminosity, reducing systematics in the luminosity monitor acceptance. CDF has measured $\sigma_{p\bar{p}}^{tot} = 80.6 \pm 2.3\ mb$. Using the W sample described in Section 3.1, they find $\sigma_W = 23.2 \pm 1.2\ nb$, where $\sigma B(W \to \ell\nu)$ has been divided by $B(W \to e\nu) = 0.1084$.[24] The 4.6% measurement uncertainty is now close to the 3.8% spread in predictions of different parton distribution functions (see Figure 31), although the luminosity uncertainty (3.6%) continues to dominate the uncertainty of this measurement.

4.2 Charge Asymmetry of W Production

The charge asymmetry of leptons from W decays in $p\bar{p}$ collisions may be used to gain information on the difference between the parton distributions $d(x)$ and $u(x)$ in the region $x \sim 0.04$ - 0.20, $Q \sim M_W$.[82] It is known that u quarks in the proton have a stiffer momentum spectrum than d quarks.[83] Thus the W^+ tends to move in the antiproton direction and the W^- tends to move in the proton direction. The charge asymmetry of the W is:

$$A(y) = \frac{d\sigma(W^+)/dy - d\sigma(W^-)/dy}{d\sigma(W^+)/dy + d\sigma(W^-)/dy},$$

where y is the rapidity of the W. Because the dominant contribution to W^+ (W^-) production is $u\bar{d}$ ($\bar{u}d$) annihilation, the asymmetry may be written as

$$A(y) \approx \frac{u(x_1)d(x_2) - d(x_1)u(x_2)}{u(x_1)d(x_2) + d(x_1)u(x_2)}$$

where $x_1, x_2 = \frac{M_W}{\sqrt{s}} \exp(\pm y)$. Introducing the ratio $R(x) = d(x)/u(x)$, the asymmetry for small y is found to be $A(y) \approx x_0 y\, R'(x_0)/R(x_0)$, where $x_0 = \frac{M_W}{\sqrt{s}}$. Hence, $A(y)$ is sensitive to $d(x)/u(x)$.

Because of its magnetic analysis of charged particles, CDF is able to measure the charge asymmetry of leptons from W decays.[84] Both $W \to e\nu$ and $W \to \mu\nu$ decays are selected. In addition to the central leptons used in Section 3, electrons in the plug end-cap ($1.1 < |\eta| < 2.4$) calorimeters are used in this analysis. The momentum measurement in the CTC is less accurate

in this region, but charge-determination is still precise. To suppress backgrounds, the lepton and neutrino are required to have $p_T > 25\ GeV$, and events with hadron jets $> 20\ GeV$ are rejected.

The asymmetry measured by CDF is actually not the W charge asymmetry, but the lepton charge asymmetry, $A(y_\ell)$. At FNAL energies, the low x in W production makes it difficult to choose the correct p_L^ν solution, as was done by UA1. For the lepton rapidity acceptance described above, the range of W rapidities is approximately $-1.8 < y_W < 1.8$. The observed lepton asymmetry from CDF data is shown in Figure 32, where CP invariance has been invoked to fold the data across $y_\ell = 0$: $A(-y_\ell) = -A(y_\ell)$. Because the quantity measured is a ratio, the effects of lepton efficiencies, detector acceptances, *etc.*, cancel so long as they are charge-independent. Small corrections must be made for the background content in the data, as indicated in the figure. Also shown are NLO predictions[85] for the asymmetry calculated with different parton sets.

From Figure 32, all the CTEQ2 parton distributions are inconsistent with the CDF data. This is interesting, since CTEQ2 is consistent with all deep-inelastic scattering data, and in fact gives a reasonable description of the NMC $F_2^{\mu n}/F_2^{\mu p}$ data, a quantity which is also sensitive to d/u in the same x region as the CDF data (although at much smaller Q^2). The reason for this is that $F_2^{\mu n}/F_2^{\mu p}$ is also sensitive to differences in the $\bar{u}$ and $\bar{d}$ distributions, but $A(y_\ell)$ is not. The CTEQ fits compensate their large d/u slope with different $\bar{u}$ and $\bar{d}$ parameterizations to fit the NMC data, but their resulting u and d distributions do not fit the CDF $A(y_\ell)$ data well.

4.3 Transverse Motion of *W* Bosons

W's can be produced at $O(\alpha_s)$ and above in processes such as $qg \to Wq$ or $q\bar{q} \to W + (n\ g)$, where the W appears to recoil against high-p_T jets of hadrons. In these cases, the W moves with momentum transverse to the $p\bar{p}$ beamline, in contrast to the lowest order quark-antiquark annihilation, where the W is at rest in the transverse plane. A measurement of the transverse momentum spectrum at high P_T^W could be used to indicate new physics producing high-p_T W's.

A measurement of the differential cross section $d\sigma/d(P_T^W)^2$ also tests the non-perturbative régime of QCD. At large and moderate values of P_T^W, the cross section for W and Z^0 production in $p\ \bar{p}$ collisions may be computed pertubatively and have the form $d\sigma/d(p_T)^2 \sim \alpha_w \alpha_s\ (u_1 + u_2\alpha_s + u_3\alpha_s^2\ ...)$, but at low p_T the terms diverge like $\alpha_s^n \ln^n(p_T^2/M_W^2)$, even though α_s may be small. The technique of soft-gluon summation[86] may be used in the low-P_T^W régime, and the result matched to the perturbative result at $\alpha_s^n \ln^n(p_T^2/M_W^2) \sim 1$, or

$P_T^W \sim 20\ GeV/c$, to calculate $d\sigma/d(P_T^W)^2$ over all ranges of P_T^W.[87] The differential cross section $d\sigma/d(p_T)^2$ is expected to be similar for W's and Z^0's.[88]

These measurements have been carried out by the UA1,[51], UA2,[89] and CDF[44] collaborations. The CDF differential cross sections are shown in Figure 33. The results are in agreement with predictions of QCD and the W and Z^0 transverse momentum distributions are seen to be similar in shape.

4.4 Hadron Jets Produced with W Bosons in $p\bar{p}$ Collisions

As mentioned above, the W is produced at $O(\alpha_s)$ and above in $p\bar{p}$ collsions in association with high-p_T jets of hadrons. Aside from being of topical interest because they are a major background to top quarks at Fermilab (see below), these jets produced with the W are of interest in their own right in that α_s can be measured from the relative probabilities of radiating zero and one extra jets (each jet coming at the price of a power of α_s), as done by UA2[90] and DØ[91].

The measured cross sections evidently depend upon the experimental definitions of a jet, such as the angular acceptance of the detector, jet cone size, and the minimum E_T of jets considered in the analysis. The DØ analysis has benefitted from a next-to-leading order Monte Carlo[85] of $W + 0,1$ jet production with which they can simulate experimental effects. The cross sections are parameterized as $\sigma(W + 0\ \text{jet}) = A_1 + \alpha_s A_2$, $\sigma(W + 1\ \text{jet}) = \alpha_s B_1 + \alpha_s^2 B_2$, where the coefficients A and B depend upon experimental conditions and the Q^2 scale and are calculated by the Monte Carlo for the choice $Q^2 = M_W^2$. They obtain:

$$\text{DØ:}\ \ \alpha_s(M_W^2) = 0.126 \pm 0.005\ (stat.) \pm 0.016\ (sys.)$$
$$\text{UA2:}\ \ \alpha_s(M_W^2) = 0.123 \pm 0.018\ (stat.) \pm 0.017\ (sys.)$$

For reference, the LEP value of α_s,[6] scaled to $Q^2 = M_W^2$, is $\alpha_s = 0.124 \pm 0.005$.

It has been noted,[92] however, the Q^2 scale at which $\alpha_s(Q^2)$ is to be evaluated in $W +$ jet events is not clear, and a change in scale from $Q^2 = M_W^2$ to $Q^2 = \frac{1}{4}M_W^2$ shifts α_s by 0.01. A measurement of the $W +$ jets distribution by the CDF collaboration for all jet multiplicities (see Figure 34), shows good agreement with a tree-level Monte Carlo calculation,[93] but the theoretical calculation is quite sensitive to the choice of Q^2. In fact, probably both the Q^2 scale and α_s evolve *vs.* N_{jet}.

5. New Particle Searches Using the W

5.1 Search for $W' \to e\nu$ and a Right-Handed Current

The weak interaction is quite remarkable in that it is purely left-handed. Extended gauge models[94] have proposed that there is actually left-right symmetry in the weak interaction at a mass scale much larger than the electroweak scale $M_W \approx 80\ GeV/c^2$, and introduce heavy right-handed bosons, W'. It is therefore interesting to see if the W' may be observed directly, for example, via the process $p\bar{p} \to W' \to \ell\nu$. In its simplest form, the W' appears as a heavier version of the left-handed W and decays primarily via $W' \to WZ^0$. In extended gauge models the W' can decay with large probability to right-handed $\ell_R \bar{\nu}_R$ pairs, since it is expected[95] that the coupling at the $W'WZ^0$ vertex is suppressed by a left-right mixing angle $\xi \sim \left(\frac{M_W}{M_{W'}}\right)^2$.

Many indirect limits exist on the W'. For very light neutrino masses, the most stringent limits are astrophysical or cosmological (all 90% C.L. unless otherwise noted): for $m_{\nu_R} < 1\ MeV$ constraints from big bang nucleosynthesis[96] imply $M_{W'} > 1\ TeV$, and the energetics of Supernova 1987A can in some models imply[97] $M_{W'} > 16\ TeV$. Assuming manifest left-right symmetry, a limit of $M_{W'} > 1.3\ TeV$ has also been derived[98] using experimental data from muon decay,[99] the measured difference between the K_L and K_S masses,[100] the semileptonic branching ratio $b \to X\ell\nu$,[101] B_d-$\bar{B}_d$ mixing,[102] and neutrinoless atomic double beta decay.[103]

Direct searches for the process $p\bar{p} \to W' \to \ell\nu$ have been performed[104] by DØ[105] and CDF[106]. Searches for $W' \to \ell\nu$ assume that the decay $W' \to WZ^0$ is suppressed and that the ν_R is sufficiently light (but not necessarily massless), that the decay $W' \to \ell_R \bar{\nu}_R$ occurs, and that the ν_R is stable and non-interacting. The W' signature is a new peak in the transverse mass spectrum of lepton + $\not\!\!E_T$ data. Note that a 600 GeV/c^2 W' leaves a 300 GeV/c lepton in the detector! Figure 35 shows the transverse masses of the CDF and DØ $e\nu$ events. To set a mass limit for the W', the experimental limit on $\sigma B(p\bar{p} \to W' \to \ell\nu)$ is compared to a theoretical model of the W' cross section. Figure 36 shows the 95% C.L. limits from CDF and DØ. Also shown is the expected σB, calculated with a lowest-order Monte Carlo program with a K-factor enhancement. CDF establishes the limit $M_{W'} > 652\ GeV/c^2$ (95% C.L.) and DØ obtains $M_{W'} > 600\ GeV/c^2$ (95% C.L.) with the assumptions stated above. Mass limits for different models may be obtained by overlaying their expected cross section predictions on these cross section limit curves.

5.2 Search for W + Jet(s) Mass Resonances.

As discussed in Section 4, W production at hadron colliders is well-described by perturbative QCD, and at higher orders the W is expected to be produced in association high-p_T jets of hadrons. Nevertheless, one can investigate whether a heavier object is producing W + jet(s) final states by reconstructing the the W-jet invariant mass distribution.

Models of composite quarks[107] exist in which excited states of these quarks can decay via $q^* \to qg$, $q^* \to q\gamma$, $q^* \to qW$, or $q^* \to qZ^0$ with branching ratios 83.4%, 2.2% (0.6%), 10.9%, and 3.5% (5.1%) for the u^* (d^*). CDF[108] has searched for excited quarks in the W + 1 jet (with $W \to \ell\upsilon$, $\ell = e,\mu$) and the γ+ jet modes.[109] The principal background to the W + jet channel is the W + 1 jet production described in Section 4, while in the γ+ jet channel it is Compton-like process $qg \to q\gamma$ and hadron dijet processes, where one jet fagments to a leading π^0. The resulting W/γ+ jet mass distributions are shown in Figure 37. From the theoretical cross section[107] CDF excludes excited quarks with masses $M^* < 540\ GeV/c^2$ (95% C.L.).

Models also exist for W + 2 jet mass resonances. These would be sensitive to QCD WW and WZ^0 production,[110] $p\bar{p} \to W' \to WZ^0$ or to $p\bar{p} \to W \to WH^0$, with $H^0 \to b\bar{b}$.[111] These searches are underway, and Fermilab could have sensitivity to $m_{Higgs} \sim 100\ GeV/c^2$ with $1\ fb^{-1}$ of data. The $W' \to WZ^0$ search is quite complementary to the $e\upsilon$ search (see Section 5.1) and tests different models of W' couplings. The W + 2 jet channel also provides another way to look for W' in the decay $W' \to t\bar{b} \to Wb\bar{b}$,[112] where the reconstructed $\ell\upsilon$+1 jet mass (= m_{top}) and the $\ell\upsilon$+2 jet mass (= $M_{W'}$) provides a W' signal which circumvents assumptions about the υ_R. With b tagging of the jets, as is possible at CDF, this W' signal, if observed, would be quite striking.

5.3 Search for the Top Quark

The top quark is required in the Standard Model as the weak isodoublet partner to the b quark. Measurements of the forward-backward asymmetry of the b at the Z^0 pole show that the b quark's axial and vector couplings are those of a weak isospin $\frac{1}{2}$ particle, suggesting that it has a partner. The measured Z^0 width requires $m_{top} > \frac{1}{2} M_Z$. The measured value of the W width, or rather the leptonic branching ratio (see Section 3.1), implies $m_{top} > 65\ GeV/c^2$ (95% C.L.). Direct searches for the top at $p\bar{p}$ colliders establish $m_{top} > 91\ GeV/c^2$ (95% C.L.)[113], and, more recently, $m_{top} > 132\ GeV/c^2$ (95% C.L.)[114]. Unlike the limits from the W and Z^0 widths, the

limits from direct searches must assume $B(t \rightarrow Wb) = 100\%$, and that other decay channels, such as charged Higgs modes $t \rightarrow H^+ b$, are not available to the top.[115]

At the Tevatron, top quarks are expected to be produced in pairs, via $gg \rightarrow t\bar{t}$ or $q\bar{q} \rightarrow t\bar{t}$. Calculations of the cross section for $\sqrt{s} = 1800\ GeV$ show[116] that the expected cross section is between $\sigma_{t\bar{t}} \sim 150\ pb$ ($m_{top} = 90\ GeV/c^2$) and $\sim 3\ pb$ ($m_{top} = 200\ GeV/c^2$). The top is expected to decay predominantly to a W boson and a b quark. When both W's from the $t\bar{t}$ pair decay leptonically (the "dilepton" mode), two isolated high-p_T leptons, two hadronic jets (from the b quarks) and $\not\!\!E_T$ (from the two neutrinos) are observed. When only one W decays leptonically (the "lepton + jets" mode), a single isolated high-p_T lepton, missing energy, and four jets (two from the two b quarks, and two from the hadronic W decay) are observed.

Last year, evidence was presented by the CDF collaboration[117] for $t\bar{t}$ production in $20\ pb^{-1}$ of $p\bar{p}$ collisions at $\sqrt{s} = 1800\ GeV$. The Tevatron collider has continued to run since 1993, and this year, based on a data set of $67\ pb^{-1}$, CDF[118] has reported definitive evidence for the top which the DØ collaboration[119] has also confirmed from its data set of $50\ pb^{-1}$.

The primary CDF lepton + jets search begins with a sample of $\sim 52{,}000\ W \rightarrow \ell\nu$ events, and searches for jets consistent with b quarks in the event, either through the signature of secondary vertices in their SVX or through additional leptons from the semileptonic decay $b \rightarrow c\ell\nu$ or $b \rightarrow c \rightarrow s\ell\nu$. The SVX search is very powerful because of the precision of the SVX and the resulting clean signature of secondary verteces displaced from the primary $p\bar{p}$ interaction. The CDF SVX and soft lepton background estimates in the W + 1,2 jets agree well with the observed tags, plus a small $t\bar{t}$ contribution, but the signal region of ≥ 3 jets shows a clear excess of tags (Figure 38, Table 9). Seven of the events even have two separate jets tagged! The lifetime distribution (see Figure 38) of the SVX-tagged jets is in good agreement with that expected from b decay. As a check of their tagging, CDF studies their Z^0 + jet data, where no top is expected. They observe 15, 3, and 2 b tags in the Z^0 + 1, 2, and ≥ 3 jet data, in good agreement with their background expectations of 17.5, 4.2, and 1.5 tags.

The DØ Collaboration's search in the lepton + jets mode incorporates the fact that the jets in $t\bar{t}$ events tend to be more energetic than Monte Carlo models [93] of W + jets production. Because of their better calorimeter hermeticity, DØ considers only $W + \geq 4$ jet events. A cut was imposed on a kinematic variable, H_T, which is the $\sum E_T$ of all jets and the leading electron (if

any) in the event: $H_T > 200\ GeV$. If a soft ($p_T > 4\ GeV/c$) muon b-tag was found, only three jets were required and a relaxed cut $H_T > 140\ GeV$ imposed. Figure 49 shows H_T for $t\bar{t}$ (estimated by the ISAJET[120] Monte Carlo program) and the $W + \geq 4$ jets background (estimated by the VECBOS[93] Monte Carlo program). Correcting for trigger biases, and allowing for variations in the Q^2 scale of the Monte Carlo (Section 4.4), they show good agreement with the background Monte Carlo in the $W + 1$, 2 and 3 jet bins, where the top contribution is small. DØ observes 14 $W + \geq 4$ jet events passing all cuts, with an estimated background of 3.14 ± 0.53 events.

Both collaborations consider the $e\mu$, ee, and $\mu\mu$ dilepton modes, where in addition to the two leptons, two jets and $\not\!\!E_T > 25\ GeV$ are required (see Tables 9 and 10). CDF observes 5 $e\mu$ candidates and 1 $\mu\mu$ candidate,[121] and DØ observes 2 $e\mu$ candidates and 1 $\mu\mu$ candidate. Three of the CDF dilepton events, furthermore, are observed to contain a total of 5 jets that are tagged as b quarks. If the $t\bar{t}$ content of the CDF sample were zero, only 0.5 such tags would be expected (3.6 tags are expected with top), making these events quite spectacular.

The two searches, including overall sensitivity, are summarized in Tables 9 and 10. CDF benefits from its powerful SVX analysis, which has sensitivity 2.5 for $m_{top} = 180\ GeV/c^2$. The DØ searches achieve sensitivities of 0.9 to 1.6 at this mass. The probability of CDF's candidates to be consistent with background is 1×10^{-6}, or 4.8σ (in terms of deviations from a Gaussian distribution). The additional check of the b-tags in the CDF dileptons add confidence to the top signal. DØ calculates the background probability of their signal to be 2×10^{-6}, or a 4.6σ excess. The DØ cross section as a function of top mass is shown in Figure 40. The CDF measured cross section, $\sigma_{t\bar{t}} = 6.8^{+3.6}_{-2.4}\ pb$, is also shown at its measured top mass (see below).[122]

CDF measures the mass of the top by fully reconstructing the lepton + jets final state in which the lepton, neutrino, and four highest-E_T jets are assumed to be the $t\bar{t}$ daughters. There are multiple solutions, due to the quadratic ambiguity in the neutrino longitudinal momentum and the combinatorics of jet assignments to W daughters or b quarks. The mass resolution suffers in the absence of b tagging because of the jet combinatorics and because the non-$t\bar{t}$ background increases. Both the mass resolution and the background fraction improve by requiring a b tag in the event and the fit solution to be one in which the b tagged jet(s) are assigned to b quarks. The resulting mass distribution shows a strong peak at $m_{top} = 176 \pm 8\ (stat.) \pm 10\ (sys.)\ GeV/c^2$ (see Figure 41). The quoted uncertainties are conservative, pending study of the soft gluon jets[123] expected in top events which could confuse kinematic fits. The mass peak, combined with the number of CDF top candidates, establishes the top quark's existence at the 5.0σ level.

Table 9: Summary of CDF Top Search Modes[117,118]

	SVX b Tag Search	Soft Lepton Tag Search	Dilepton Search
Total Efficiency × Branching Ratio, m_{top} = 140, 160, 180 GeV/c^2	0.029 ± 0.008 0.033 ± 0.009 0.035 ± 0.009	0.014 ± 0.004 0.016 ± 0.004 0.017 ± 0.004	0.008 ± 0.001 0.008 ± 0.001 0.009 ± 0.001
Total # $t\bar{t}$ events expected in search [a] m_{top} = 140, 160, 180 GeV/c^2	33 ± 10 18 ± 5 10 ± 3	16 ± 5 9 ± 3 5 ± 1	4.4 ± 0.6 3.0 ± 0.5 2.4 ± 0.4
Total backgrounds in search	6.7 ± 2.10	15.4 ± 2.0	1.3 ± 0.3
Search Sensitivity [b] m_{top} = 140, 160, 180 GeV/c^2	5.2 3.6 2.5	2.9 1.8 1.1	1.8 1.5 1.3
Observed # Events in CDF Data	21	22	6

Table 10: Summary of DØ Top Search Modes[119]

	Lepton + Jets Search	Lepton + Jets + μ Tag Search	Dilepton Search
Total Efficiency × Branching Ratio, m_{top} = 140, 160, 180 GeV/c^2	0.008 ± 0.001 0.014 ± 0.002 0.020 ± 0.004	0.006 ± 0.001 0.008 ± 0.002 0.009 ± 0.002	0.003 ± 0.001 0.005 ± 0.001 0.006 ± 0.001
Total # $t\bar{t}$ events expected in search [a] m_{top} = 140, 160, 180 GeV/c^2	6.5 ± 1.1 5.1 ± 0.8 3.8 ± 0.8	4.5 ± 0.8 2.9 ± 0.5 1.8 ± 0.3	2.9 ± 0.4 2.0 ± 0.3 1.2 ± 0.2
Total backgrounds in search	1.93 ± 0.50	1.2 ± 0.2	0.65 ± 0.15
Search Sensitivity [b] m_{top} = 140, 160, 180 GeV/c^2	2.2 1.9 1.6	1.9 1.4 1.0	1.5 1.2 0.9
Observed # Events in DØ Data	8	6	3

[a] Assuming theoretical $t\bar{t}$ cross section of Reference [116]

[b] Defined as (Number of Expected Signal Events)/$\sqrt{\text{Signal+Background}}$

DØ also estimates the top mass from kinematic fits to their $W + 4$ jet data. They fit to the masses, m_{3j} and m_{2j}, of the 3 jets assigned in their fit to the hadronically-decaying top and to the smallest-mass jet pair within the hadronic top decay. Jets with μ tags, when present, were assigned to b quarks. The variables m_{2j} *vs.* m_{3j} are shown in Figure 42 (a) for top Monte Carlo, (b) $W + 4$ jet Monte Carlo, and (c) DØ data. They find $m_{top} = 199^{+31}_{-25}$ (*stat.*) GeV/c^2 (see Figure 43(a)). DØ repeats this analysis with no H_T requirement, since it could bias the fitted mass. In this second determination they have more events, but suffer from a larger background fraction in the sample: $m_{top} = 199^{+19}_{-21}$ (*stat.*) ± 22 (*sys.*) GeV/c^2, (see Figure 43(b)). DØ will greatly benefit from the anticipated installation of a Silicon tracker in 1998, since b jet tagging is very powerful in reducing backgrounds and combinatorics of incorrect jet assignments.

6. Conclusions

In this article, I have reviewed several tests of the electroweak theory using the W boson. The W is now beyond the discovery stage of the earlier UA1 and UA2 experiments, and first-rate measurements are coming available. With the many parameters of the theory that are specified by low-Q^2 deep-inelastic scattering data, atomic data, and the high-Q^2 neutral-current data at the Z^0, the Standard Model predicts many of the properties of the W. There is a wealth of information incorporated into the Standard Model fits. So, it is with some degree of awe that we can look upon the extraordinary agreements between the predictions and the direct measurements of the W and the top quark made at the Fermilab Tevatron.

The measurements presented here from the Fermilab Tevatron collider will see substantial improvements in the next era of experiments. Fermilab plans a major upgrade to its luminosity through its replacement of the Main Ring by the Main Injector in 1998. Instantaneous luminosities of 10^{-32}–$10^{-33}\ cm^{-2}sec^{-1}$ are foreseen, implying datasets of $\sim 1\ fb^{-1}$ for the collider detectors there (this amounts to 10^6 $W\rightarrow\ell\nu$ decays per experiment). As well, the LEP e^+e^- collider plans within the next couple of years to increase its centre-of-mass energy to $\sqrt{s} \sim 180\ GeV$, enabling study of the W through pair production $e^+e^-\rightarrow W^+W^-$. The vastly different physics environment at LEP-200 will in some cases provide very complementary measurements to those at the Tevatron.

The long-awaited observation of the top quark also opens up a number of new and exciting questions. First, the fact that the measured cross section is in agreement with the predicted cross section suggests that the top quark is characterized solely by the decay $t\rightarrow Wb$. It will be interesting to continue searches for other decays of the top (such as Reference [115]). It also remains of interest to reduce the top mass uncertainty in the pre-LHC era. With its exceptionally large mass, one is led to ask whether the top plays a special role in the Standard Model beyond the large radiative corrections. It possesses large Yukawa couplings to the Higgs, and in some models[124] the Higgs itself is thought to be a $\bar{t}t$ condensate.

Both LEP-200 and FNAL expect to be able to achieve W mass measurements with uncertainties $\sim 50\ MeV/c^2$. The major challenge for LEP-200 is to accumulate enough statistics (in 5 years, only 10,000 W pairs are expected), while for CDF and DØ the major challenge will be to control their momentum scales to such precision. The relative branching fractions of the W into various final states will probably be best measured by LEP-200, since the indirect extraction

from σ_W/σ_Z at the Tevatron will be systematics limited. Direct searches at the Tevatron for new W decay modes and for new W' bosons, however, will still be quite fruitful with a potential reach of a few TeV. LEP-200 will have difficulty determining the W width without devoting costly time to a scan above and below $2M_W$. The best measurement of the $\Gamma(W)$ will come from the Tevatron (Section 3.2). Studies of the gauge structure of the $W\gamma$ couplings, however, will be best studied at LEP-200, where departures of κ and λ spoil the gauge cancellation in $e^+e^- \to W^+W^-$, even at the modest energy of LEP-200.[125] In light of the measurements already performed I believe both Fermilab and LEP enjoy bright prospects for further precision study of the W, and I view it a mistake to simply await LEP-200 for definitive measurements of the W.

With the many studies to come, the pre-LHC era can take many turns. LEP-200 might discover any number of oddities between $\sqrt{s} = 90$ and $180\ GeV$. With the Tevatron measurements of M_W and m_{top}, we may know where to look for the Higgs before the LHC turns on. CDF and DØ, furthermore, will continue to study the top, with particular interest on any new decay modes that might be observed and its extraordinarily large mass. We may await with interest to see if any surprises should arise.

Acknowledgements

The work summarized in this paper is the result of the efforts of many individuals and several major collaborations. I thank my many CDF and DØ colleagues whose dedicated work has produced many of the fruitful results summarized here. In addition, I owe a debt of thanks to Geary Eppley, Robert Harris, Young-Kee Kim, Hugh Montgomery, Steven Playfer, David Saltzberg, and Darien Wood and for their cooperation in providing me with their results. I am especially grateful to Henry Frisch, Jonathan Rosner, James Stirling, and James Cronin for valuable discussions, and to Henry Frisch and for helpful comments on this manuscript.

References

§ Present address: Department of Physics, Syracuse University, Syracuse NY 13244.

[1] S. Weinberg, Phys. Rev. Lett. **19** 1264 (1967).

[2] A. Salam, *Elementary Particle Theory*, ed. N. Svartholm (Stockholm: Almqvist, 1968).

[3] S.L. Glashow, Nucl. Phys. **22** 579 (1961).

[4] G. Arnison *et al.*, Phys. Lett. **B 122**, 103 (1983); Phys. Lett **B 126**, 398 (1983).

[5] M. Banner *et al.*, Phys. Lett. **B 122**, 476 (1983); P. Bagnaia *et al.*, Z. Phys. C **24**, 1 (1984).

[6] For a review of the Z^0, see D. Schaille, *Proceedings of the XXVII International Conference of High Energy Physics*, Glasgow, Scotland (1994). For other electroweak results, see the references in P. Langacker and J. Erler in Ref. [49].

[7] See, for example, the lectures of M. Peskin in the *Proceedings of the XVII SLAC Summer Institute*, Stanford California, July 1989 and F. Jegerlehner in the *Proceedings of the Theoretical Advanced Study Institute (TASI)*, Boulder, Colorado, June 1990.

[8] This idea was first proposed by O. Klein, in *Les Nouvelles Théories de la Physique*, Proceedings of a Symposium held in Warsaw, Poland, June 1938 (Institut International de Cooperation Intellectuelle, Paris, 1938), pg. 6.

[9] R.N. Cahn, Phys. Rev. **D 36**, 2666 (1987).

[10] M. Peskin and T. Takeuchi, Phys. Rev. Lett. **65**, 964 (1990).

[11] For recent discussions, see W.F.L. Hollik, Fortschr. Phys. **38**, 165 (1990); W.J. Marciano and A. Sirlin, Phys. Rev. **D 22**, 2695 (1980).

[12] G. Buchalla, A.J. Buras, and M. Harlander, Nucl. Phys. **B 349**, 1 (1991).

[13] CERN Preprint CERN/SPSC 78-06 (1978).

[14] A more thorough review may be found in the review paper by H. Edwards, Ann. Rev. Nucl. Part. Sci. **35**, 605 (1985), or the lectures by M. Shochet at the Les Houches Summer School, École de Physique Thèorique, Les Houches, France, 1991.

[15] F. Abe *et al.*, Nucl. Instr. and Meth. **A 271**, 387 (1988), and references therein.

[16] At collider experiments, spherical coordinates are typically used: θ is the polar angle in spherical coordinates and is measured from the proton beam axis (+z axis). The azimuthal angle ϕ is measured from the plane of the Tevatron. The pseudo-rapidity, η, which is approximately equal to the rapidity for relativistic particles, is defined as $\eta \equiv -\ln(\tan(\theta/2))$.

[17] D. Amidei *et al.*, Nucl. Instr. Meth. Res., Sect. **A 350**, 73 (1994).

[18] S. Abachi *et al.*, Nucl. Instr. and Meth. **A 338**, 185 (1994).

[19] Radiation damage suffered during the collider run, unfortunately, has reduced the muon coverage to $|\eta| < 1.0$.

[20] F. Abe *et al.*, Phys. Rev. Lett. **68**, 1104 (1992).

[21] R. Ansari *et al.*, Phys. Lett. **B 186**, 452 (1987).

[22] The component of the momentum transverse to the proton beam-line is called the transverse momentum, p_T, defined by $p_T \equiv p \sin\theta$.

[23] V. Barger and R. Phillips, *Collider Physics*, (New York: Addison Wesley Publishers), pp. 258-260 (1987).

[24] J. Rosner, M. Worah, and T. Takeuchi, Phys. Rev. **D 49**, 1363 (1994). I have used the world average for $M_W = 80.27 \pm 0.15\ GeV/c^2$ (see Section 3.3) in their calculation of $\Gamma(W)$.

[25] N. Cabbibo, III Topical Conference on Proton-Antiproton Collider Physics, Rome, Jan. 1983; F. Halzen and M. Marsula, Phys. Rev. Lett. **51**, 857 (1983); K. Hikasa, Phys. Rev. **D29**, 1939 (1984); N.G. Deshpande *et al*, Phys. Rev. Lett. **54**, 1757 (1985); A.D. Martin, R.G. Roberts, and W.J. Stirling, Phys. Lett. **B189**, 220 (1987); E.L. Berger, F. Halzen, C.S. Kim, and S. Willenbrock, Phys. Rev. **D40**, 83 (1989).

[26] Aside from the couplings, the major difference between σ_W and σ_Z is the u/d ratio in the proton, which is well-constrained by the W charge asymmetry measurement (Section 4.3).

[27] C. Albajar *et al.*, Phys. Lett. **B253**, 503 (1991)

[28] J. Alitti *et al.*, Phys. Lett. **B276**, 365 (1991).

[29] S. Abachi *et al.*, submitted to Phys. Rev. **D**, May 1995.

[30] F. Abe *et. al.*, Phys. Rev. Lett. **69**, 28 (1992).

[31] F. Abe *et. al.*, Phys. Rev. Lett. **73**, 220 (1994).

[32] The values of σ_W/σ_Z are calculated with different sets of parton distribution functions, and the collaborations typically used the same parton sets in their acceptance calculations. The low-x density of the partons has been increasing as new HERA data emerges, and these affect σ_W/σ_Z and the acceptance calculations that go into R. It may be true that R is not stable with respect to knowledge of parton sets, but fortunately $\frac{R}{(\sigma_W/\sigma_Z)}$ is.

[33] P. Colas, D. Denegri, and C. Stubrauch, Z. Phys. C **40**, 527, (1987).

[34] A.D. Martin, W. J. Stirling, and R.G. Roberts, Phys. Lett. **B 228**, 149 (1989).

[35] R. Hamberg, W.L. van Neerven, and T. Matsuura, Nucl. Phys. **B 359**, 343 (1991).

[36] A.D. Martin, W. J. Stirling, and R.G. Roberts, Phys. Rev **D 50**, 6734 (1994); and W.J. Stirling, private communication.

[37] A. Denner and T. Sack, Zeit. Phys. **C46**, 653 (1990).

[38] A. Denner, Fortschr. Phys. **41**, 307 (1993).

[39] C. Albajar *et al.*, Z. Phys. C **44**, 15 (1989).

[40] R. Ansari *et al.*, Phys. Lett. **B 186**, 440 (1987).

[41] F. Abe *et al.*, Phys. Rev. Lett **74**, 341 (1995).

[42] F. A. Berends, "Z Line Shape," in "Z Physics at LEP I," CERN-89-08.

[43] J. Rosner, private communication.

[44] F. Abe *et. al*, Phys. Rev. Lett. **66**, 2951 (1991); Phys. Rev. Lett. **67**, 2937 (1991).

[45] R. G. Wagner, Comput. Phys. Commun. **70**, 15 (1992), based on calculations by F. Berends *et al.*, Z. Phys. **C27**, 155 (1985) and F. Berends and R. Kleiss, Z. Phys. **C27**, 365 (1985).

[46] P. Roudeau *et. al.*, in the "EFCA Workshop on LEP200," CERN-87-08.

[47] It is probably true, however, that the full one-loop corrections, including fermion masses and photon emission diagrams, *etc.*, will have to be applied to the Breit-Wigner form for the theory to make meaningful predictions at the future experimental sensitivity of 30 *MeV*.

[48] The curves are calculated by F. Halzen and B.A. Kniehl, Nucl. Phys. **B 353**, 567 (1990), with some modification (F. Halzen and B.A. Kniehl, private communication) to include effects of the running with Q^2 of the top mass, and other QCD corrections. The values used to calculate the curves are $M_Z = 91187 \pm 7\ MeV/c^2$, $\Delta\alpha_{had}(M_Z^2) = 0.0283 \pm 0.0007$, $\alpha_s(M_Z^2) = 0.117 \pm 0.005$. See also S. Fanchiotti, B. Kniehl, and A. Sirlin, Phys. Rev. **D 48**, 307 (1993). The uncertainty band on the curves is from folding in quadrature uncertainties on the Z^0 mass, α, and α_s evaluated at $Q^2 = M_Z^2$ (see M.L. Swartz, SLAC-PUB-6710, Nov. 1994 and also A. Martin and D. Zeppenfeld, UW preprint MAD-PH-855, Nov. 1994). My thanks to Steve Errede for providing these curves.

[49] G. Arnison *et al.*, Europhys. Lett. **1**, 327 (1986).

[50] R. Ansari *et al.*, Phys. Lett. **B 186**, 440 (1987).

[51] C. Albajar *et al.*, Z. Phys. **C 44**, 15 (1989).

[52] F Abe *et al.*, Phys. Rev. Lett. **65**, 2243 (1990); Phys. Rev **D 43**, 2070 (1991).

[53] J. Alitti *et al.*, Phys. Lett. **B 276**, 354 (1992). I have calculated the W mass from their measurement of M_W/M_Z using $M_Z = 91188 \pm 4\ MeV/c^2$ from Ref. [6].

[54] C.K. Jung, "Measurement of the W Boson Mass," in the *Proceedings of the XXVII International Conference of High Energy Physics*, Glasgow, Scotland (1994).

[55] F Abe *et al.*, Phys. Rev. Lett. **75**, 11 (1995).

[56] L. Montanet *et al.*, Particle Data Group, Phys. Rev. **D 50**, 1173 (1994).

[57] Q. Zhu, *Topical Workshop on $\bar{p}p$ Collisions*, Tsukuba, Japan, October 1993; A.I. Mincer, *Proceedings of the 9th Meeting of the Division of Particles and Fields*, Albequerque, New Mexico, August 1994; and H. Montgomery, private communication.

[58] J. Alitti *et al.*, Phys. Lett. **B 280**, 137 (1992).

[59] F. Abe *et al.*, Phys. Rev. Lett. **68**, 3398 (1992).

[60] J.R. Patterson, "Weak and Rare Decays," invited talk at the XXVII International Conference on High Energy Physics, Glasgow, Scotland, August 1994.

[61] J.M. Roney, *Proceedings of the Second Workshop on Tau Lepton Physics*, The Ohio State University, Columbus, Ohio, U.S.A., September, 1992 (World Scientific, publishers). This reference uses a TRIUMF result, D.L. Britten *et al.*, Phys. Rev. Lett. **68**, 3000 (1992).

[62] L. Arnell, W. Marciano, and Z. Parsa, Nucl. Phys. **B 196**, 378 (1982); G. Lepage and S. Brodsky, Phys. Lett. **B 87**, 359 (1979); and G. Kane, private communication.

[63] P. Abreu *et al.*, Phys. Lett. **B 268**, 296 (1991).

[64] F. Abe *et al.*, Phys. Rev. Lett. **69**, 2160 (1992); F. Abe *et al.*, submitted to Phys. Rev. Lett..

[65] See, for example, C. Quigg, Gauge Theories of the Strong, Weak, and Electromagnetic Interactions, (New York: Addison Wesley Publishing, 1983), pp. 100-102.

[66] G. Arnison *et al.*, Phys. Lett. **B 129**, 273 (1983). Note that the higher $\sqrt{s}$ of the Tevatron makes this measurement difficult as a test of *V-A*. See Section 4.2.

[67] C. Stubenrauch, Ph.D. Thesis, Universitè Paris-Sud, CEA-N-2532 (1987).

[68] B. Blake *et al.*., Phys. Rev. **D 37**, 587 (1988).

[69] U. Baur, Nucl. Phys. **B 308**, 127 (1988).

[70] J.M. Cornwall, D.N. Levin, and G. Tiktopolous, Phys. Rev. Lett. **30**, 1268 (1973); Phys. Rev. **D 10**, 1145 (1974); C.H. Llewellyn Smith, Phys. Lett. **B 46**, 233 (1973); S.D. Joglekar, Ann. of Phys. **83**, 427 (1974).

[71] J. Ellison, in the *Proceedings of the 9th Meeting of the Division of Particles and Fields*, Albequerque, New Mexico, August, 1994.

[72] F. Abe *et al.*, Phys. Rev. Lett. **74**, 1936 (1995).

[73] M.S. Alam *et al.*, Phys. Rev. Lett. **74**, 2885 (1995).

[74] S. Chia, Phys. Lett. **B 240**, 465 (1990); K. Peterson, Phys. Lett. **B 282**, 207 (1992); T. Rizzo, Phys. Lett. **B 315**, 471 (1993); U. Baur, in *Proceedings of the Summer Workshop on B Physics*, Snowmass, Colorado (1993); X. He and B. McKellar, Phys. Lett. **B 320**, 165 (1994).

[75] S.D. Drell and T.-M. Yan, Phys. Rev. Lett **25**, 316 (1970).

[76] C.S. Kim, F. Halzen University of Wisconsin preprint MAD/PH/454.

[77] Although at this centre-of-mass energy $c\bar{s}$ annihilation is also important at the 5-10% level. See A.D. Martin, W.J. Stirling, and R.G. Roberts, Phys. Lett. **B 228**, 149 (1989).

[78] R. Hamburg, T. Matsuura and W.L. van Neerven, Nucl. Phys. **B 345**, 331 (1990); Nucl. Phys. **B 359**, 343 (1991); W.L. van Neerven and E.B. Zijlstra, Nucl. Phys. **B 382**, 11 (1992).

[79] J. Botts, J. Morfin, J. Owens, J. Qui, W.-K. Tung, and H. Weerts, Phys. Lett. **B 304**, 159 (1993).

[80] A.D. Martin, R.G. Roberts, and W.J. Stirling, Phys. Lett. **B 306**, 145 (1993).

[81] F. Abe *et al.*, Phys. Rev. **D 50**, 5518 (1994); *ibid* **50**, 5535 (1994); *ibid* **50**, 5550 (1994).

[82] P.N. Harriman, A.D. Martin, R.G. Roberts, and W.J. Stirling, Phys. Rev. **D 42**, 798 (1990).

[83] This may be understood as a consequence of the Pauli exclusion principle.

[84] F. Abe *et al.*, Phys. Rev. Lett **74**, 850 (1995).

[85] W.T. Giele, N. Glover, and D. Kosower, Fermilab preprint FNAL-92/230-T (1992).

[86] J. Collins and D. Soper, Nucl. Phys. **B 193**, 381 (1981); J. Collins, D. Soper, and G. Sterman, Nucl. Phys. **B 250**, 199 (1985).

[87] P. Arnold and P. Kauffman, Nucl. Phys. **B 349**, 381 (1991).

[88] M. H. Reno, Phys. Rev. **D 49**, 4326 (1994).

[89] J. Alitti *et al.*, Z. Phys. **C 47**, 523 (1990).

[90] J. Alitti *et al.*, Phys. Lett. **B 263**, 563 (1991).

[91] J. Kotcher for the DØ Collaboration, *Proceedings of the 9th Meeting of the Division of Particles and Fields, Albequerque, New Mexico*, August, 1994.

[92] I. Hinchcliffe, Phys. Rev. **D 50**, 1297 (1994).

[93] W. Giele, E. Glover, and D. Kosower, Nucl. Phys. **B 403**, 633 (1993).

[94] J. Pati and A. Salam, Phys. Rev. **D 11**, 566 and 2558 (1975); R.N. Mohapatra and J.C. Pati, Phys. Rev. **D 11**, 566 (1975); Phys. Rev. **D 11**, 2558 (1975); G. Senjanovic and R.N. Mohapatra, Phys. Rev. **D 12**, 1520 (1975).

[95] P. Ramond, Ann. Rev. Nucl. Part. Sci. **33**, 31 (1983).

[96] G. Stiegman, K.A. Olive, and D. Schramm, Phys. Rev. Lett. **43**, 239 (1979); Nucl. Phys. **B 180**, 497 (1981).

[97] R. Barbieri and R.N. Mohapatra, Phys. Rev. **D 39**, 1229 (1989); G. Raffelt and D. Seckel, Phys. Rev. Lett. **60**, 1793 (1988).

[98] For a review, see P. Langacker and S. Uma Sankar, Phys. Rev. **D 40**, 1569 (1989).

[99] A.E. Jodidio *et al.*, Phys. Rev. **D 34**, 1967 (1986); *Erratum* Phys. Rev. **D 37**, 237 (1988); J. Imazato *et al.*, Phys. Rev. Lett. **69**, 877 (1992).

[100] G. Beal, M. Bander, and A. Soni, Phys. Rev. Lett. **48**, 848 (1982); F.I. Olness and M.E. Ebel, Phys. Rev. **D 30**, 1034 (1984).

[101] F.J. Gilman and M.H. Reno, Phys. Rev. **D 29**, 937 (1984).

[102] G. Altarelli and P. Franzini, Z. Phys. **C 37**, 271 (1988).

[103] R.N. Mohapatra, Phys. Rev. **D 34**, 909 (1986).

[104] Similar searches by UA1 (C. Albajar *et al.*, Z. Phys. **C 44**, 15 (1988)) and UA2 (K. Jacobs, Int. J. Mod. Phys. **A 9**, 2903 (1994)) are superceded by the CDF and DØ limits.

[105] G. Eppley, *Proceedings of the 9th Meeting of the Division of Particles and Fields*, Albequerque, New Mexico, August 1994. I have multiplied their limits on $\sigma_{W'}/\sigma_W$ by the measured values for σ_W from CDF.

[106] F. Abe *et al.*, Phys. Rev. Lett. **67**, 2609 (1991); Phys. Rev. Lett. **74**, 2900 (1995).

[107] U. Baur, I. Hinchliffe, and D. Zeppenfeld, Int J. Mod. Phys. **A 2**, 1285 (1987); U. Baur, M. Spira, and P. Zerwas, Phys. Rev. **D 42**, 815 (1990). Here excited quarks have spin and weak isospin $\frac{1}{2}$ and the first doublet u^* and d^* are degenerate in mass.

[108] F. Abe *et al.*, Phys. Rev. Lett **72**, 3004 (1994).

[109] Earlier limits by UA1[51] are superceded because of the higher $\sqrt{s}$ of the Tevatron.

[110] F. Abe *et al.*, submitted to Phys. Rev. Lett., March, 1994.

[111] Willenbrock et al Phys. Rev. **D 49**, 1354 (1994).

[112] J. Rosner and E. Takasugi, Phys. Rev. **D 42**, 241 (1990).

[113] F. Abe *et al.*, Phys. Rev. Lett **68**, 447 (1992); Phys. Rev. **D 45**, 3921 (1992).

[114] S. Abachi *et al.*, Phys. Rev. Lett **72**, 2138 (1994).

[115] Searches have been carried out specifically for $t \rightarrow H^+ b$, where the mass limits of these searches depend upon the the parameter $tan\beta = v_1/v_2$ and v_1 and v_2 are the vacuum expectation values for the two charged Higgs fields: F. Abe *et al.*, Phys. Rev. Lett. **72**, 1977 (1994); Phys. Rev. Lett. **73**, 2667 (1994)).

[116] P. Nason, S. Dawson, and R.K. Ellis, Nucl. Phys. **B 303**, 607 (1988); W. Beenaker, H. Kuijf, W.L. van Neerven, Phys. Rev. **D 40**, 54 (1989); G. Altarelli, M. Diemoz, G. Martinelli, and P. Nason, Nucl. Phys. **B 308**, 724 (1988).

[117] F. Abe *et al.*, Phys. Rev. Lett **73**, 225 (1994); Phys. Rev. **D 50**, 2966 (1994); Phys. Rev. **D 50**, 4623 (1995).

[118] F. Abe *et al.*, Phys. Rev. Lett **74**, 2626 (1995).

[119] S. Abachi *et al.*, Phys. Rev. Lett. **74**, 2632 (1995).

[120] F. Paige and S. Protopopescu, BNL Report No. BNL-38034, 1986 (unpublished).

[121] An additional dimuon event was discarded from the final sample because one of the two observed jets was consistent with a photon and the $\mu\mu\gamma$ mass was 86 GeV/c^2, making it consistent with a radiative decay $Z^0 \rightarrow \mu\mu\gamma$.

[122] If the CDF and DØ masses are combined, assuming uncorrelated uncertainties, the weighted average is negligibly shifted from the CDF value: $m_{top}^{avg.} = 179 \pm 12\ GeV/c^2$.

[123] L. Orr and W.J. Stirling, Phys. Rev. **D 51**, 1077 (1995).

[124] reference to Nambu model here.

[125] K. Hagiwara, R.D. Peccei, and D. Zeppenfeld, Nucl. Phys. **B 282**, 253 (1987). It is also noted therein that the LHC probes much higher $W\gamma$ masses than the Tevatron or LEP-200.

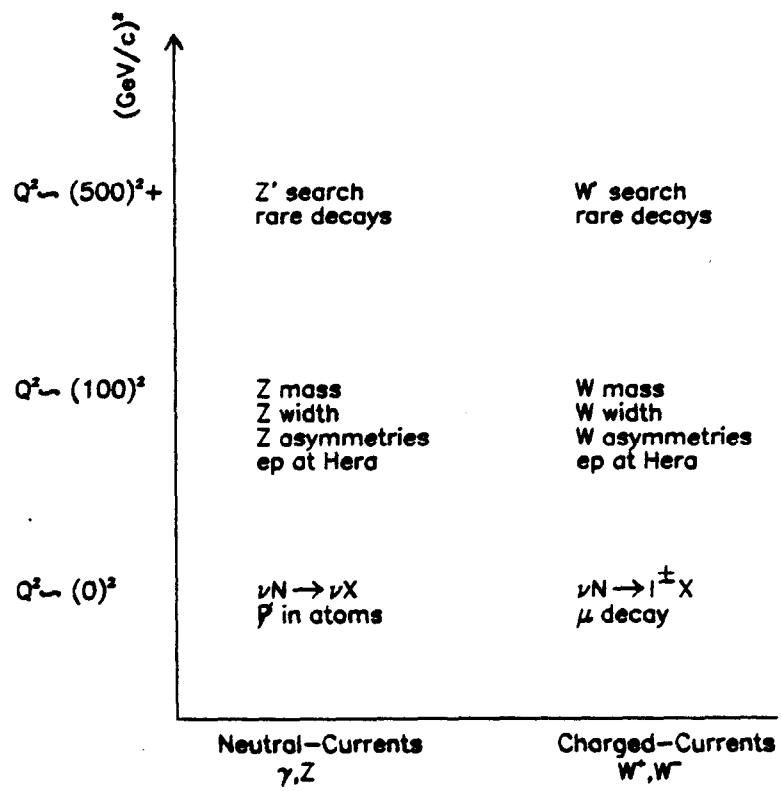

Figure 1: Relationship between different Standard Model measurements. The Standard Model, with other input data, extrapolates between low- and high-Q^2 and from the neutral current sector to the charged current. The direct measurements of the W at high Q^2 test this extrapolation in an energy régime where new physics may begin to be observable.

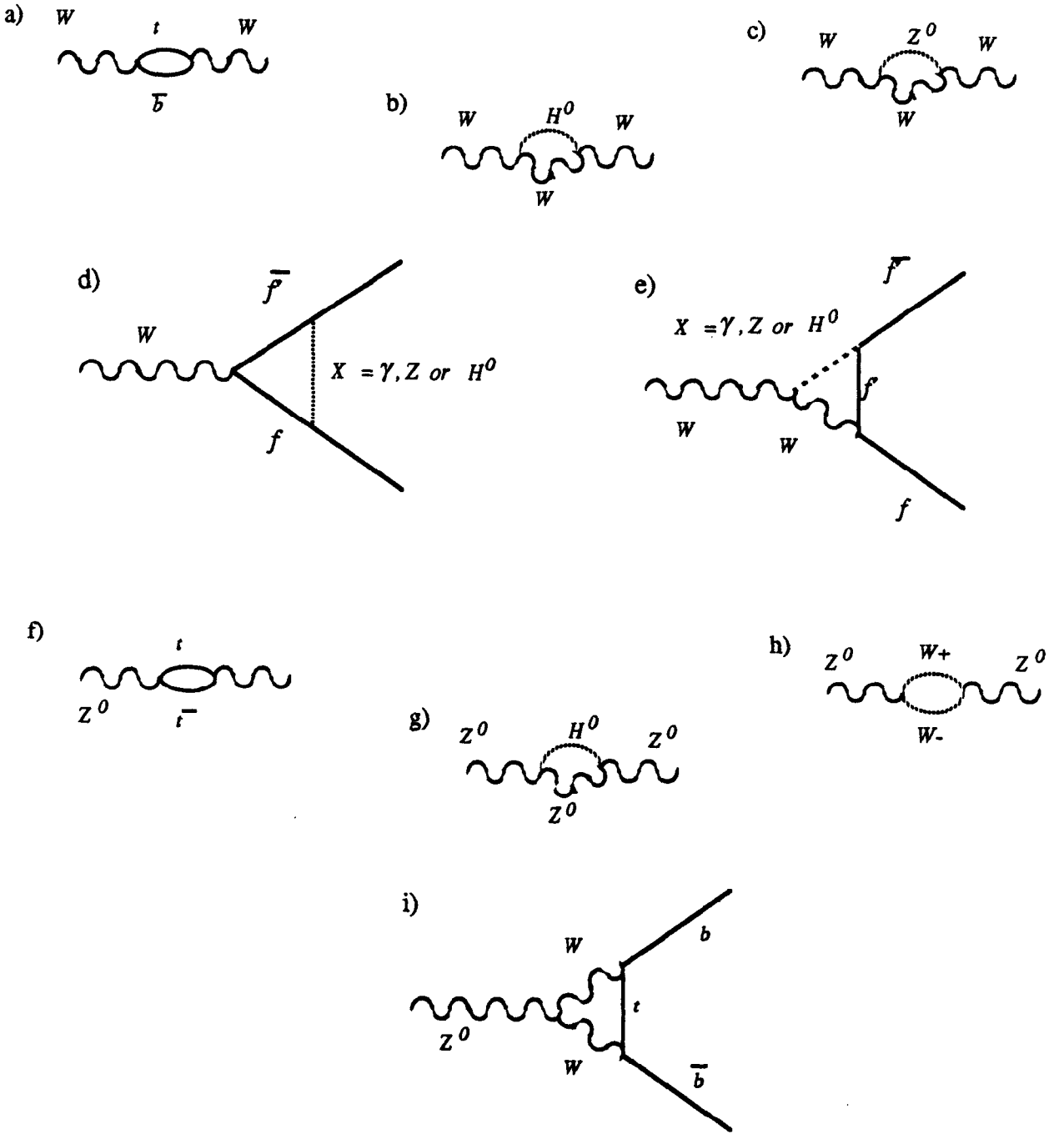

Figure 2: Feynman graphs which alter the (a)-(c) the W pole mass; (d)-(e) the W-fermion coupling; (f)-(h) the Z^0 pole mass; and (i) the $Z^0 \to b\bar{b}$ decay amplitude.

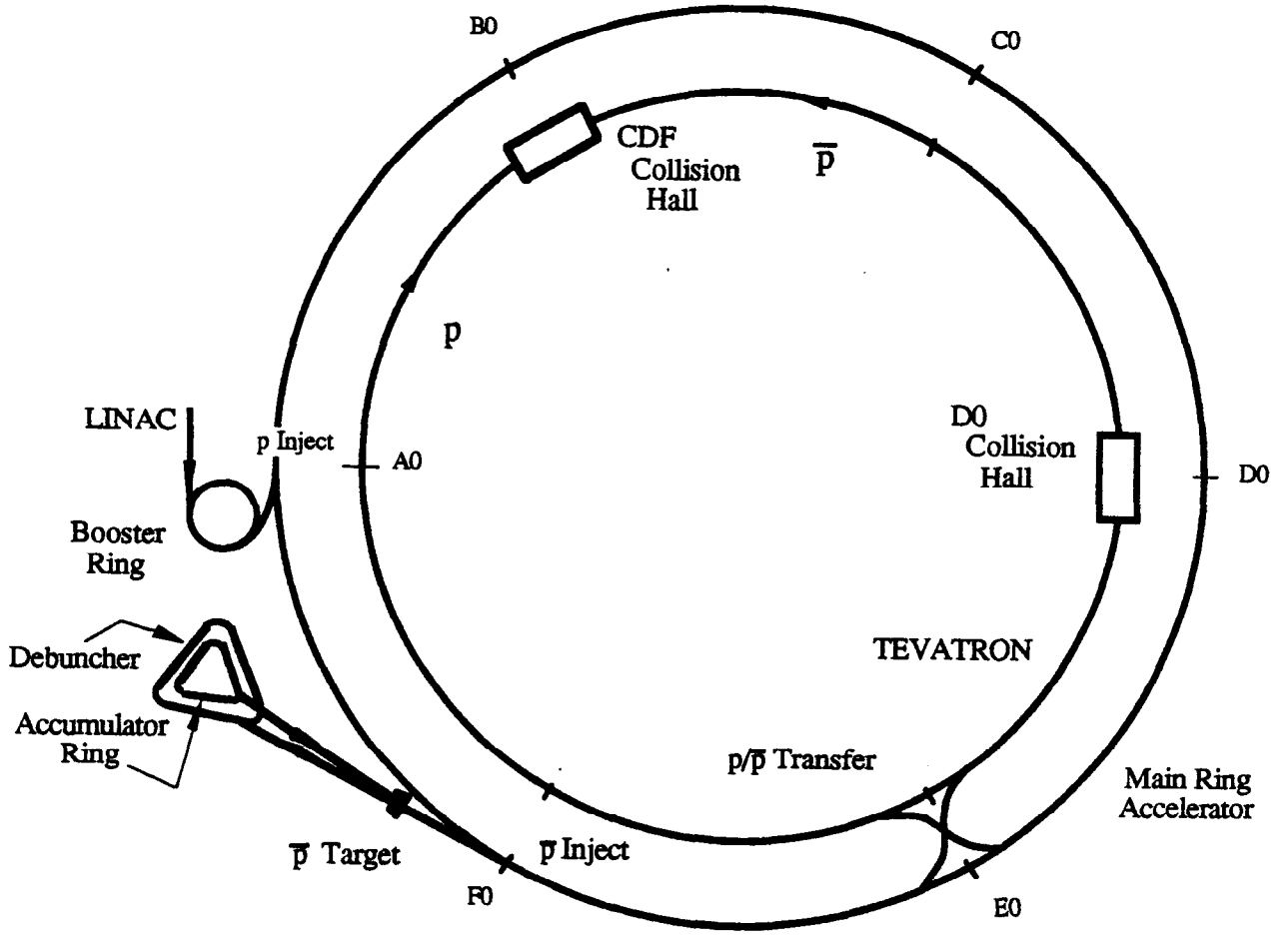

Figure 3: The Fermilab Tevatron. Of the five intersection points of the p and $\bar{p}$ beams, the BØ interaction region is occupied by CDF and the DØ interaction region by the new DØ detector.

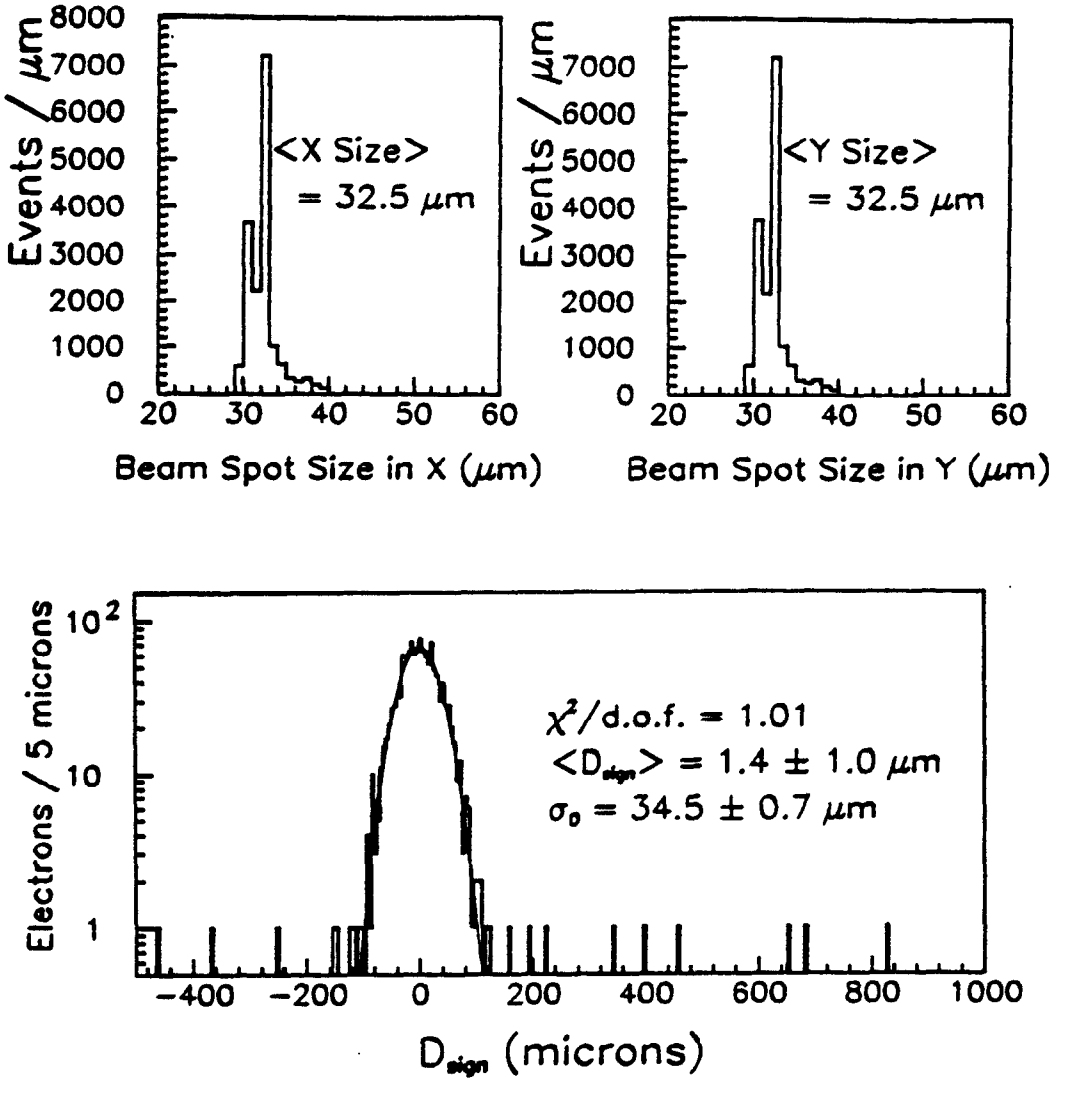

Figure 4: (a) The cross-sectional size of the $p\bar{p}$ beams' overlapping region, as measured by tracks in the CDF Silicon Vertex Detector; (b) The impact parameter distribution of electrons from $Z^0 \rightarrow e^+e^-$ decays at CDF. For charged particle tracks with $p_T > 1$ *GeV/c*, the dominant contribution to the impact parameter resolution is the transverse size of the $p\bar{p}$ interaction region, which causes a location uncertainty in the primary interaction vertex position. For electron tracks, the impact parameter experiences a 10.7 μm smearing due to the effect of Bremsstrahlung radiation in addition to the 32.5 μm smearing due to the primary vertex location.

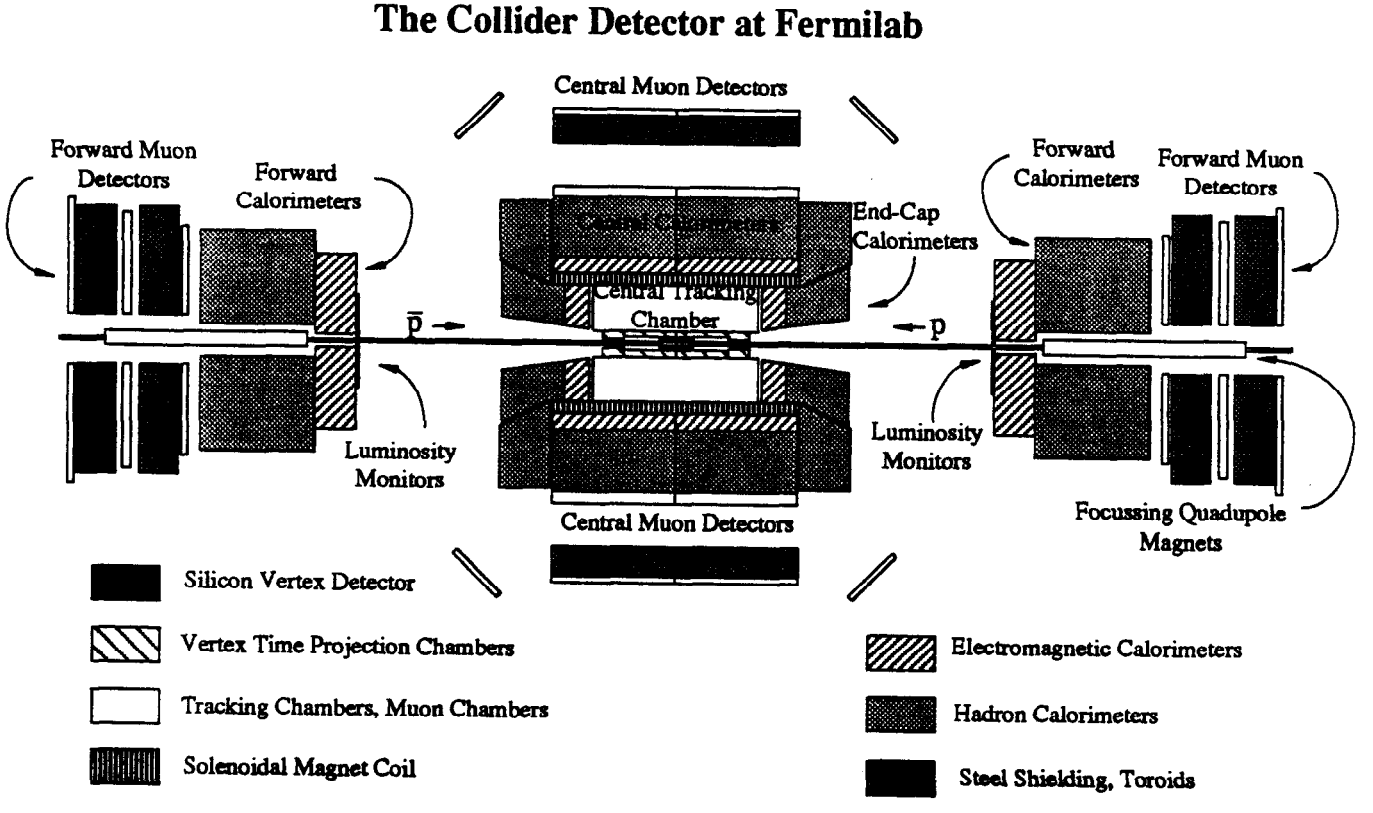

Figure 5: The Collider Detector at Fermilab (CDF). Charged particle tracking chambers immersed in a 1.4 T solenoidal field surround the beam pipe. Outside the solenoid, calorimeters measure the deposition of electromagnetic and hadronic showers.

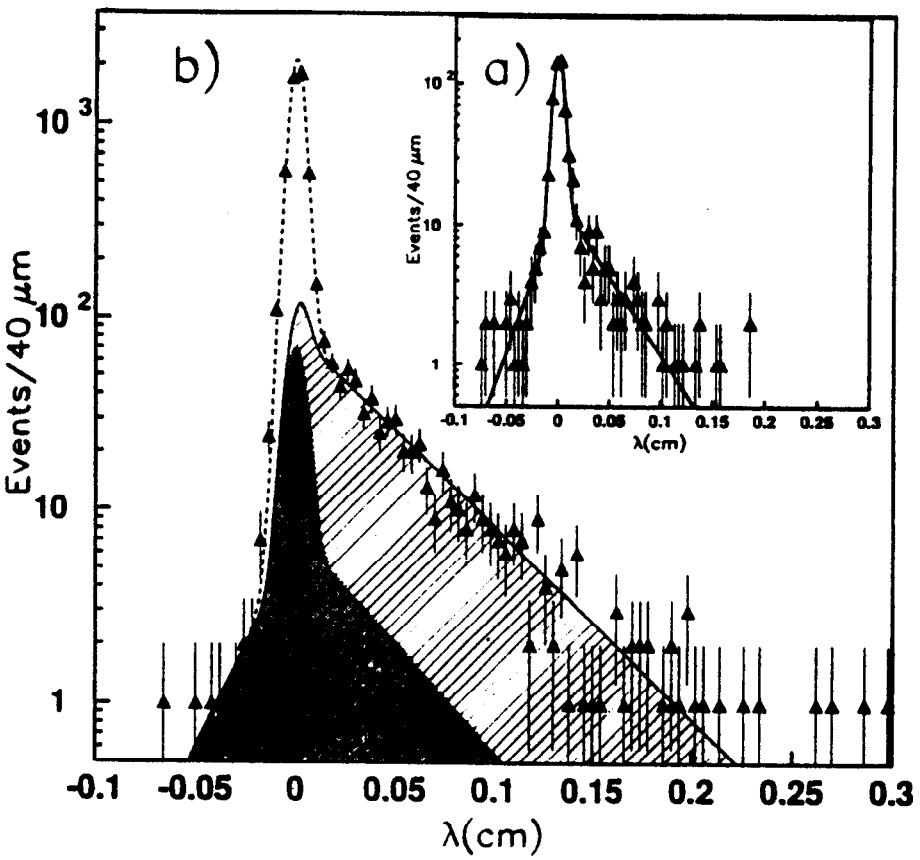

Figure 6: The two-dimensional flight path distribution of $\mu^+\mu^-$ pairs in the J/ψ mass region from the CDF collaboration, along with a fit including a background parameterization (shaded distribution), prompt J/ψ's consistent with coming from the primary vertex (dotted gaussian at zero), and J/ψ's from b decays (light shaded curve). The long tail to the positive side of zero is the signature of the secondary decay of a long lived parent particle to the J/ψ. The inset shows the flight path distribution of the mass sidebands used to parameterize the background distribution.

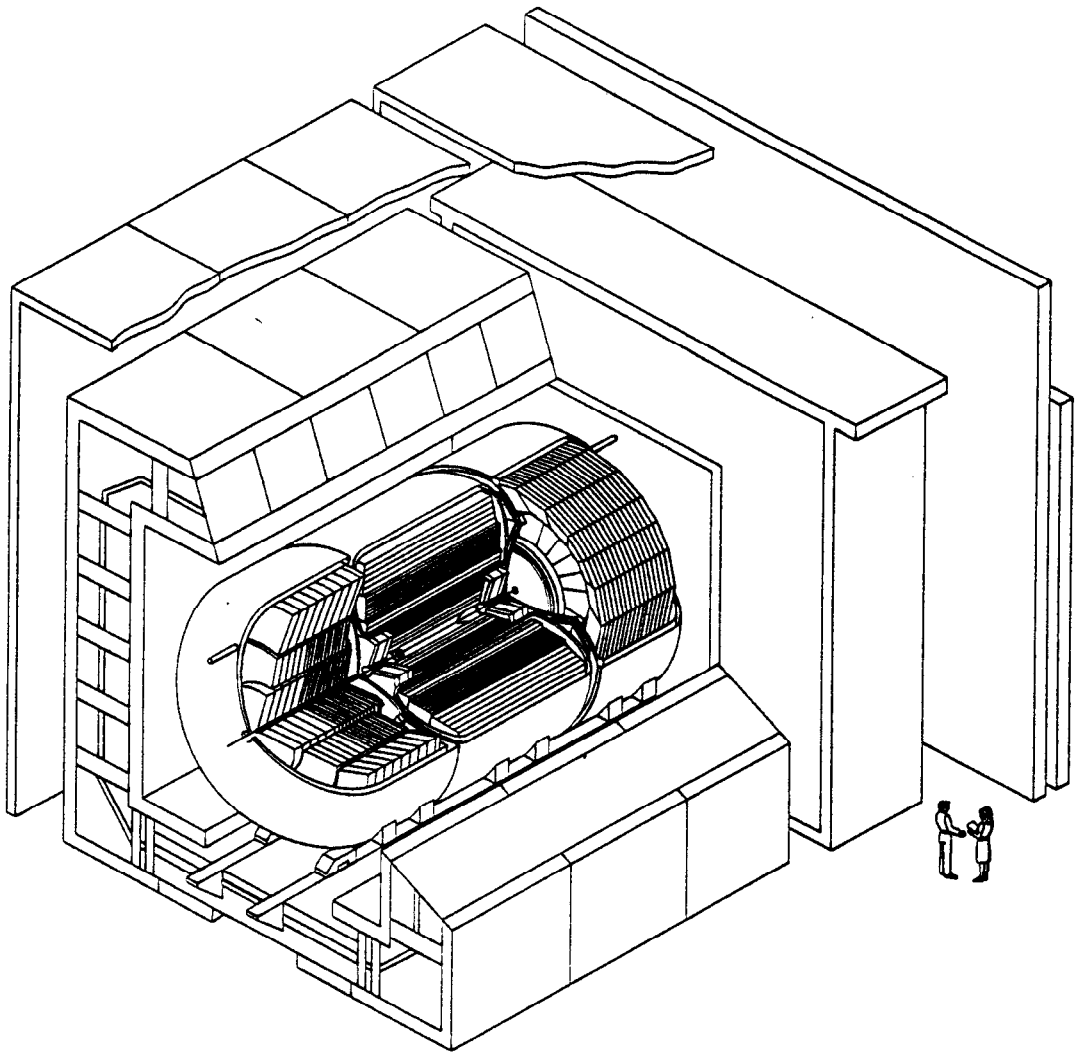

Figure 7: The DØ detector. In addition to charged particle tracking chambers surrounding the $p\bar{p}$ beams, a Uranium-liquid Argon calorimeter records electromagnetic and hadronic showers. A magnetic field in the DØ design was forsaken so as to obtain a more compact, hermetic calorimeter.

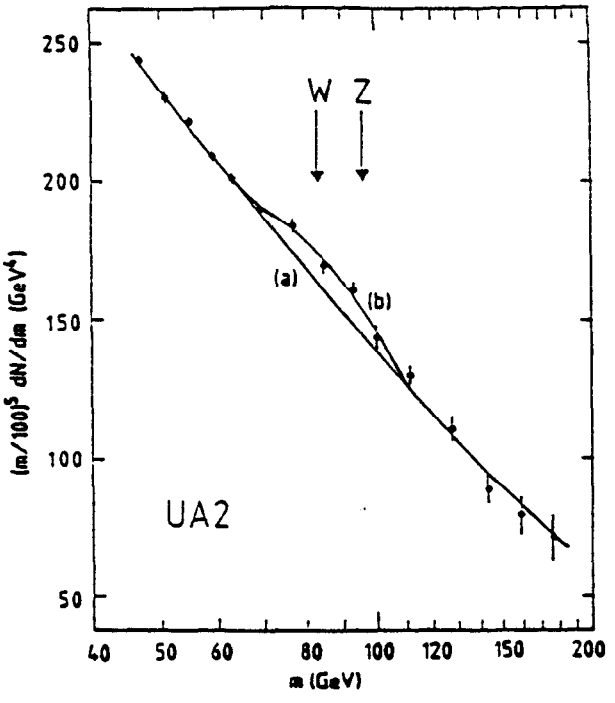

Figure 8: The invariant mass distribution of two-jet events from UA2. In addition to the falling spectrum expected from QCD 2→2 processes, a marked excess near the W and Z^0 masses is visible. The calorimeter resolution was insufficient to resolve the two mass peaks.

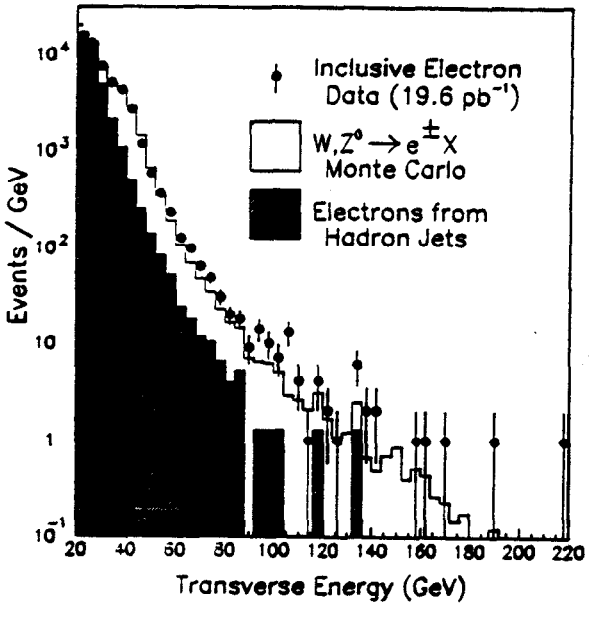

Figure 9: The transverse energy of all electrons from CDF. The components expected from fragmentations of hadron jets ($b \rightarrow ce\nu$, *etc.*) and W/Z^0 decay are indicated. An additional cut of lepton isolation (not imposed here) preferentially selects W/Z^0 electrons.

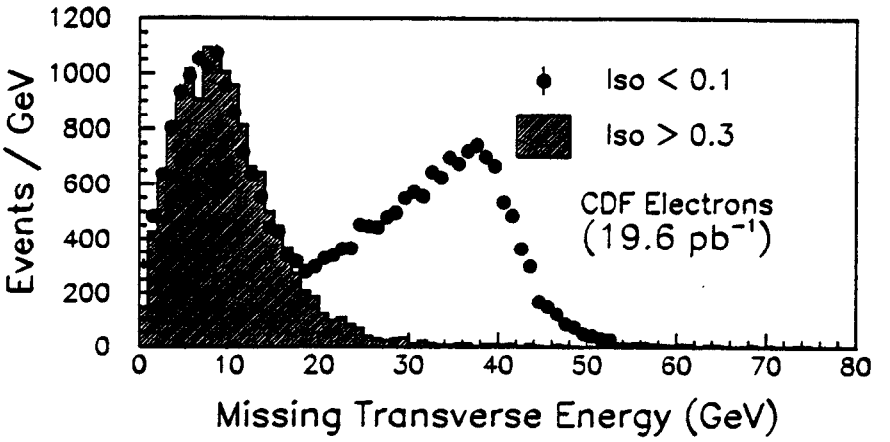

Figure 10: The $\not\!\!E_T$ of the isolated ($Iso < 0.1$, open histogram) and non-isolated ($Iso > 0.3$, shaded histogram) electrons from the CDF collaboration. The isolated electrons show a $\not\!\!E_T$ peak consistent with energetic neutrinos from $W \rightarrow e\nu$ decays on top of a lower-energy lump from mismeasurements. The non-isolated data (scaled up to the isolated data in the region $\not\!\!E_T <$ 10 *GeV*) exhibit only the peak from mismeasurement.

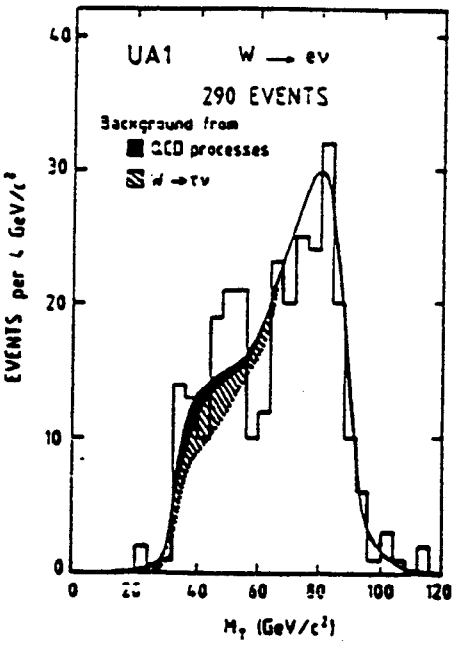

Figure 11: The transverse mass (see Section 2.3) of $W \rightarrow e\nu$ decays from UA1. The transverse mass peaks near M_W and only the detector resolutions and the finite W width allow events to populate the region $M_T > M_W$.

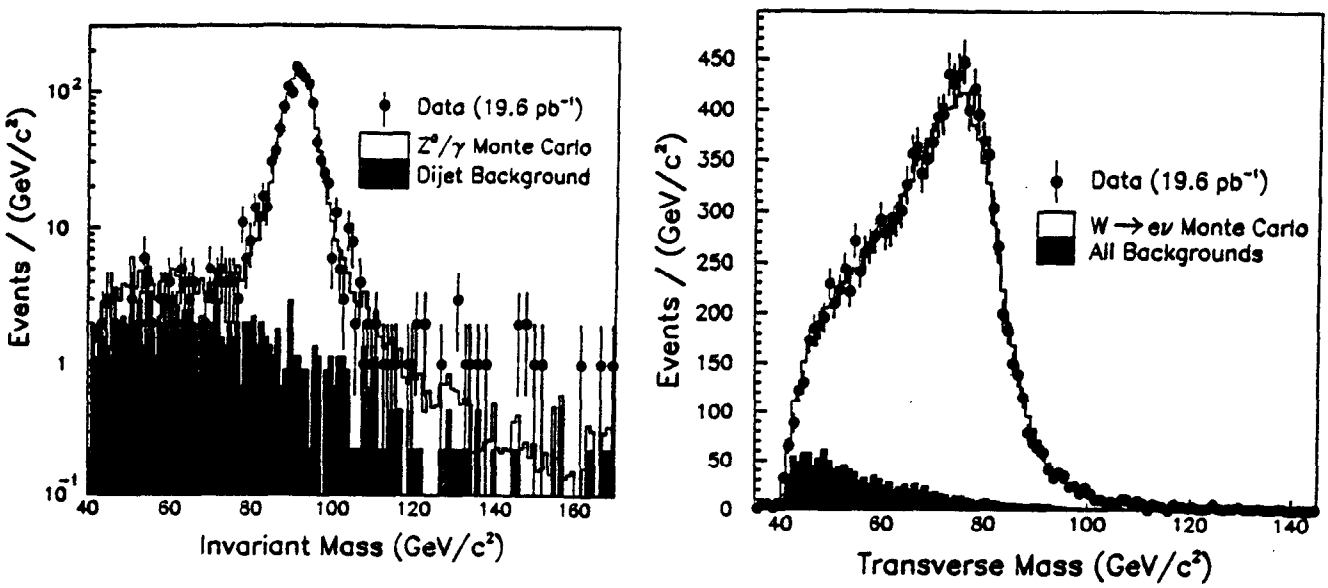

Figure 12: (a) Invariant mass of $Z^0 \rightarrow e^+e^-$ candidates; (b) Transverse mass of $W \rightarrow e\upsilon$ candidates from CDF. Also indicated are backgrounds from all sources, and the expected distributions from the Monte Carlo used to calculate the kinematic "acceptances" (see text).

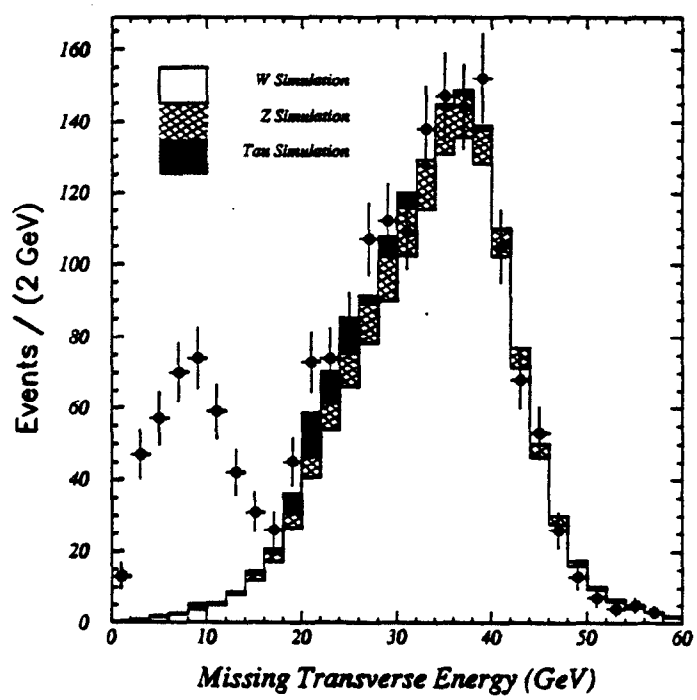

Figure 13: Missing transverse energy of $W \rightarrow \mu\upsilon$ candidates from CDF. Also indicated are the backgrounds from all sources, and the expected distribution from the Monte Carlo used to calculate the kinematic "acceptances" (see text).

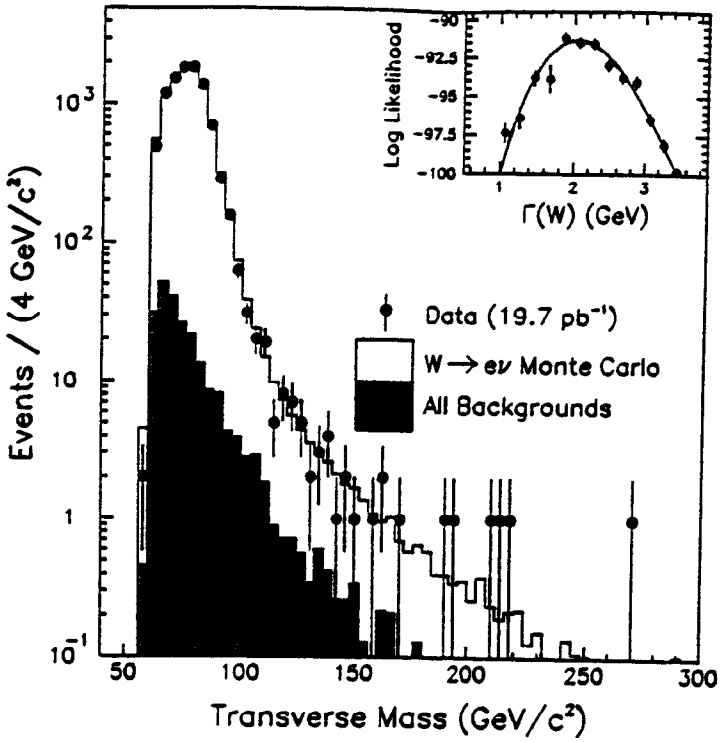

Figure 14: CDF transverse mass distribution of 9701 $W \rightarrow e\upsilon$ candidates surviving a cut of $P_T^W < 20\ GeV/c$, along with the background expectation. A Monte Carlo W shape with $\Gamma(W) = 2.067\ GeV$ is overlaid. Inset: Log likelihood fit of the data for the best W width. Each point is the result of a fit performed over $M_T > 110\ GeV/c^2$.

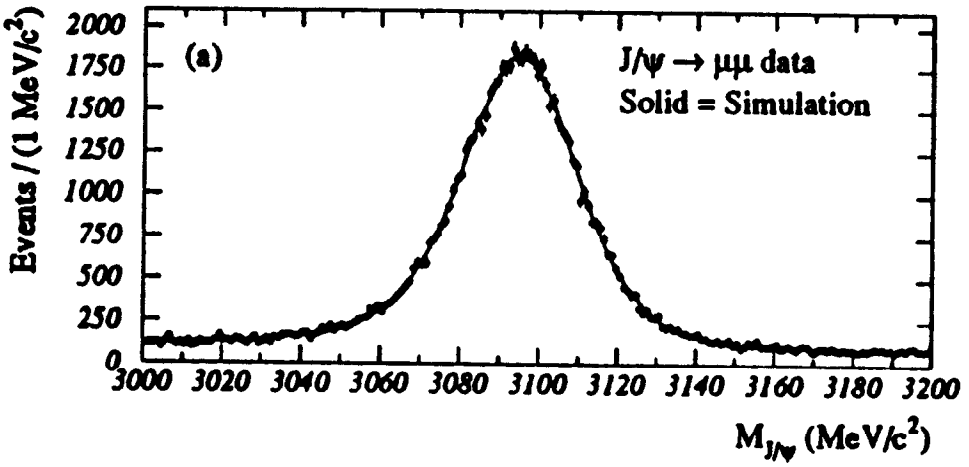

Figure 15: Invariant mass of $\mu^+\mu^-$ pairs near the J/ψ from CDF. The curve is a Monte Carlo calculation including detector resolutions and the effect of radiative decays, $J/\psi \rightarrow \mu^+\mu^-\gamma$.

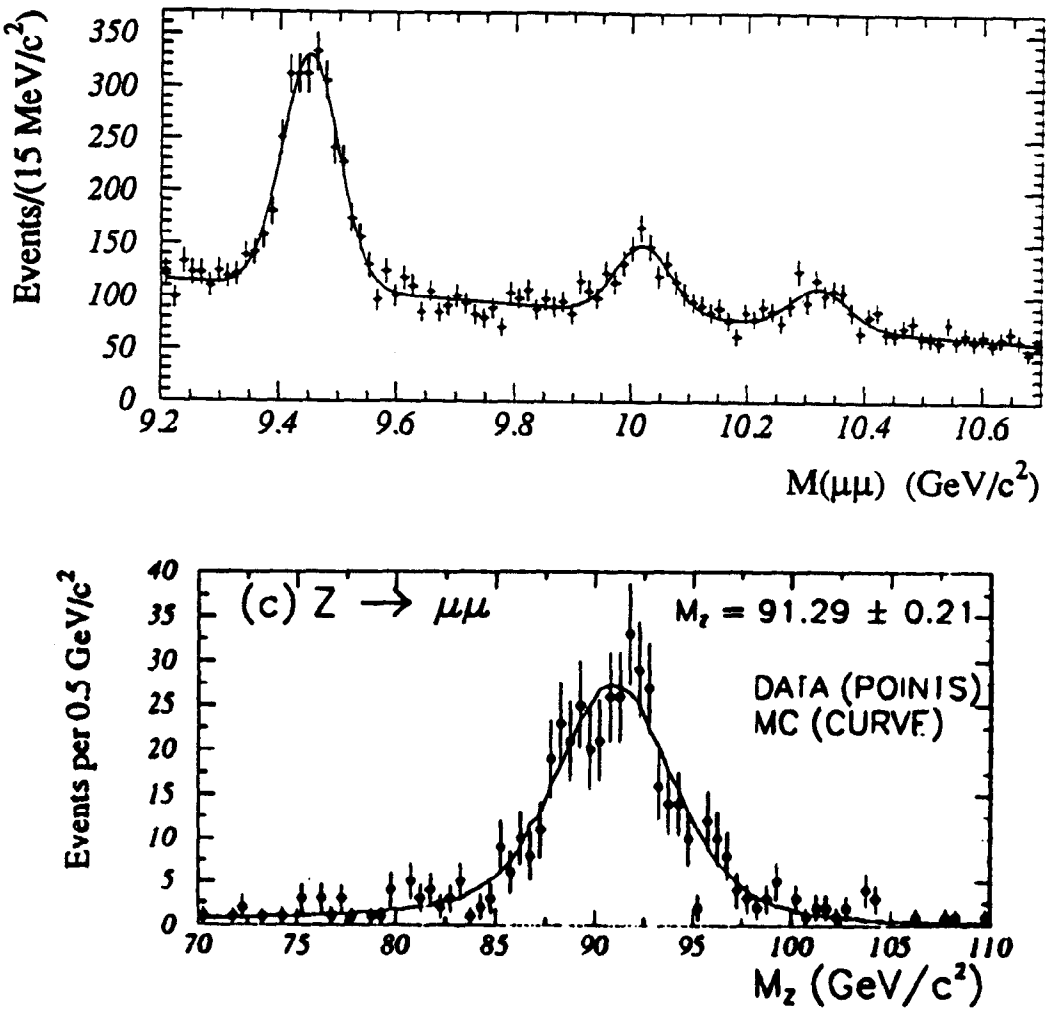

Figure 16: Invariant mass distribution of $\mu^+\mu^-$ pairs near the (a) Υ and (b) Z^0 regions. In (a) the curve is a sum of gaussian fits on a qaudratic polynomial background, and in (b) it is a Monte Carlo calculation including detector resolutions and the effect of radiative decays, $Z^0 \rightarrow \mu^+\mu^-\gamma$.

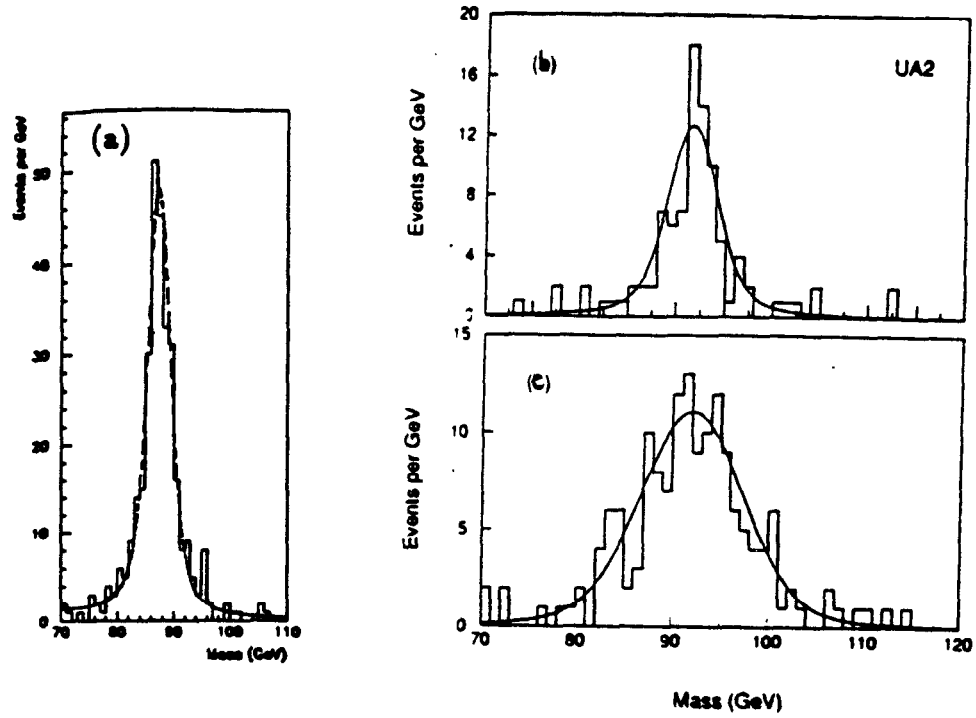

Figure 17: Invariant mass of e^+e^- pairs near the Z^0 for (a) central electron pairs from DØ; (b) central pairs from UA2; and (c) central-non-central pairs from UA2. The LEP Z^0 mass is used to establish the energy scales of their calorimeters.

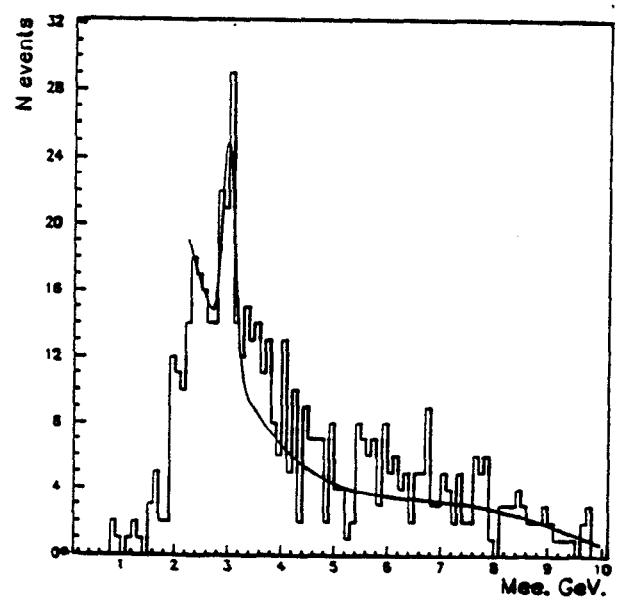

Figure 18: Invariant mass of e^+e^- pairs near the J/ψ from the DØ experiment. The curve is gaussian fit on a polynomial parameterization of the background. Studies are being undertaken by DØ to use this peak and the reconstructed $\pi^0 \rightarrow \gamma\gamma$ peak to help fix the calorimeter energy scale.

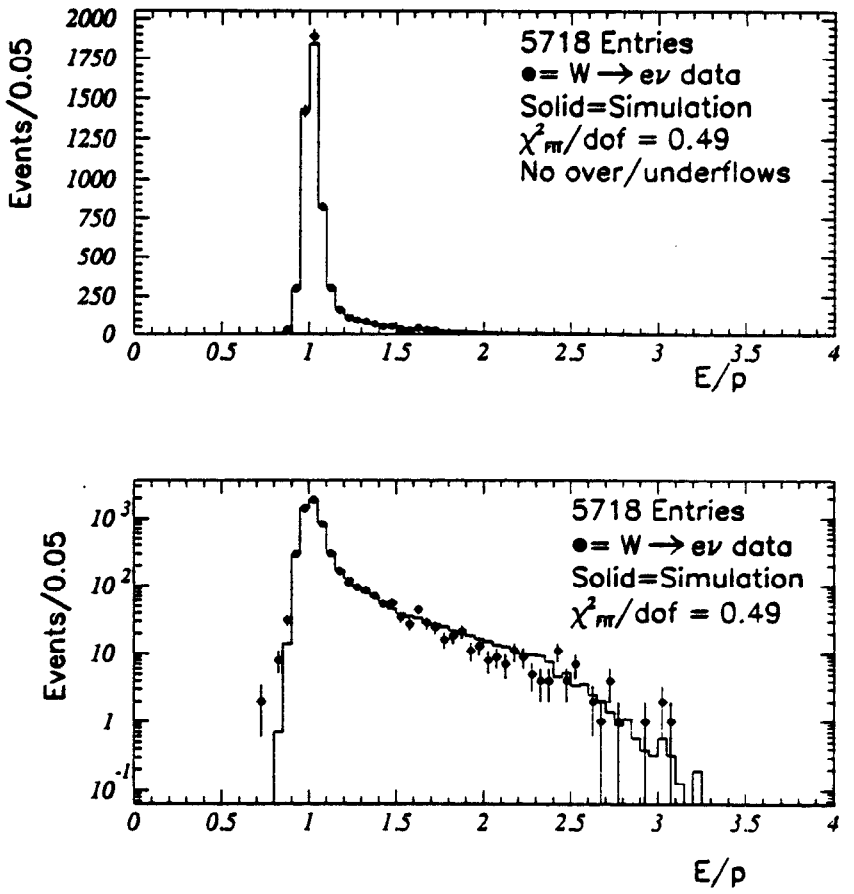

Figure 19: The E/p distribution of electrons from $W \rightarrow e\upsilon$ decays from CDF. Bremsstrahlung radiation causes the high side tail to E/p. The curve is a Monte Carlo model which includes effects of Bremsstrahlung radiation in the detector material and radiative decays $W \rightarrow e\upsilon\gamma$.

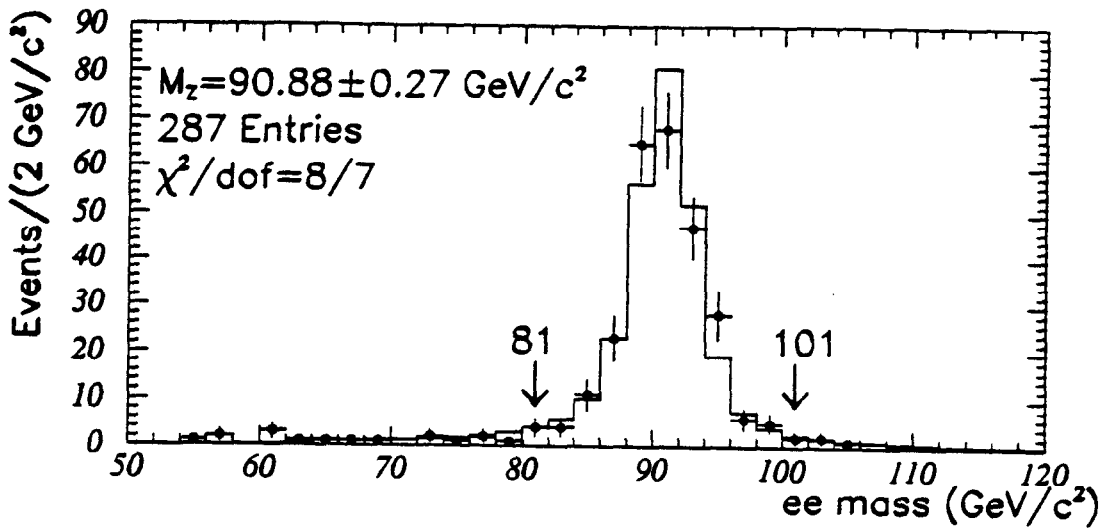

Figure 20: Invariant mass of e^+e^- pairs near the Z^0 for central electron pairs from CDF. The curve is a Monte Carlo model which includes effects of Bremsstrahlung radiation in the detector material and radiative decays $Z^0 \rightarrow e^+e^-\gamma$. The position of the peak is measured absolutely and is a check of the calorimeter energy scale.

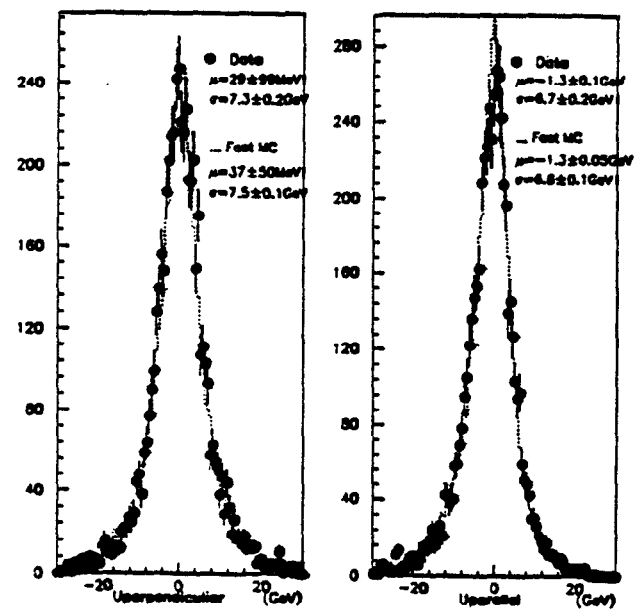

Figure 21: Components of the **u** vector (a) perpendicular ($u_\perp$) and (b) parallel ($u_{//}$) to the electron in $W \rightarrow e\upsilon$ decays from DØ. The curve is a Monte Carlo model which uses $Z^0 \rightarrow e^+e^-$ data to parameterize the calorimeter response to hadrons recoiling against the W. Since, for W's nearly at rest, $M_W \cong 2p_T^e + u_{//}$, shifts in $u_{//}$ in the Monte Carlo cause biases in M_W.

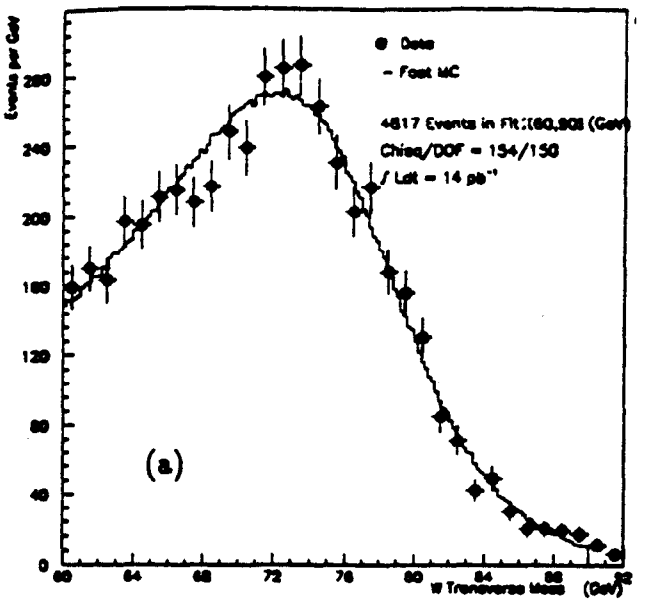

Figure 22: The transverse mass distribution of the 5830 $W \rightarrow e\nu$ candidates in the DØ W mass fit. The fit region is 60 $GeV/c^2 < M_T^W < 90$ GeV/c^2. The curve is a Monte Carlo model (see text).

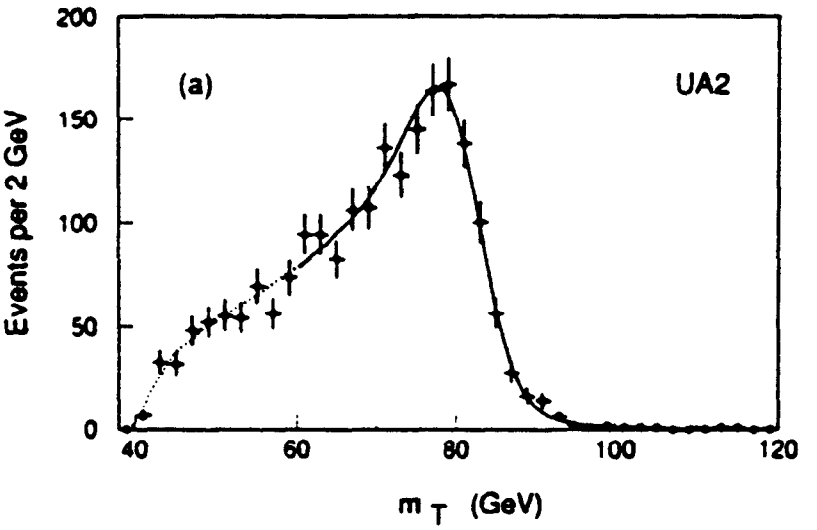

Figure 23: The transverse mass distribution of 2065 $W \rightarrow e\nu$ candidates in the UA2 mass fit. The fit region is 60 $GeV/c^2 < M_T^W < 120$ GeV/c^2. The curve is a Monte Carlo model (see text).

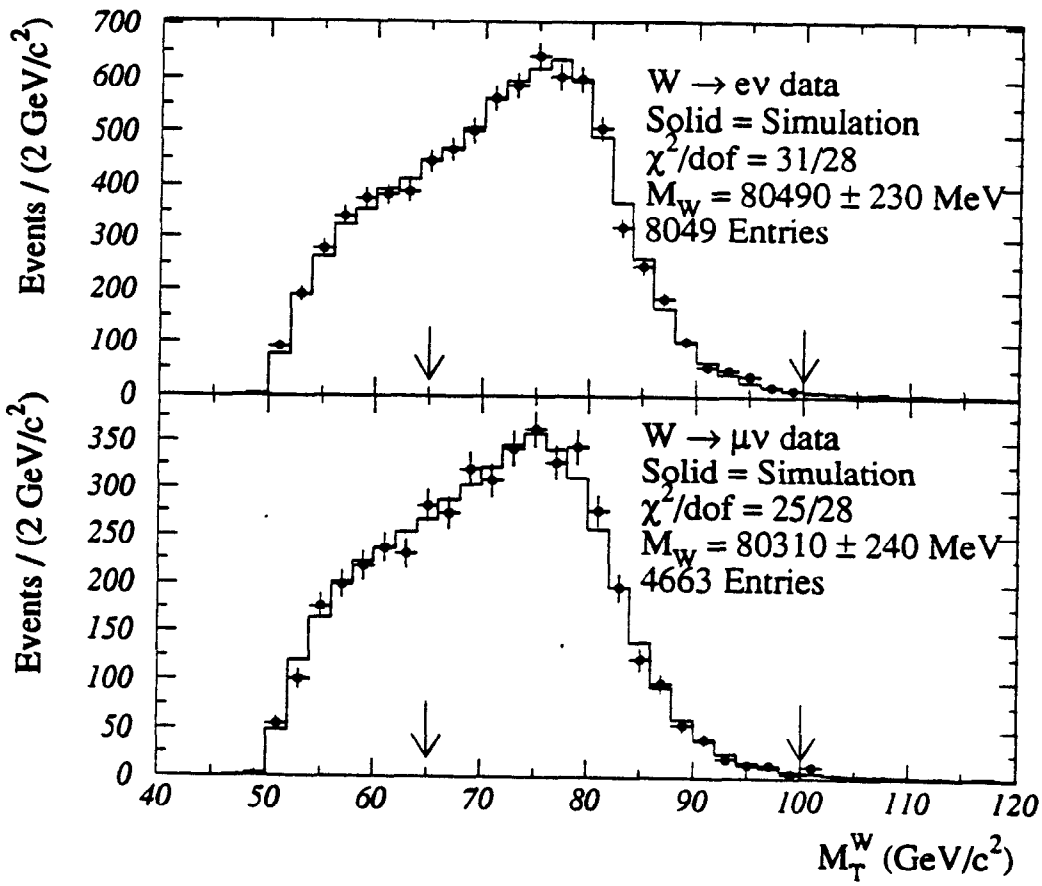

Figure 24: The transverse mass distribution of 8049 $W \rightarrow e\upsilon$ and 4663 $W \rightarrow \mu\upsilon$ candidates in the CDF W mass fit. The fit region is 65 $GeV/c^2 < M_T^W < 100\ GeV/c^2$. The curve is a Monte Carlo model (see text).

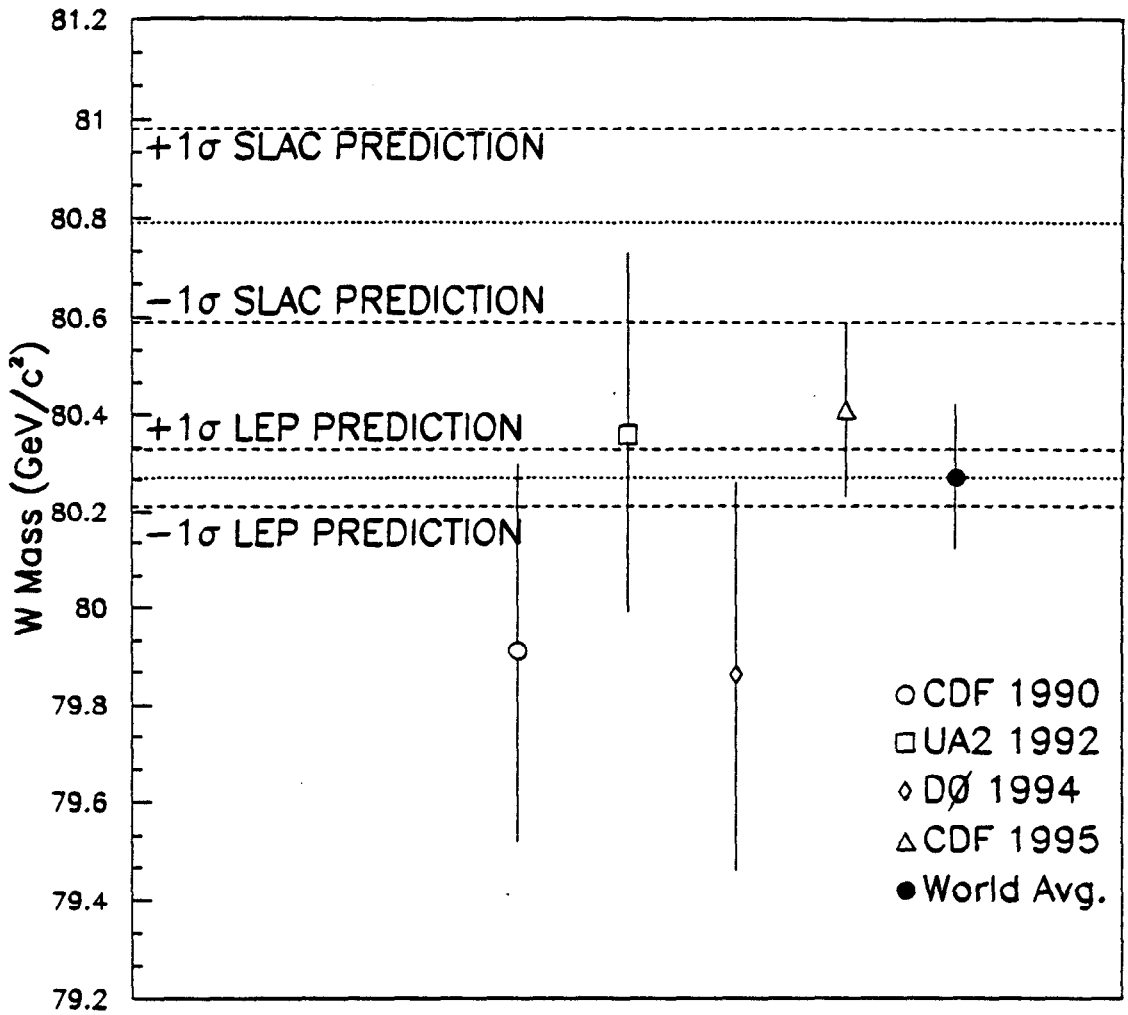

Figure 25: The direct measurements of the W mass and the world-average measurement, along with the predictions from the Standard Model fits to the LEP Z^0 data and the SLD Z^0 data.

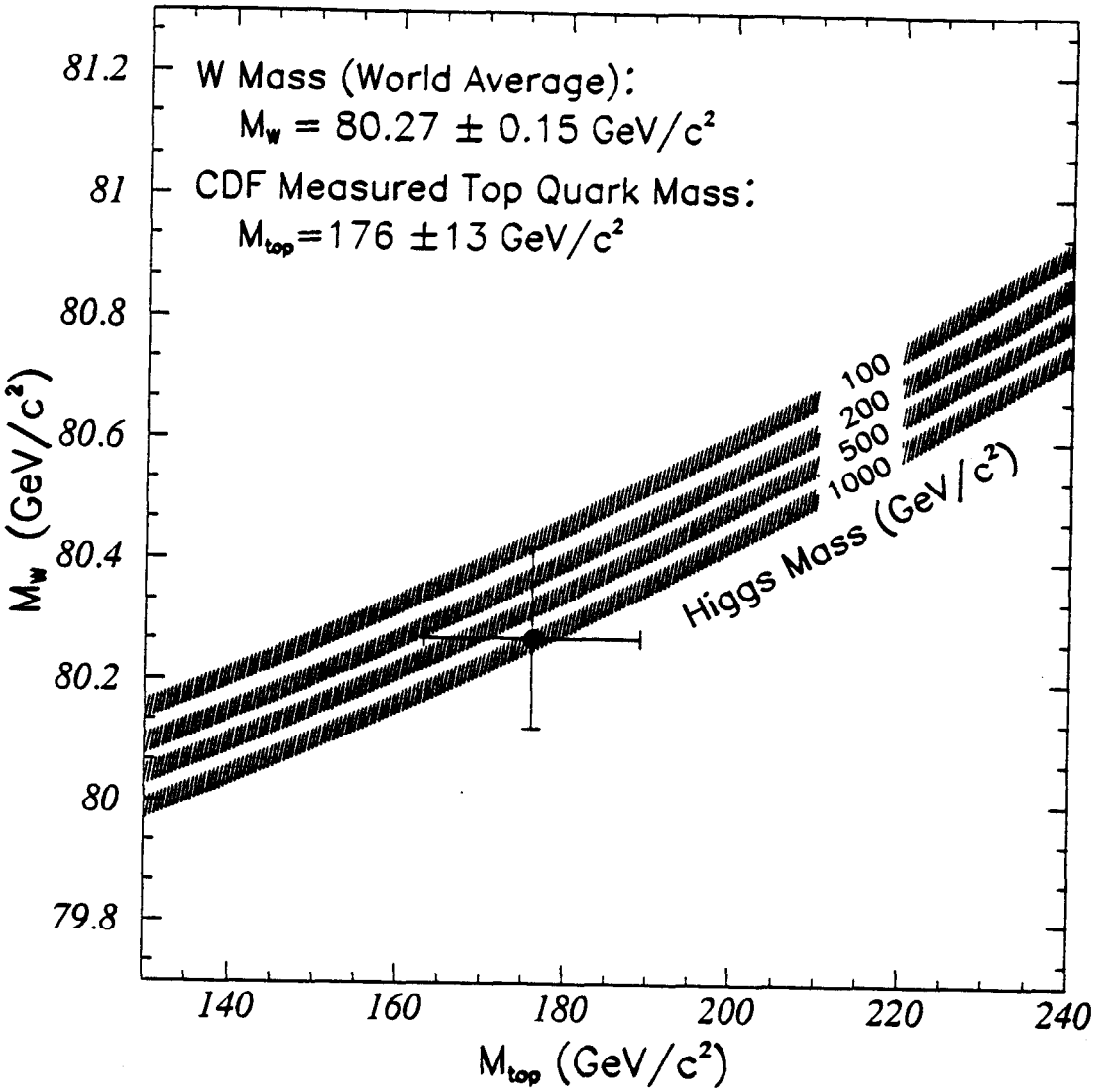

Figure 26: The data point represents the world-average direct measurement of the W boson mass and the CDF measurement of the top quark mass (See Section 5.3). The curves are from a theoretical calculation[48] of the dependence of the W mass on the top quark mass in the minimal Standard Model using several Higgs masses.

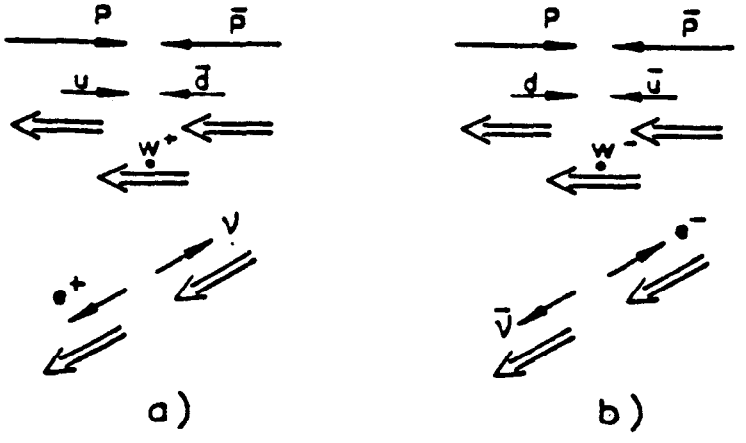

Figure 27: Schematic view of spin directions in W production and decay. Because the weak interaction is pure V-A, the W couple to purely left-handed quarks. Angular momentum conservation thus implies the W^- (W^+) is polarized along the proton (antiproton) direction. The left-(right-)handed neutrino (antineutrino) preferentially boosts the positron (electron) in the W^+ (W^-) direction, producing a charge-dependent asymmetry.

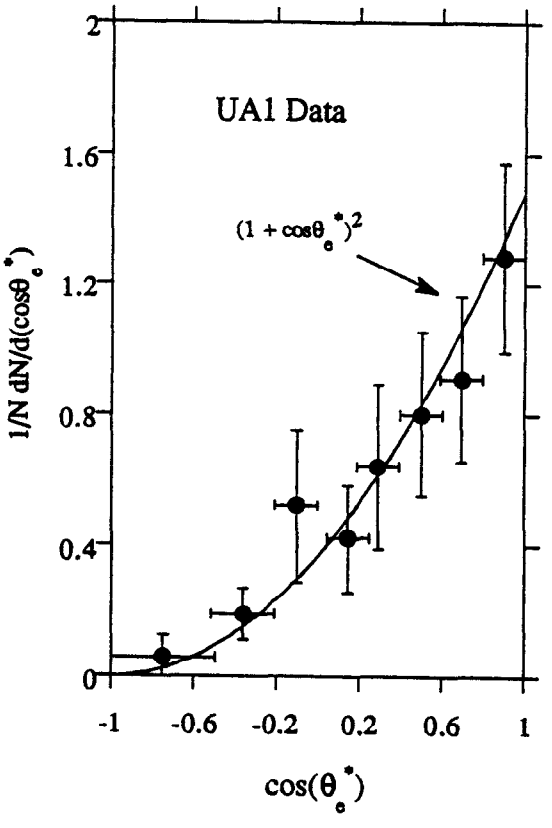

Figure 28: The UA1 corrected W asymmetry data. The angle θ_e^* is the angle of the electron (positron) with respect to the proton (antiproton) direction in the W centre-of-mass frame. The curve $(1 + \cos\theta_e^*)^2$ is expected if the weak interaction is pure V-A.

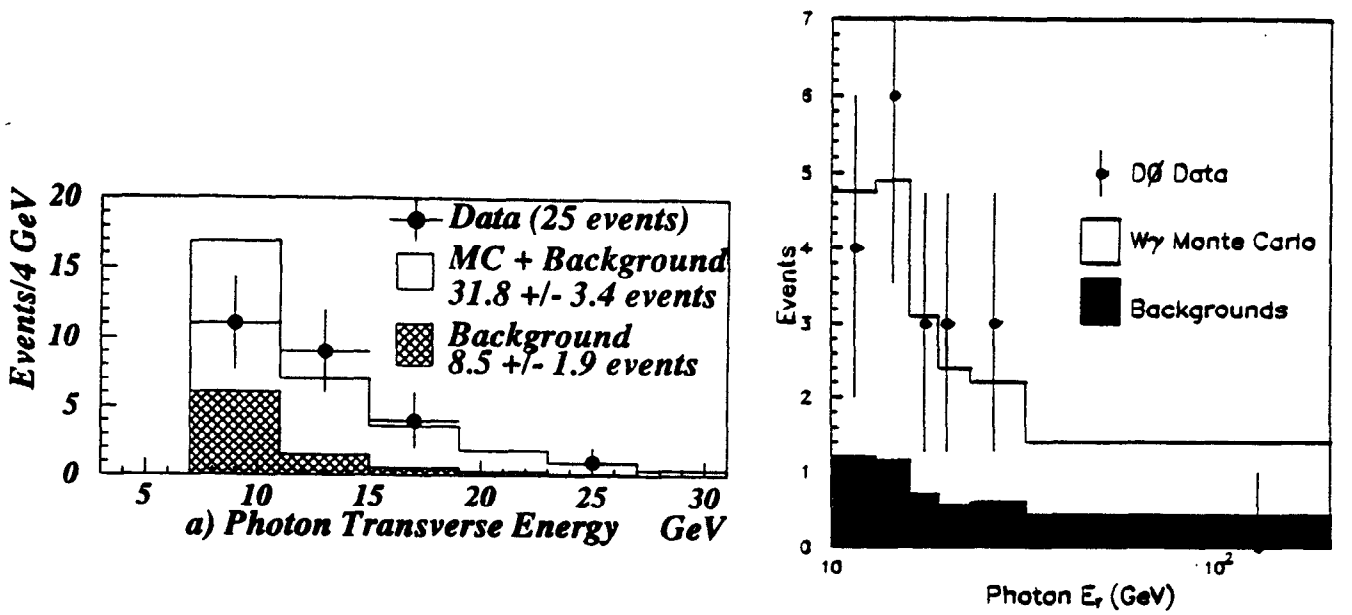

Figure 29: The p_T^γ distributions for the CDF (left) and DØ (right) $W\gamma$ candidates. Anomalous $W\gamma$ couplings would tend to produce photons with exceptionally large p_T.

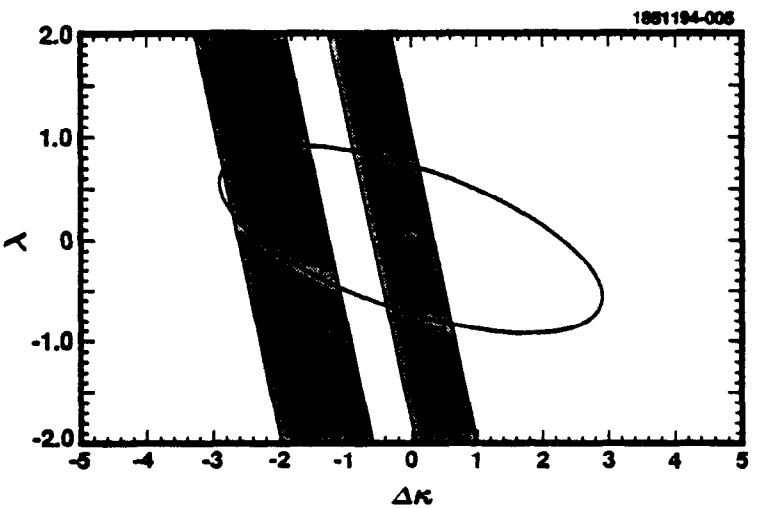

Figure 30: The limits on the anomalous coupling parameters $\Delta\kappa = \kappa - 1$ and λ obtained by DØ by fitting their p_T^γ spectrum. The area inside the ellipse is allowed by the DØ data. The CDF collaboration obtains an essentially identical ellipse. Also shown are the bands indicating the allowed parameter space from the CLEO inclusive $b \to s\gamma$ measurement.

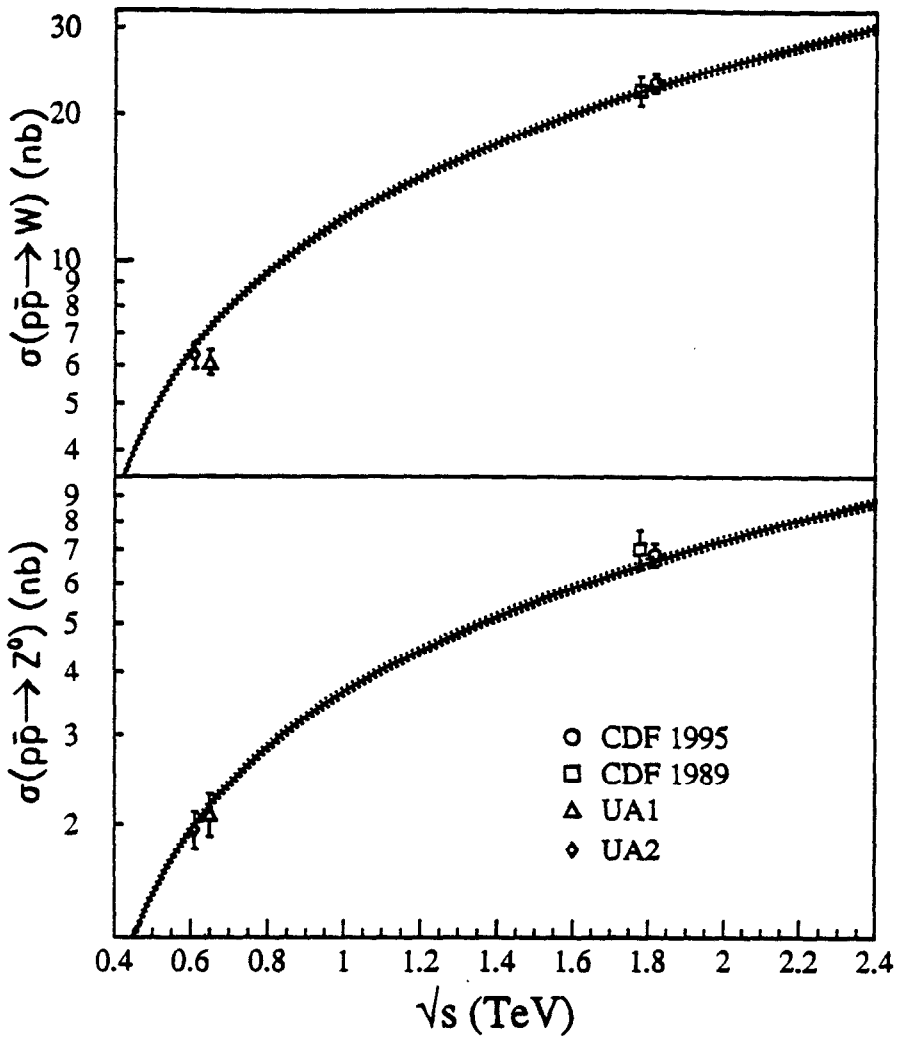

Figure 31: The evolution of the W and Z^0 production cross sections in $p\bar{p}$ collisions with $\sqrt{s}$. Shown are the theoretical predictions for several different parton distribution sets and the measurements by the UA1, UA2, and CDF collaborations. The measured σB's have been scaled by $B(W \to \ell\nu) = 0.1084$ and $B(Z^0 \to \ell\ell) = 0.0336$ to convert to the total cross sections.

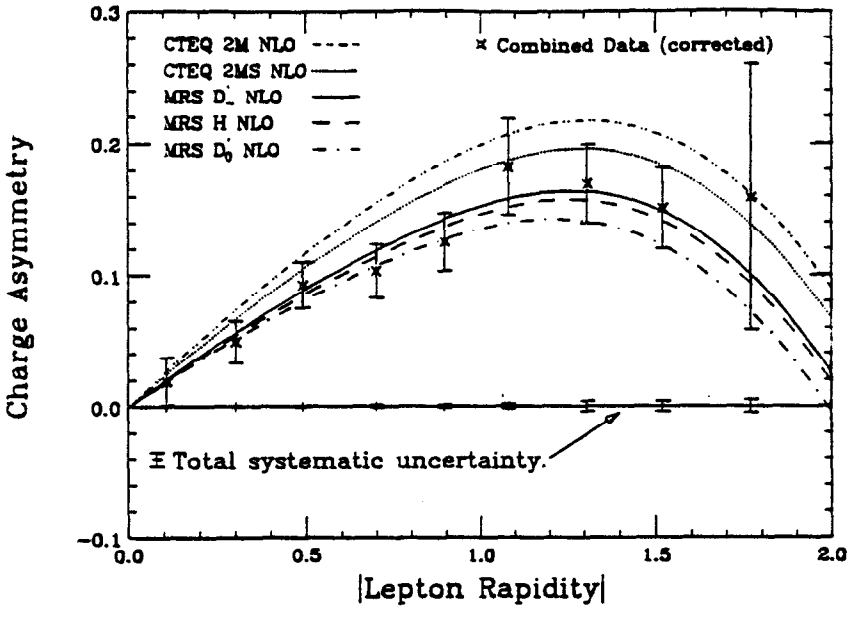

Figure 32: The lepton charge asymmetry from W decays in $p\bar{p}$ collisions at $\sqrt{s} = 1800\ GeV$ from the CDF collaboration. CP invariance has been invoked in order to fold the data across $y_\ell = 0$: $A(-y_\ell) = -A(y_\ell)$. Also shown are the predictions of a NLO Monte Carlo calculation[85] using different parton distribution functions.

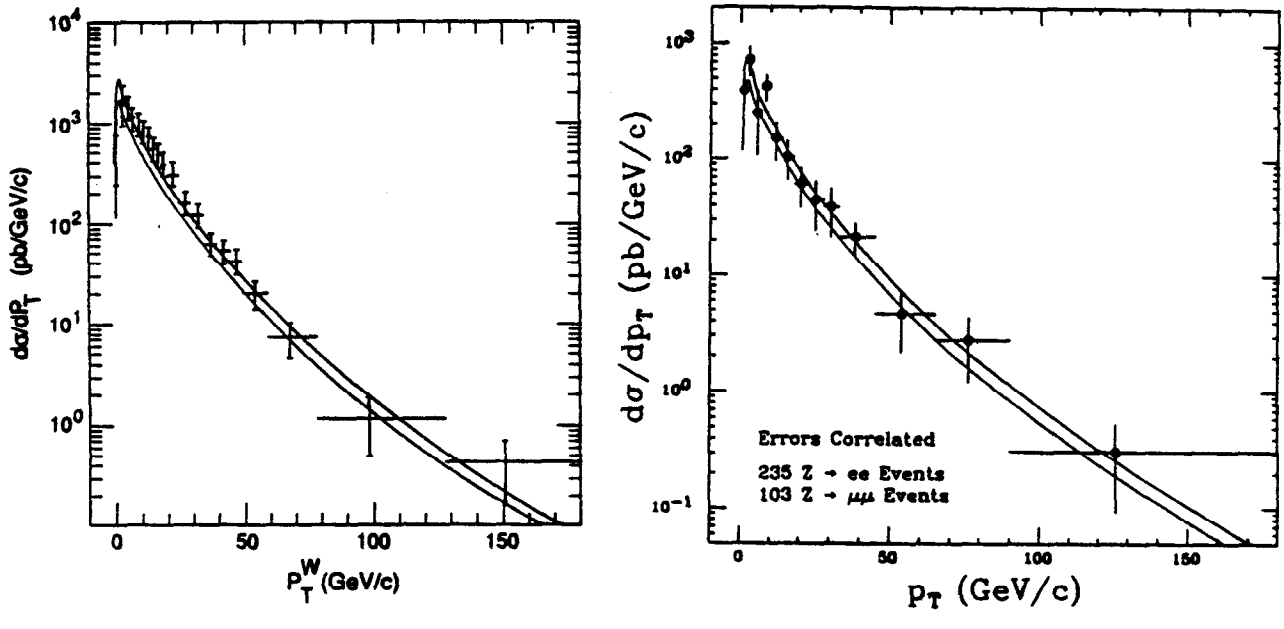

Figure 33: The measured P_T^W and P_T^Z distributions from the CDF collaboration. Also shown are the theoretical predictions of reference [87].

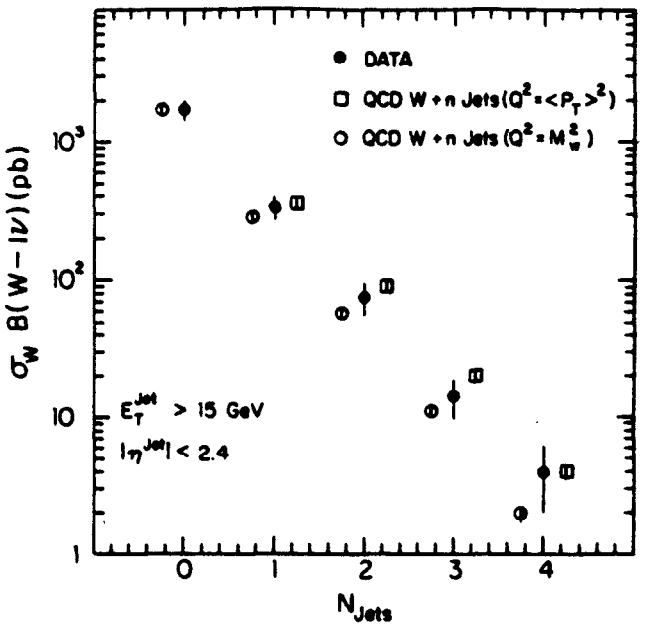

Figure 34: The jet multiplicity distribution of jets produced in association with W's in $p\bar{p}$ collisions at $\sqrt{s} = 1800\ GeV$. Also shown are the tree-level predictions of the VECBOS Monte Carlo program[93] for two different choices of the Q^2 scale: $Q^2 \sim M_W^2$ and $Q^2 \sim (P_T^W)^2$.

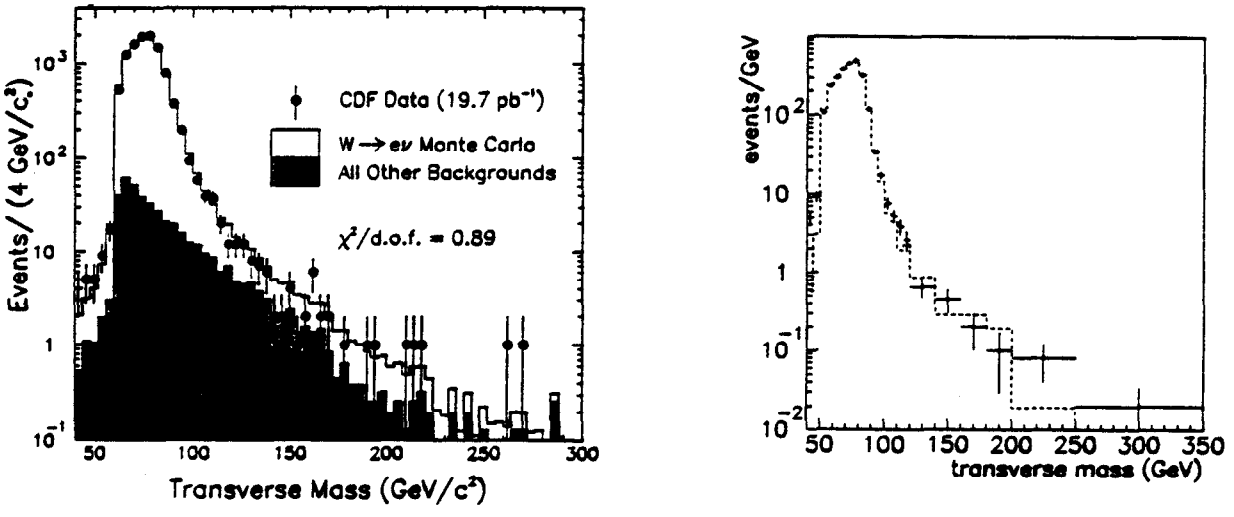

Figure 35: Transverse mass distribution of electron plus $\not{E}_T$ events in the CDF and DØ $W' \to e\upsilon$ searches. Also shown are the expected contributions from $W \to e\upsilon$ decays and other backgrounds. A W' would show up as a new peak near $M_T \sim M_{W'}$.

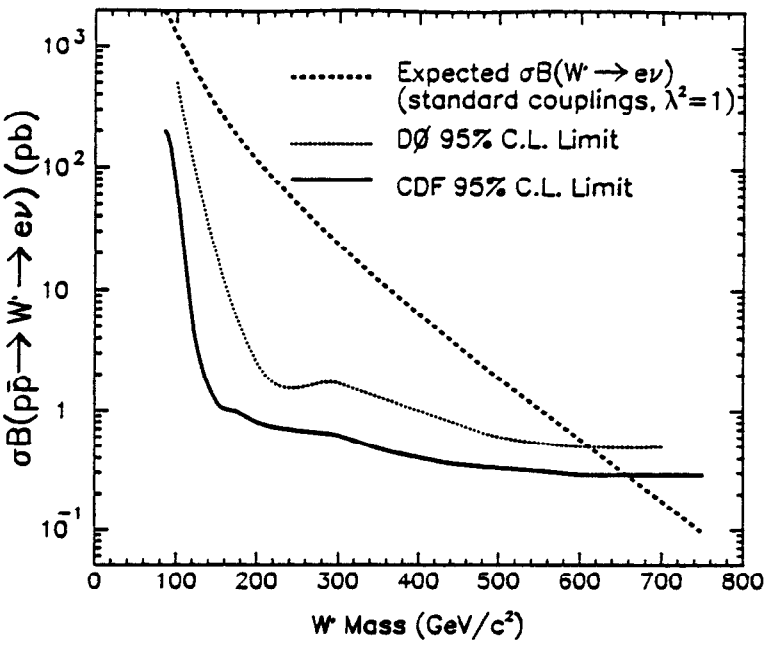

Figure 36: The 95% C.L. upper limit on the W' cross section times leptonic branching ratio derived from the CDF and DØ data as a function of the W' mass, and the theoretical expectation for the W' cross section, assuming "standard" couplings.

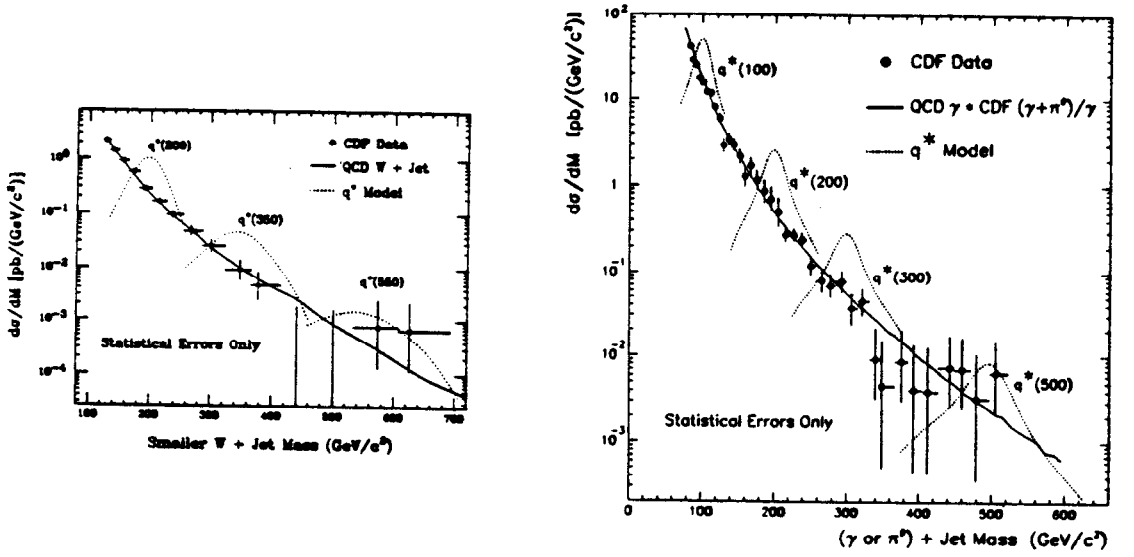

Figure 37: $W+1$ jet and $\gamma+1$ jet invariant mass distributions from the CDF collaboration, along with the expectation from QCD. Also shown are the expected mass peaks from excited quark $q^* \to qW$ and $q^* \to q\gamma$ decays of different masses. In solving for the neutrino longitudinal momentum in $W+$ jet events, the solution resulting in the smaller $W+$ jet mass is chosen in both the data and the Monte Carlo models.

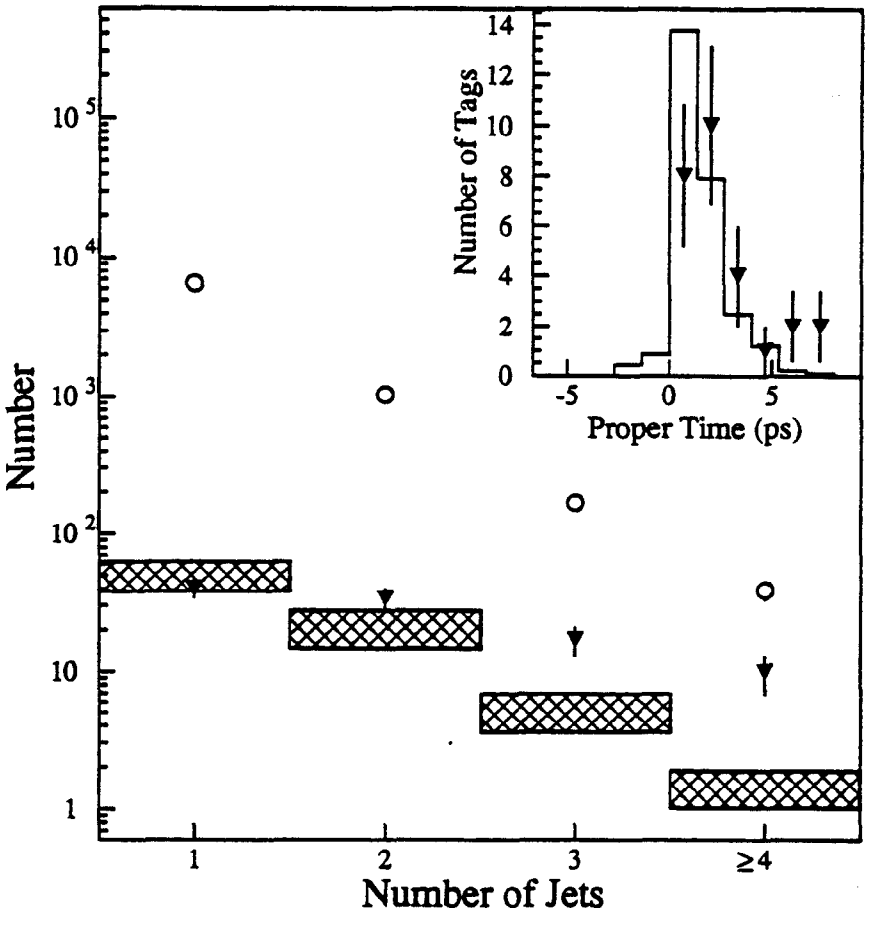

Figure 38: The CDF observed yields of $W+N$ jets, with $N = 1, 2, 3, \geq 4$ ($W \rightarrow e\upsilon$ and $W \rightarrow \mu\upsilon$ decays combined), before b tagging (open circles), after b-tagging using the SVX detached vertex algorithm (filled circles), and the backgrounds from non-$t\bar{t}$ processes (hatched regions). Based upon the excess of tags in the ≥ 3 jets, an additional 0.5 and 5 tags from $t\bar{t}$ decay are expected in the 1 and 2 jet bins, respectively. The inset shows the secondary vertex proper time distribution of the 27 tagged jets in the $W + \geq 3$ jets (triangles) compared to the expectation for b quarks from $t\bar{t}$ decay.

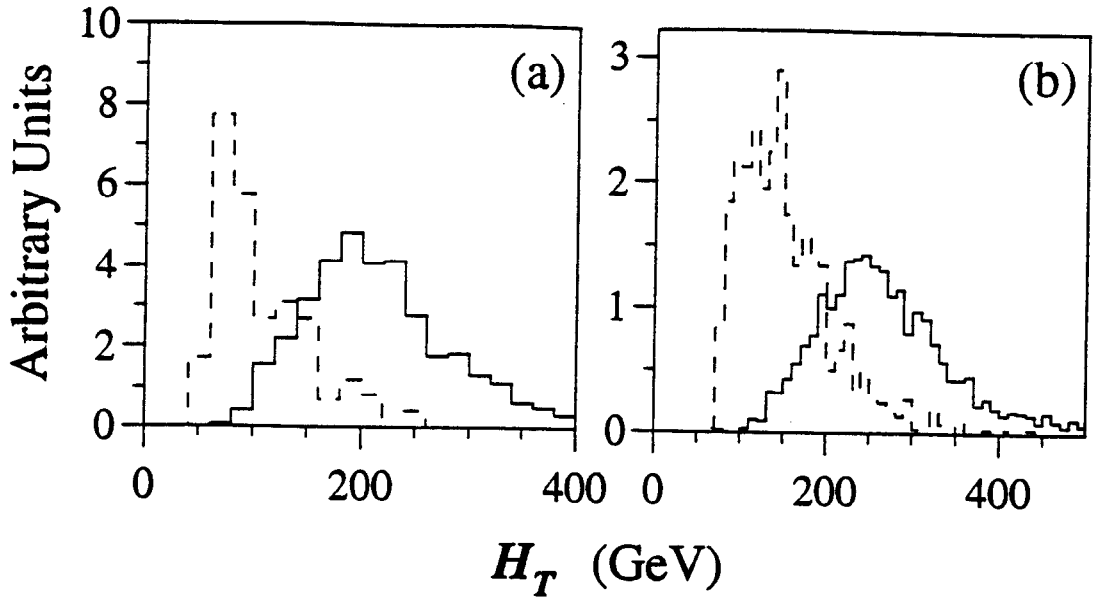

Figure 39: The shape of the H_T distributions (see text) expected in the DØ detector for the principal backgrounds (dashed lines) and for 200 GeV/c^2 top quarks (solid histograms) for (a) the $e\mu$ + jets, and (b) the untagged single lepton + jets events.

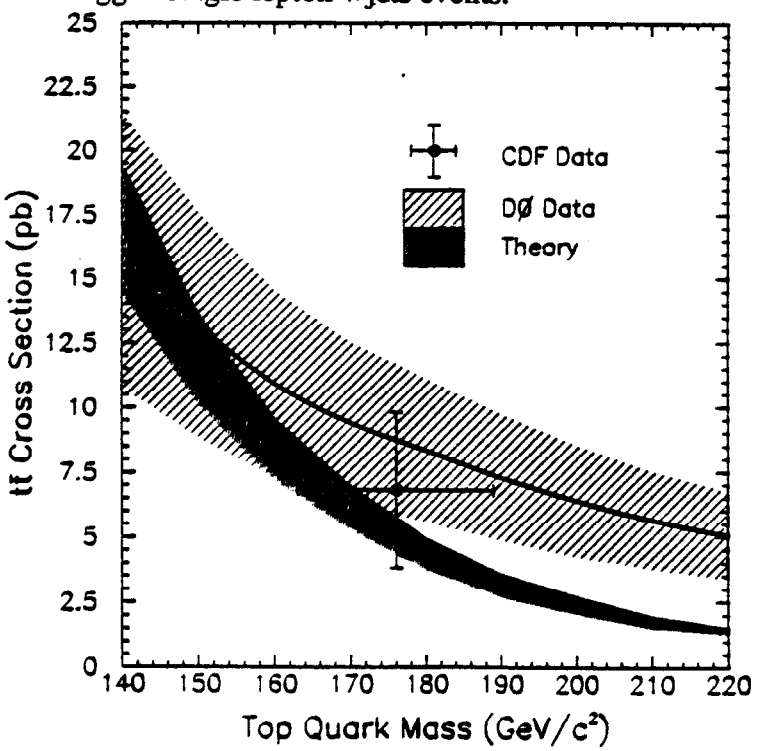

Figure 40: The theoretical $t\bar{t}$ production cross section $\sigma_{t\bar{t}}$ as a function of the top quark mass at $\sqrt{s}$ = 1800 GeV[116], as well as the DØ observed cross section *vs.* mass and the CDF cross section at its measured value of the top mass, $m_{top} = 176 \pm 13$ GeV/c^2.[122]

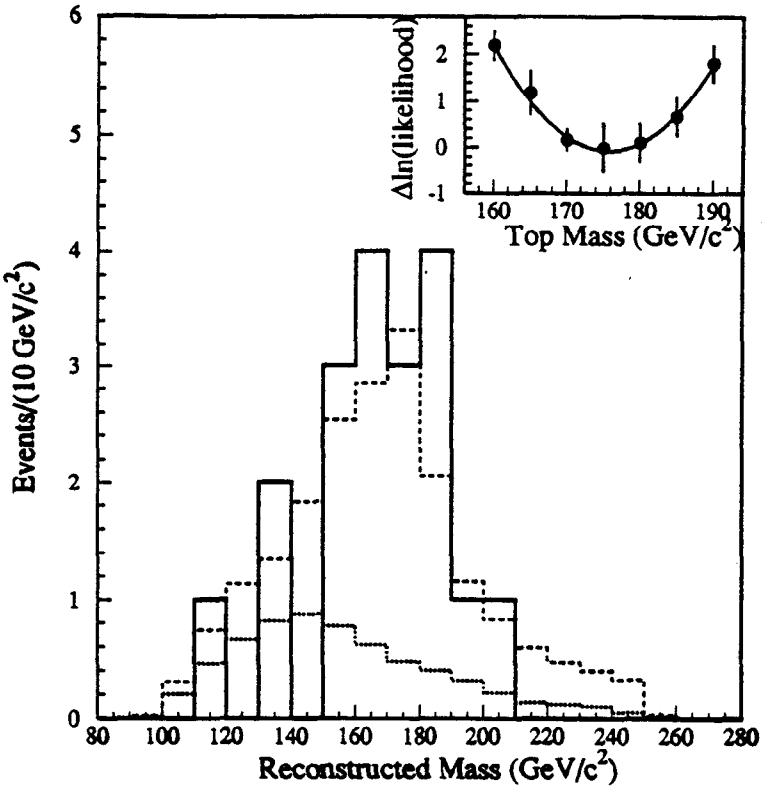

Figure 41: The CDF reconstructed mass distribution for the b-tagged $W + \geq 4$-jet (solid histogram). Also shown are the expected background shape (dotted histogram) and the sum of background plus $t\bar{t}$ Monte Carlo for $m_{top} = 175\ GeV/c^2$ (dashed histogram). The inset shows the likelihood fit used to determine the top mass.

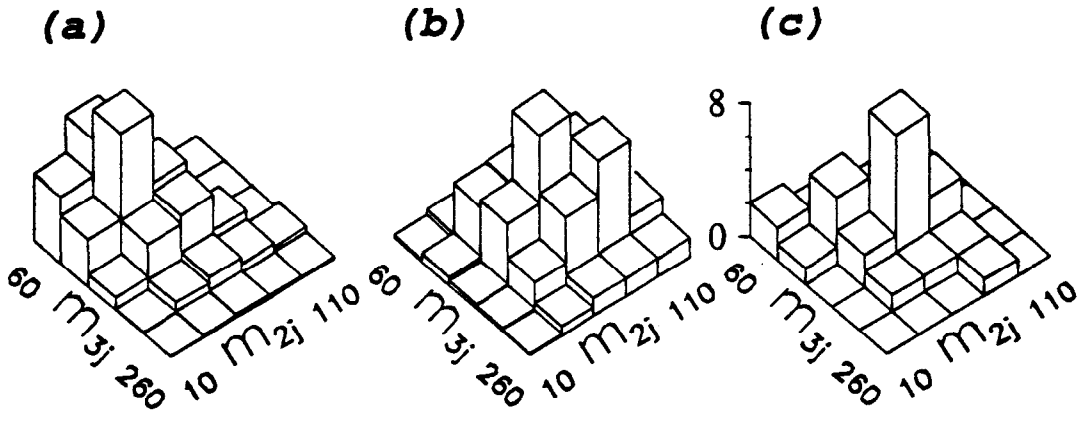

Figure 42: The DØ two-jet *vs.* three-jet invariant mass distributions in single lepton + ≥ 4 jet events for (a) background; (b) 200 *GeV/c*^{2} ISAJET top Monte Carlo; and (c) DØ data.

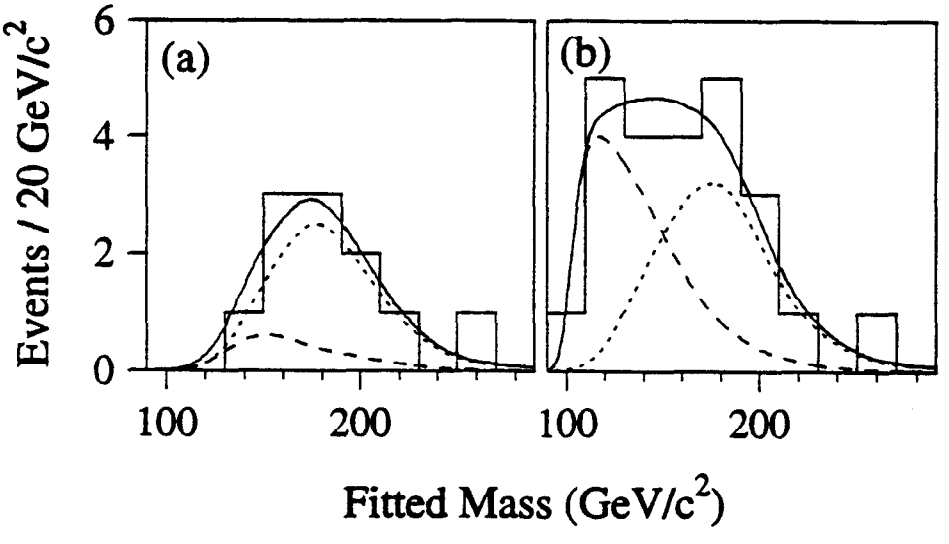

Figure 43: The DØ fitted mass distributions for candidate events (histogram) with the expectation for 199 *GeV/c*^{2} top quark events (dotted curve), background (dashed curve), and the sum of the two (solid curve) for (a) events with the H_T cut imposed and (b) events with relaxed cuts and no H_T cut (see text).